Physics-based energy estimation during the loading phase of a TSHD

D.G.J. Janssen

TUDelft

Van Oord

Marine ingenuity

Physics based energy estimation during the loading phase of a TSHD

The development of a simulation tool in order to potentially reduce dredging emissions.

by

D.G.J. Janssen

Student number:	4484355
Contact:	*janssen.dgj@gmail.com* | +31 6 81296109
Study:	MSc Hydraulic Engineering
Project duration:	May 2, 2022 - March 22, 2023

Thesis committee:	Prof. dr. ir. M. van Koningsveld,	TU Delft / Van Oord (chair)
	ir. M. de Geus,	Van Oord (supervisor)
	dr. ir. J.A.A Antolinez ,	TU Delft
	ir. M. Jiang,	TU Delft
	ir. A. Sepehri,	TU Delft

An electronic version of this thesis is available at http://repository.tudelft.nl/.

Cover: TSHD HAM318 Van Oord - (Photo from database Van Oord)

Preface

Before you lies the thesis "Physics based energy estimation during the loading phase of a TSHD". It has been written to fulfill the graduation requirements of the Masters program Hydraulic Engineering at Delft University of Technology. This work was conducted at Van Oord, a contractor in the maritime industry, over a period of 11 months from May 2022 to March 2023. As a family-owned company, Van Oord always treated me with kindness and provided ample support. Therefore, I highly recommend doing a graduation internship at this company!

I would like to thank my thesis committee for helping me deliver this master thesis. Thank you, Martin de Geus; my daily supervisor at Van Oord. Your personal attention and guidance really stood out. You always made time to passionately explain the engineering profession, which was greatly appreciated. Secondly, I would like to thank the chair of the committee, Mark van Koningsveld. Your enthusiasm and passion for solving maritime problems from a higher perspective have always helped me to zoom out and focus on the overall goal of the research. Thirdly, I would like to extend a special thanks to Jose Álvarez Antolínez. Our engaging discussions on data analysis and academic writing greatly contributed to the improvement of the report's academic standard. Furthermore, I would like to thank Man Jiang and Arash Sepehri for their guidance and insightful discussions during our meetings. Their input greatly assisted me in presenting the research more effectively and focusing on the ultimate goal.

Last but not least, I would like to thank my family and friends. Especially, Leo Janssen for getting me excited about the engineering profession and for always being available to discuss the overarching structure and steps to take during this research.

D.G.J.Janssen
Rotterdam, March 2023

Abstract

The dredging industry is a contributor to the greenhouse gas (GHG) emissions due to the energy-intensive process of dredging and transporting sediment. This industry has to reduce the GHG emissions due to future possible restricting regulations on GHG emissions. The dredging industry is shifting towards more environmentally friendly fuels, but designing new vessels which can run on these fuels will be a time consuming transformation. Though, the demand of dredging activities is growing, think of construction of offshore wind farms and creating flood defences against sea level rise. To minimize the costs due to the high GHG footprint in the short term, Van Oord should be able to estimate the energy consumption (GHG emissions) based on different dredging strategies.

Van Oord uses a model to estimate energy consumption that accurately describes the majority of dredging projects, based on the power installed, dredging time, and a power coefficient term. This power coefficient term is based on empirical data and may result in a less accurate estimation of more complex (new) projects such as offshore wind farms and cable dredging, which are the new opportunities arising for dredging companies. To better estimate energy consumption during these complex dredging operations, a physics-based and semi-empirical method is developed that can more accurately estimate energy consumption based on certain dredging strategies. Previous research already looked at the sailing phases of the dredging cycle, therefore the main objective of this thesis is:

To quantify the energy consumption of different TSHD dredging strategies based on physics for the loading phase.

To achieve this research objective, first a literature study is conducted to list the different physics-based methods available to estimate the energy consumption. The energy consumption of a TSHD is divided into five main energy consumers (propulsion system, dredge pumps, jet pumps, bow thrusters and board net) in which the energy of the individual components is described by a power and a time term. The time component is represented by the duration of the loading cycle, which in this study is limited to the filling process of the hopper until overflow. The power term of the jet- and dredge pumps have been estimated by the (adjusted) in-house physics-based methods of Van Oord. The board net and the bow thrusters have been estimated by data analysis of a case study. The goal of this research is to develop a method to estimate the required propulsion power and a tool to bring all methods together to simulate the total energy consumption during the loading phase based on different dredging strategies.

A model is developed to estimate the required propulsion power during loading. The model development is divided into three phases; The first phase describes the development of a semi-empirical physics based model. In this, the various resistance forces acting on the vessel, suction pipe, and draghead are calculated based on stationary parameters such as vessel dimensions, and project parameters. The project parameters, including water depth, trailing speed, and visor angle, are extracted by filtering the actual data from the case study. In this way the estimation model is set equal to a reference case. Finally, the output of the estimation model is calibrated by comparison with the actual data of the case study. This calibration phase is an iterative process in which the accuracy of the model is described and increased.

The model shows that it is possible to calculate the required propulsion power based on operational parameters, such as trailing speed. Furthermore, the model provides insight into the amount of resistance on the three components (draghead, suction pipe and vessel). The power curve follows a quadratic pattern for increasing trailing speed, which appears to be a reasonable estimate. When comparing the model to the actual data it can be seen that the model underestimates at lower trailing speed and over estimates at higher trailing speed. By finding correlations between visor angle and trailing speed the model is calibrated and seems to better fit the dataset, however the slope of the curve still has a large deviation compared to the regression line based on the actual dataset. Therefore, the model needs to be further developed before it can be included as an addition to the existing models within Van Oord. The static friction term is not included, which could compensate the underestimation of the model and the high cutting forces are the potential reason for the overestimation at high

trailing speed. For now, the current developed model falls within the reference dataset for the trailing speed between 1.6 [kn] and 1.9 [kn], thus making it a reasonable first estimate of the required propulsion power.

The OpenCLSim python package, which can be used to simulate discrete events, is used to simulate the dredging processes of the loading phase. A plugin for this python package is developed to calculate the total energy consumption during these processes. The propulsion model is integrated (with the set limitations) in this plugin together with the four other power estimation methods (dredge pumps, jet pumps, bow thrusters and board net). The simulation tool runs based on four input characteristics: vessel parameters (TSHD), site characteristics, dredging strategy, and data describing the bow thrusters and board net. The output of the simulation includes required power, duration, and consumed energy. Additionally, the simulation estimates the fuel usage, emissions, and project costs associated with energy consumption.

The main ability of the simulation tool is that it can visualize the energy consumption (and emissions) based on dredging strategies and location. This enables the prediction and potential reduction of emissions in sensitive areas, such as fine dust emissions near cities. By using this simulation tool, a dredging plan can be created based on dredging strategies (trailing speed) to reduce emissions in these sensitive areas. To better demonstrate the other capabilities of the developed plugin within the OpenCLSim Python package, the simulation tool is applied to an imaginary project called Barachi. This project has strict regulations that prohibit overflow and apply emission taxes. Two dredging strategies are compared based on the limitations of the developed propulsion model: trailing speeds of 1.6 [kn] and 1.9 [kn]. The results show that, first of all, the project duration will decrease with an increasing trail speed. Secondly, the increase in power has a greater effect on energy consumption than the decrease in project duration, meaning that energy consumption will increase. Since fuel use and corresponding emissions are linked to energy consumption, they will also increase. However, the cost analysis provides a different view. In this case, because the ship's operating costs are governing, faster trailing is the most cost-efficient, even if an emission tax of 200 euros/ton CO2e is applied.

To conclude, by creating a model to estimate the propulsion power and by integrating this model in a simulation tool, it is possible to quantify the energy consumption of different TSHD dredging strategies based on physics for the loading phase. Subsequently, the simulation also provides insight into the fuel usage, carbon emissions, and costs of the project. Further development and validation of the propulsion model is needed to give a more accurate estimation of the required power. Firstly, the static friction component should be included in the estimation model which could potentially solve the underestimation at lower trailing speed. Secondly, a maximum trail speed limit should be set based on the available propulsion power with respect to the total power distribution of the vessel. This limit should be included in the simulation tool, since it is linked to the other power consumers and the operational parameters. Thirdly, the propulsion model can only be used in saturated sand projects. Other cutting models based on cutting of silt, clay and rock should be added in the propulsion model to be able to apply the model in these soil conditions. Finally, the use of the tool is limited to dredging projects where overflow is not allowed. The suction production and the settling process within the hopper should be added to expand the capabilities of the tool to projects where overflow is possible.

Contents

1 | Introduction

1.1 Context

Climate change is one of the biggest challenges for the current and future generations. Fortunately there is an increasing willingness to reduce the emission of greenhouse gases (GHG) in almost every sector in the world. The link to the dredging industry is quickly made if you look at GHG emissions. The big dredging vessels need a lot of energy to pick up, transport and deposit sediment from one location to the other. Multiple energy consuming installations are applied to execute this process. Normally a dredger is designed on heavy fuel oil (HFO) and marine gas oil (MGO) and the combustion of these oils will lead to high GHG emissions.

Fortunately, also in this industry big companies are motivated to decrease their GHG emissions. The shift is coming from fossil- to more environmentally friendly fuels (Mestemaker et al., 2020). First, transitions fuels are used as natural gas and bio fuels. These fuels have equivalent CO2 emissions but less other GHG are emitted during combustion. In the future these fuels will probably be converted into hydrogen or other renewable energy sources (Jacoby, 2022). This transformation to environmental friendly solutions will not come immediately, while on the other hand the need for dredging activities is growing. The dredging industry is key in providing different solutions to current global issues, think off the construction of offshore wind parks to switch to renewable energy, creating artificial islands to cope with the world's growing population and protecting people from sea level rise by creating flood defenses. When in fact there's a growing demand for the dredging industry, opportunities should be created to decrease environmental impact of the big dredging vessels.

There are multiple ways to decrease the emissions in dredging. The main impact will be made by the government, which can create restricting regulations on maximum allowable emissions in this sector (Castro et al., 2014). To be able to win new tenders a contractor should find technology solutions to comply with these new regulations and project conditions. Contractors are shifting to more environmental friendly fuels, but designing new vessels which can run on these fuels will be a time consuming transformation. In the short term, to reach these goals the dredging industry needs to improve their current methods of energy estimation and corresponding emissions of vessels during a project. Only then when the energy consumption (GHG emissions) of a specific dredger is known, decisions can be made how to approach a project to reduce GHG emissions and to comply with the new legislation.

Up til now a contractor wants to minimize vessel operating costs by minimizing project duration. This normally means that a dredger is working on full power and it's consuming a lot of fuel and therefore emitting high amount of emissions. New regulations will change this way of approaching a project and the environmental impact of the project will be key on winning new projects. The greenhouse gas emissions are divided into three categories for businesses and organizations – scope 1,2 and 3 (World Economic Forum, 2022). For a contractor as Van Oord this means the following. Scope 1 emissions are direct emissions from combustion of fossil fuels in the company-owned vessels. Scope 2 emissions are the indirect emissions from the electricity used to power the dredging equipment and any on-site facilities, such as offices or workshops. Scope 3 emissions are the emission of the dumped material and the end-of-life dredging equipment. New tenders can not only be won on costs efficiency, the environmental impact of a project, based on the three scopes, can also play a critical role in determining the outcome of a tender. An example of process is the recent tender for an offshore wind park in the North Sea, important subjects in this tender are marine protected areas, species protection, the impact on fisheries and other environmental scope 3 criteria (RVO, 2023). Additionally, the reduction of greenhouse gas emissions during the construction phase, which falls under scope 1, can also become a crucial factor in determining the winning bid.

1.2 Trailing Suction Hopper Dredger

The Trailing Suction Hopper Dredger [TSHD] is a self-propelled dredging vessel, which can be used as sea going or inland waterway vessel. The vessel is mainly applied at projects where the distances to the dump areas are too large for a direct discharge and supply with pipelines. The vessel makes use of box (hopper) where it can store its dredged material until it can be disposed at the dumping area, The vessel does not use an anchorage system during dredging which allows it to be used in many different places. A TSHD is applied with powerful pumps and engines which enables the vessel to dredge different kind of material like sand, silt and clay and sometimes even gravel. The material will be stored in the vessel (hopper) and the leftover water will be discharged overboard (when allowed) to maximize capacity.

1.2.1 Working method of TSHD

The general working method of a TSHD can be divided into four stages. Sailing empty to the borrow area, loading of the dredged material into the hopper, sailing full to the deposit area and dumping the dredged material. A schematic overview of this process is shown in figure 1.1.

The vessel will first sail at full speed with a (nearly) empty hopper to the dredging area. The loading stage will start when the vessel reduces its speed to approximately 2 knots ($\pm$ 1.0 m/s) whereas the suction pipes will be swung outboard and be lowered. When the suction inlets arrive at the bottom of the sea the drag heads are lowered and the dredging pumps are started. The hopper will be filled with a mixture of sediment and water. To maximize the loading capacity the hopper will discharge the leftover water overboard, which makes it in non-linear process. If the hopper is fully filled (or sometimes before fully filled) the pumps will be turned off and the suction pipes will be brought back inboard. The sailing full stage will start when the vessel starts accelerating to full speed. The vessel, with a filled hopper, will sail to the dumping area where the final stage will begin, the depositing stage. A TSHD can use multiple methods to deposit its load. By simply opening the bottom doors, by rain-bowing (spraying the sediment) and by discharging the sediment via pipelines. Site specific parameters will have to show which method is the most appropriate.
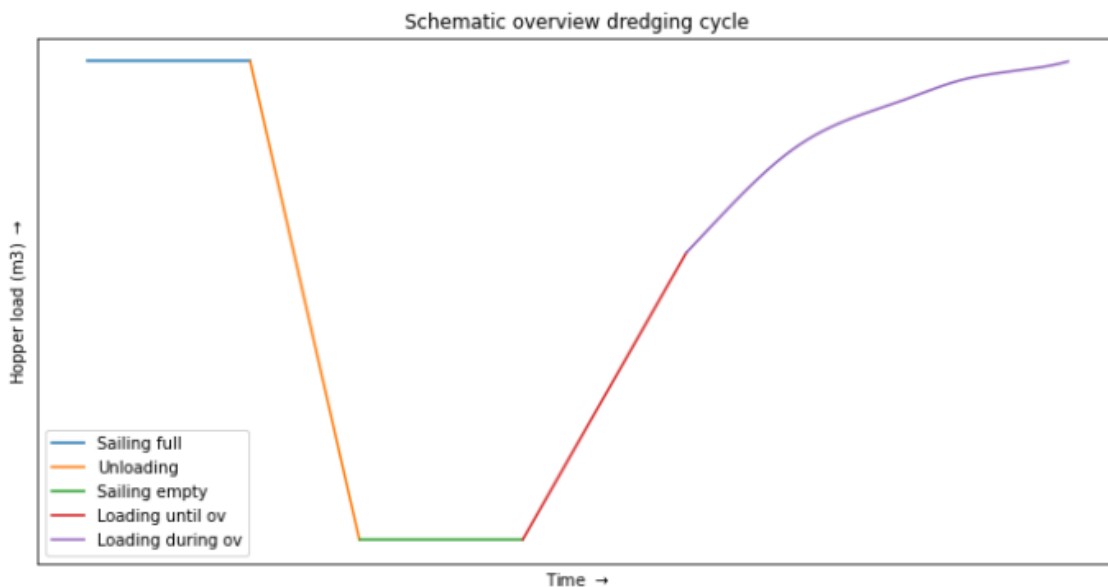

Figure 1.1: Schematic overview dredging cycle with different colors per dredging phase. y-axis represents the hopper loading and the x-axis the time

1.2.2 Energy consumers

To get insight in the energy consumption of the TSHD the main power systems are analysed. Multiple engines are present on the vessel which are activated and dis-activated during different stages of the dredging process. This overview provides some background information of the energy consumers.

Propulsion system The propulsion system is used at full power during the sailing stages and on less power during the loading stage. The vessel should always aim to sail on full speed to limit the total dredging cycle time and therefore limit the costs. During the loading phase it is not possible to sail on full speed due to the overboard suction arms. The speed should therefore be limited to approximately 2 knots which result in a decrease of energy consumption. Overall the propulsion system is seen as one of the main energy consumers of the TSHD.

Inboard dredge pumps (IBP) The IBP is normally a centrifugal pump installed on the vessel deck. This pump is used to suck up and discharge the mixture in the hopper. The centrifugal dredge pump is one of the main energy consumers on board of the TSHD and is activated during the loading and unloading stages of the dredging cycle.

Underwater dredge pumps (UWP) The UWP is mainly installed on the bigger THSDs which are used to dredge at very large extraction areas. The UWP is installed in the suction pipe and is used in combination with the IBP to overcome the high pressure losses that occur in these large suction arms. Both pumps have a comparable power demand.

Jet pumps The jet pumps are used to cut the soil before pumping the soil-water mixture onboard. By jetting water in the soil the soil will disengage and a soil-water mixture will be formed. This mixture will then be sucked up by the dredging pumps.

Bow thrusters The thrusters can apply a force perpendicular on the vessel to increase the maneuverability of the vessel. This makes it possible to turn the vessel in confined spaces. The thrusters should always stay under the waterline to exert the required force.

Board net The board net can be seen as a collection term of the remaining energy consumers on board of the TSHD. These remaining energy consumers are the hydraulic systems, winching systems, board lighting and electricity for daily business of the crew.

Not every energy consumer is active during all dredging stages. Table 1.1 will give an overview of the active energy consumers during different stages.

	Sailing empty	Loading	Sailing full	Depositing
Propulsion system	x	x	x	x
Inboard dredge pump		x		x
Underwater dredge pump		x		
Jet pumps		x		x
Bow thrusters		x		x
Board net	x	x	x	x

Table 1.1: Active energy consumers per dredging stage: all energy consumers are active during the loading cycle

1.3   Field of research

To comply with the new set legislation and to remain one of the top dredging companies of the world, Van Oord should make the switch to decrease emissions during dredging. This should be done by designing new sustainable vessels (like the new LNG vessel), by optimizing the energy consumers on board of the current vessels, by using new renewable fuels and by implementing project strategies based on reducing emissions. For dredging companies it is therefore very important to have inside in their energy consumption (GHG emissions) off their dredging vessels.

1.3.1   Current van Oord model

A world leader company as Van Oord already make use of models to estimate the energy consumption of their fleet. This model is widely used within the company and approaches the majority of the dredging projects in an accurate way. The model is described with the following formula:

$$Energy\ consumption = P_{inst} * P_{coef} * t \tag{1.1}$$

Where:

P_{inst} = Total installed power for energy consumer [kW]
P_{coef} = Power coefficient based on empirical data [%]
t = Time energy consumer is active [min]

The power installed is the maximum power which is available for a energy consumer during a dredging stage. The dredging time is calculated based on the phase which is active, for the sailing phase this means that the duration is based on the time it takes for the vessel to sail from or to the loading/dumping area. The last term in the formula is a power coefficient term. This power coefficient is based on empirical data and is valid for most dredging activities.

A dredging company as Van Oord is keeping up with the times and diverts interest in other dredging activities. The 'basic' land reclamation and maintenance dredging work will continue to exist but new opportunities arise. The construction of offshore wind farms is one of the activities where dredging companies can play a big role as well as the infield cable dredging. This type of dredging work differs from the 'basic' projects, which ensures that the use of the current power coefficients will result in a poor estimation of the current more complex projects.

1.3.2   Previous research

The foundation of this research is laid by Vibeke van der Bilt (2019). She made a simulation of the whole dredging cycle (with the OpenCLSim python tool) by calculating the power on empirical values and by simulating the dredging cycle. By making a simulation of the dredging phases she was able to optimize the dredging strategies. Figure 1.2 shows a result of the power distribution during a typical dredging project for the Dutch coastline preservation sand reclamation work van der Bilt, 2019.

A continuation on this research was done by Stijn Lamers. He made an elaboration on the sailing full and empty dredging stage by describing the power that is needed to overcome the resistance factors on the vessel during sailing. He created an estimation model and validated this model by comparing it with sensor data of a TSHD of Van Oord. By improving his model based on the comparison with actual data, the required propulsion power during sailing can now be estimated for one particular TSHD of Van Oord.

Figure 1.2: Power distribution results of study by: (van der Bilt, 2019). Power distribution is plotted for different energy consumers based on empirical coefficients

1.3.3 Research scope

This research has been done with the contractors view in mind. The main focus of this research is to better estimate the energy consumption during the loading phase. This research is done in combination with Van Oord Marine Ingenuity and will be focused on the biggest TSHD of their fleet, the HAM318.

As described in the introduction there are many ways to improve the environmental impact of these dredgers. Changing project strategy, when the energy consumption is known, can be applied on short notice and can have a great impact on reducing emissions. The focus of this study will therefore not be on improving the ship design but on improving operational parameters to define the cheapest, fastest and cleanest project strategies. In this sector there is still a lot to win if decisions are not based on project costs but also on environmental impact.

1.4 Problem description

The previous paragraph gave an impetus to the problem description which is elaborated in more detail in this paragraph. To better estimate the energy consumption for more complex situations there are two dredging stages which have not been evaluated yet, the loading and unloading stage. As figure 1.2 shows, the power distribution during the loading and unloading phase is more extensive than during the sailing stages, since all energy consumers are active. This makes it highly complex to make an accurate energy estimation during these stages. All the processes during the loading phase should be well understood to come up with the total energy consumption of a vessel.

This leads to following problems description:

1. The current model is based on empirical data, which makes an inaccurate energy consumption estimation for some complex dredging projects.

2. The current model does not make a clear enough distinction between dredging stages during estimation of energy consumption. This makes the model too general and less applicable when comparing different dredging strategies for the same project.

3. The current model is based on empirical data and lacks physics based theory and is thus not generally applicable.

4. There is currently no accessible emission simulator based on dredging strategies, which has become increasingly crucial in winning new tenders.

1.5 Research objective

The overall research aim is to contribute to the reduction of GHG emissions by creating a simulation tool where the energy consumption can be quantified for future dredging projects based on physical estimation methods and dredging strategies. Previous research already looked at the sailing phases of the dredging cycle. The focus of this study will be on the loading phase, to contribute to an overall research which is to increase the accuracy of the energy consumption estimation during the total dredging cycle.

The main research objective is:

To quantify the energy consumption of different TSHD dredging strategies based on physics for the loading phase.

To achieve this objective the following research questions are formulated:

1. Which methods are available to quantify the energy consumption during the loading phase based on physics?

2. How to develop a semi-empirical physics-based energy estimation model and calibrate with a real case study?

3. How to integrate the developed model to estimate the total energy consumption during the loading phase?

4. How can the energy consumption among different dredging strategies be compared?

1.6 Research structure

The structure of the report is divided into seven main sections. The literature section provides an answer to the first research questions and describes previous studies on the different energy consumers. The development of a propulsion model will be elaborated in section 3. Whereafter the model is integrated in a simulation tool to estimate the energy consumption of the loading phase in section 4. The findings are discussed in section 5. The research objective will be elaborated in the conclusion section in which all research questions are answered. Finally, future directions and improvements on this report will presented in section 7, Recommendations.
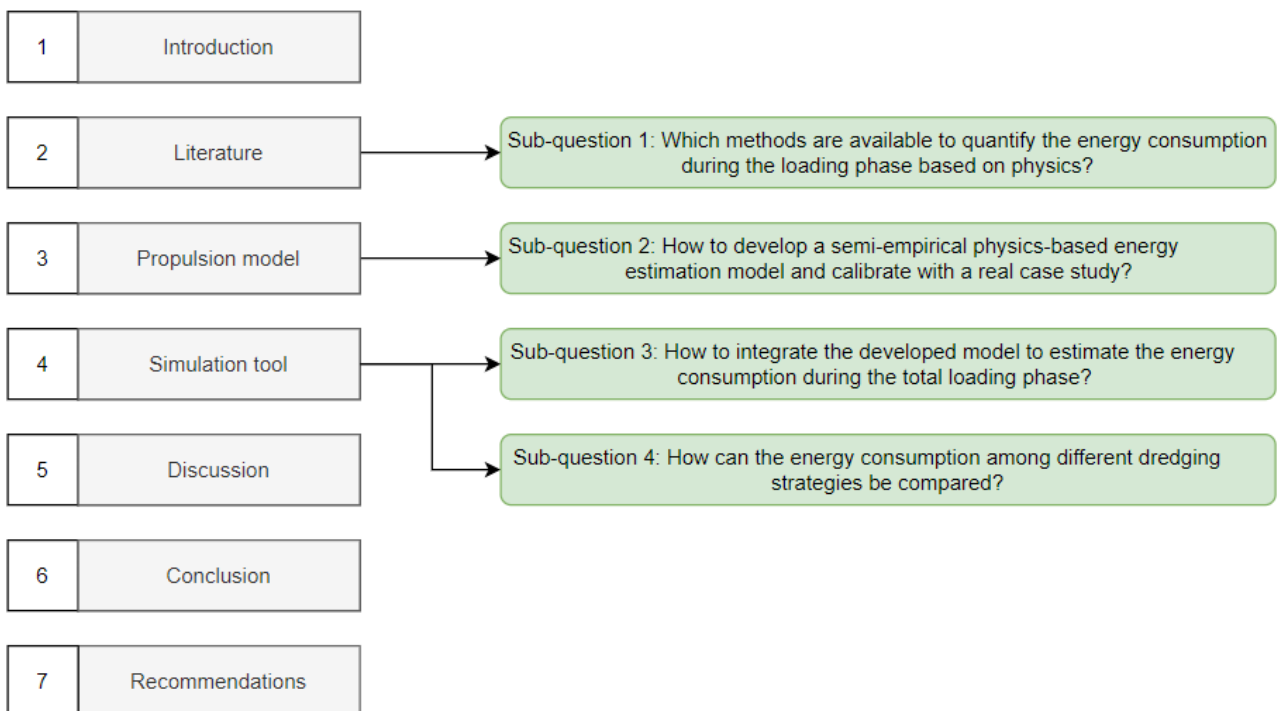

Figure 1.3: Schematic visualization of the report structure

2 | Literature

This section answers the first sub research question:

Which methods are available to quantify the energy consumption during the loading phase based on physics?

To answer this question a literature study has been performed to delve more deeply in the physical estimation methods to describe the active energy consumers during the loading phase of the TSHD. The total energy consumption during the loading phase is the sum of all active energy consumers. Figure 2.1 shows a visualization of the studied energy consumers.
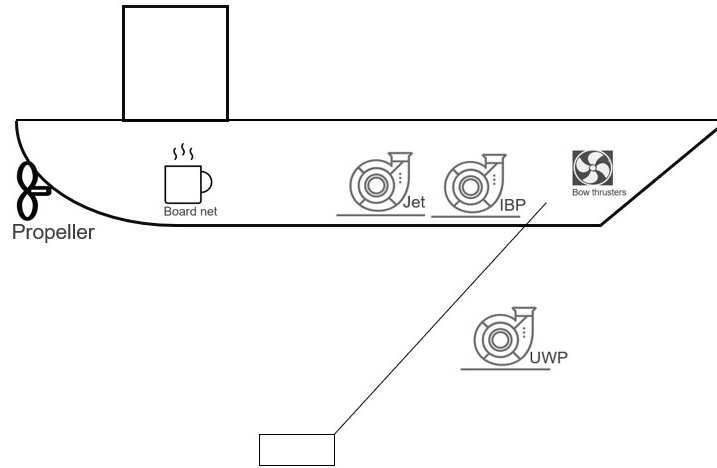
Figure 2.1: Schematization of main energy consumers on a TSHD which are elaborated in this study

The total energy consumption during the loading phase is the sum of:

$$E_{loading} = E_{propeller} + E_{dredge.pumps} + E_{jet.pumps} + E_{thrusters} + E_{board.net} \qquad (2.1)$$

Energy can be described as power times duration. It is assumed that all energy consumers, with an exception of the bow thrusters, are active during the total loading phase. This makes it possible to study the power and the duration term separately.

$$E_{loading} = \int P dt \qquad (2.2)$$

The next step is to describe the needed power per system, based on physics. Power in general can be described by different systems, and for a TSHD this can be summarized in mechanical- and hydraulic power. The mechanical power system (P_m) as the propulsion system, which is the product of a force times the object's velocity and the hydraulic power (P_h) of the pumps which is the product of pressure times discharge.

$$P_m(t) = F * v \qquad (2.3)$$
$$P_h(t) = p * Q \qquad (2.4)$$

The subsections in this literature section will deal with one of the energy consumers described in Figure 2.1. For the evaluation of the energy consumption also an estimate of the loading duration should be made (section 2.6). The background information on the software where the energy consumers will be put together is explained in section 2.7. A summary of the literature background can be found in section 2.8.

2.1 Propulsion system

The engine is the system which makes sure that the propeller rotates and the vessel can move forward. To estimate the energy which is consumed by the engine, the power during a certain time period on which the engine is active should be evaluated:

$$E_{engine} = \int P_{engine} dt \tag{2.5}$$

The loading time is the time it takes for the hopper to be filled (section 2.6) and the used power of the engine can be expressed as the power which is needed to overcome all resistance terms working on the vessel and the lost power (friction and heat) during transferring the power to the propellers. What remains after transferring the engine power to the propulsion power is called the Effective Horse power (EHP), which can also be seen as the work done by the moving vessel (van Koningsveld et al., 2021).

$$P_{engine} = P_{EHP} * \frac{1}{\eta_{tot}} \tag{2.6}$$

where:

P_{EHP} = Effective power
η_{tot} = Total efficiency terms

2.1.1 Effective power

The EHP can be seen as the power that is needed to overcome the resistance terms working on the vessel times the trailing velocity:

$$P_{EHP} = v_{trail} * R_{total} \tag{2.7}$$

where:

v_{trail} = trailing speed [m/s]
R_{total} = total resistance [kN]

The resistance working on the vessel during trailing can be split up into three components. The resistance working on the vessel, the suction pipe and the draghead (Figure 3.3). The EHP should encounter these horizontal resistance forces during dredging and should push the vessel forward with a particular trailing speed.

$$R_{total} = R_{vessel} + R_{suction.pipe} + R_{draghead} \tag{2.8}$$

The resultant of each resistance force can be transferred to each other since all components are connected. This means that the resultant of the draghead will attach at the bottom of the suction pipe (point C) and the resultant of the lower suction pipe (including draghead) will attach at point B and the resultant of the upper suction pipe (including resultant at point B) will attach at the vessel in point A. By adding these horizontal forces, the total resistance to calculate the EHP will be known. The free body diagram of this approach is show in Figure 2.2:
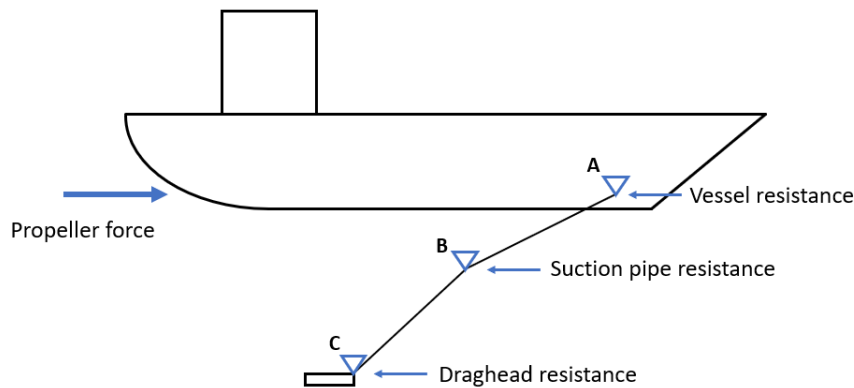

Figure 2.2: Schematization of different suction pipe compartments which is used in the resistance analysis

Vessel resistance

The vessel resistance is the resistance that works on the vessel during sailing when the suction pipe and draghead are inboard of the vessel. There are multiple methods defined to describe the resistance working on the vessel. Considering the prior research of Stijn Lamers (Lamers, 2022) it is chosen to use the Holtrop and Mennen method (Holtrop and Mennen, 1982). This makes it possible to align both studies and to combine different dredging stages with each other. The Holtrop and Mennen method describes the total resistance on a vessel during sailing by making a breakdown in different resistance components. Normally this method is applied for estimating the resistance terms for Inland Water Transport (IWT), but with some modifications it can also be used at dredging vessels. The modifications on this method are elaborated by Stijn Lamers (Lamers, 2022) based on the analyses of the same TSHD. These modifications increase the accuracy of the wave term at higher sailing speeds and includes the bulbous bow of the dredger. Since the trailing velocity is much lower than the sailing speed, the modifications of the wave term are not valid during the loading phase. The original wave term of the Holtrop and Mennen will be used during the loading phase. The modifications made by Lamers will be used during the sailing phases when simulating the total dredging cycle. The total resistance during sailing is described with the following formula, for a detailed explanation the thesis report of Lamers can be used as reference (Lamers, 2022).

$$R_{vessel} = R_F(1 + k_1) + R_{app} + R_w + R_B + R_{TR} + R_A \tag{2.9}$$

Where:

R_{vessel} = total resistance of the ship [kN]
R_F = frictional resistance [kN]
$1 + k_1$ = form factor of the hull [-]
R_{APP} = appendage resistance [kN]
R_W = wave-making resistance [kN]
R_B = pressure resistance of bulbous bow [kN]
R_{TR} = pressure resistance of immersed transom stern [kN]
R_A = model-ship correlation resistance [kN]

Suction pipe resistance

The total resistance on the upper- and lower pipe combined is the sailing pipe resistance. There are two resistance terms working on the pipe system, the drag force on the pipe due to movement through water and the gravity forces due to the weight of the pipe and the mixture moving in the pipe.

The step-by-step approach of G.ter Meulen to calculate the forces on the suction pipe by moment- and force balances (ter Meulen, 2018):

1. Free hanging situation at standstill (not touching the bed). This situation is used to determine the unknown force in the cable connected to the lower pipe. Based on the gravity forces, the static force in the cables is determined as well as the reaction force in point B.

2. Compensated vertical soil force at standstill. The cable force can be adjusted by changing the pressure in the swell compensator. To keep the tension force in the cable constant (at the previously calculated static situation) this factor is applied based on the soil type. On a sandy bed, this factors is normally set to 50% of the max compensation capacity available. Now the resulting force on the draghead can be calculated for a static situation.

3. Compensated vertical soil force and increasing trailing velocity. The same calculation is done but now by increasing the trailing velocity. This means that the drag force, which attaches in the middle of the pipes, will be added to the equation and will cause the pipe to move upwards. When the trailing speed increases this uplifting force will be bigger and on a certain point the upper or lower pipe will start floating. The angle of the pipe system will change and the situation is not static anymore. If the reaction force on the draghead becomes zero, the draghead will lift off from the bed.

4. Compensated soil excavation forces and increasing trailing velocity. The resultant forces of the draghead model is implemented to calculate the final horizontal resultant force in point A. Together with the vessel resistance, this will result in the total resistance. The vertical reaction force will be compensated by the buoyancy of the vessel.

Additions and modifications to fit the model into the scope of this research and the corresponding free body diagram are shown below:
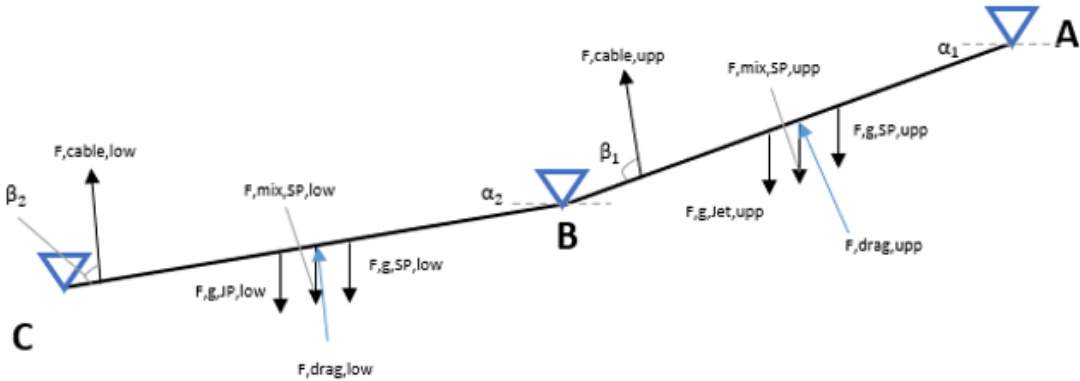

Figure 2.3: FBD of the suction pipe, cable forces, weight forces, drag forces and mixture/water force can be observed in the figure. The definition of the names are described below.

- The weight of the different parts of the suction pipe and jet pipe should be obtained via drawings of the TSHD (HAM318). Two resultant forces for both pipes should be derived from these drawings, for the upper and lower pipe. The weight of the water in the jet pipe is included in the jet forces. The application point of these resultant forces can be calculated by momentum balance at point A for the upper pipe and point B for the lower pipe:

$$R_{res} = \frac{\sum R_i * F_i}{\sum F_i}$$

F, g, Jet, upp = Submerged weight of upper jet pipe
F, g, SP, upp = Submerged weight of upper suction pipe
F, g, jet, low = Submerged weight of lower jet pipe
F, g, SP, low = Submerged weight of lower suction pipe

- The weight of the mixture in the suction pipe is derived separately. For now this weight is based on a static mxiture density of $\rho_{mix} = 1300[kg/m^3]$. The value could be adjusted during the project or be linked to the developed pump modules.

F, mix, SP, upp = Dredged mixture weight in upper pipe
F, mix, SP, low = Dredged mixture weight in lower pipe

Draghead resistance

The draghead can be seen as the dominant resistance force working on the system. At low velocities the comparison is often made with an anchor moving over the ground. The many different forces working on this system makes it complicated to analyse this system. A study by (ter Meulen, 2018) on the draghead's physical processes is summarized in this section and adjustments to this analysis are described. His work should be used as reference and a detailed explanation of the work can be found in this report (ter Meulen, 2018). First, the working principle of the draghead is analysed to understand the processes and corresponding forces within the draghead.

Working principle
Figure 2.4 is used as reference to understand the working principle of the draghead. In the figure the draghead moving direction is to the right. The figure is cut off at the suction pipe in which the mixture is transported into the hopper. The heel of the draghead is the location where the draghead rests on the ground and withholds the draghead of sinking too deep into the ground. In the heel, just right of the joint location (where the visor part starts), jets are installed to fluidize the soil. Different nozzles are installed to inject water into the soil to loosen the compact structure of the soil. The nozzles are installed across the entire width of the drag head, in which the diameter of the nozzles can be optimized to get the required flow.
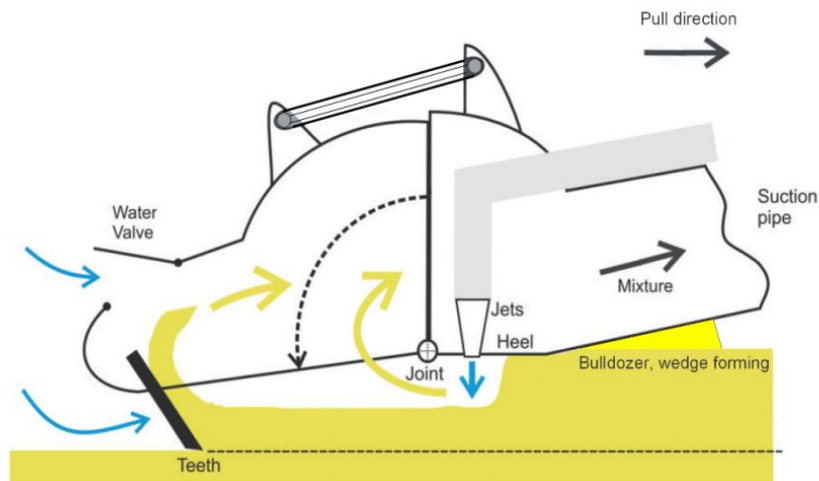
Figure 2.4: Working principle of the draghead, source (v. Bergh et al., 2015). The soil is fluidized by the jet whereas it is directly sucked upwards in the draghead. Another soil layer is cut by the teeth.

The jets will fluidize the bed layer whereby a sand-water mixture is formed. Besides the jets, cutting teeth are installed in the draghead as well. The teeth can cut the remaining soil, which is not fluidized by the jets, to increase the density of the sand water mixture. The cutting and jetting process work closely together, if too much water is penetrated in the bed no cutting will take place and the mixture will primarily exist of water. On the other hand, if too little water is used the teeth will dig into the ground and very high cutting force will arise. This can cause the draghead to jam in the ground and act like an anchor for the vessel. The formed soil water mixture will be sucked up by means of an under pressure created by the dredge pumps.

To analyse the resistance forces the draghead is split into two parts. The fixed part, which is referred to as the draghead and the movable part which is referred to as the visor. Due to the weight of the suction pipe and draghead the visor will make contact with the ground and dependent on the soil composition, even sink in the ground.

Figure 2.5: Side view of draghead configuration with a hydraulic cylinder, source: (ter Meulen, 2018). The left part of the red line is the visor, the right part is the draghead house.

The visor can be controlled in different ways (van Rhee, 2016).

1. A loose hanging visor: the visor will sink into the ground due to its weight. The angle of the visor depends on the equilibrium of the forces working on the visor, which will deviate based on the trailing speed.

2. A fixed visor: the visor is fixed at a predefined angle. The visor cannot move and will either sink in the ground or float over the ground.

3. Active control by hydraulic cylinders: the visor can be controlled during the loading process by pressing the visor down. An extra force is added therefore on top of the visor, this makes it possible to close the gap between the visor and the ground.

The loose hanging visor is described by the method of (ter Meulen, 2018) and will be described in short. The active control by the hydraulic cylinders (also referred to as force mode) is a method which is widely used at dredging companies. This control method is therefore added to the estimation model and is explained afterwards.

Another adjustment on the model described by (ter Meulen, 2018) is based on the type of draghead used. The TSHD studied by Van Oord uses a draghead with two visors (Californian model), which are installed next to each other. The described method use a single visor per draghead. For now, it will be very difficult to analyse the behaviour of two visors next to each other when no 3D models of the bed layer is present. The water depth can be analysed via sensors, but this is only for one location and not precise enough to make a distinction between the behaviour of the visors separately. Therefore, it is chosen to model the two visor of the draghead as one visor model.

Forces analysis

The focus of this section is to describe the different processes and associated forces working on the visor and draghead. The forces are extensively described by the thesis work of G. ter Meulen (ter Meulen, 2018) and this thesis is used as reference to understand the different forces working on the draghead. His work is briefly summarized below and the adjustments to make it a force mode visor are elaborated (F,hydr,visor).
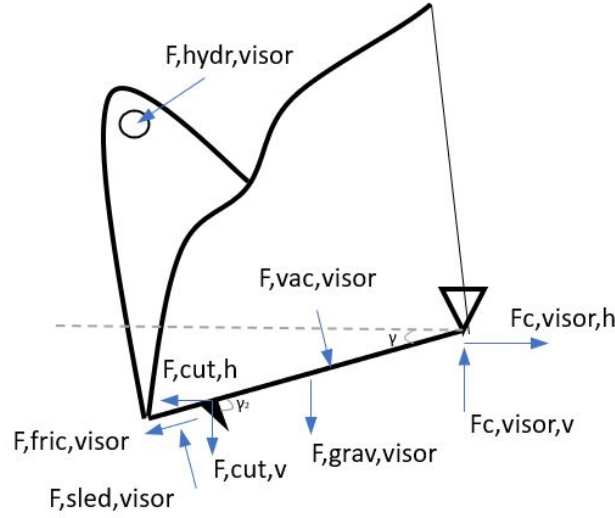

Figure 2.6: Free body diagram visor, source (modified): (ter Meulen, 2018). F,hydr,visor = hydraulic force to push visor down | F,vac,visor = under pressure created by vacuum | F,grav,visor = submerged weight of visor | F,sled,visor = reaction force contact soil | F,fric,sled = friction force contact soil | F,cut = cut force by teeth | Fc,visor = resultant force of all forces in visor

Cutting force [F,cut]: The cutting theory which is used to describe the forces working on the cutting blade is described by Sape Miedema (S. A. Miedema, 2014). His theory describes different cutting forces working on the cutting blade based on soil types. For now, this research only focuses on the cutting of saturated sand. Cutting of other soil types are left out of this study and it is recommended to add the cutting of clay and rock based on the literature of Sape Miedema to this model. A detailed description of this method can be found in the Appendix section A.1.

Vacuum force [F,vac,visor]: the under pressure that is created by the IBP and UWP will suck up the mixture that is formed in the visor. This under pressure will result in a force working on the visor, dependent on the density and velocity of the mixture and the opening of the visor.

$$F_{N,vac} = \xi * \frac{1}{2} * \rho_m * v_m^2 * l_{visor,opening} * w_{in} = \xi * \frac{1}{2} * \rho_m * v_m^2 * A_{suction} \quad (2.10)$$

where:

ρ_m = mixture density $[kg/m^3]$
ξ = resistance factor inlet [-]
v_m = mixture velocity [m/s]
$A_{suction}$ = area of inlet visor $[m^2]$

Gravity force [F,grav,visor]: The self weight of the visor results in a gravity force pushing the visor down. The gravity force cannot be calculated directly, since the visor is working under water. As a consequence the submerged force should be calculated.

$$m_{visor,eff} = m_{visor} - (V_{visor} * \rho_w) \quad (2.11)$$

$$F_{g,visor} = m_{visor,eff} * g \quad (2.12)$$

where:

m_{visor} = mass of the visor [kg]
V_{visor} = volume of inside visor [m^3]
ρ_w = water density [kg/m^3]
g = gravitational acceleration [m/s^2]

Sled and friction force [F,sled,visor and F,fric,visor]: The sled and friction forces are the forces which emerge during the contact of the visor with the bed. The forces are determined based on the soil type, visor dimensions and by the jetting process which is explained in the next section. The visor dimensions determine the area where the soil can push on the visor, the larger this area the larger the sled and friction force become. The friction force is derived from the sled force and the friction coefficient μ, which is dependent on the external friction angle δ between sand and steel.

$$F_{sled,N} = \frac{2 * w_{wearing} * h_{i,sled}^2 * q_{sled} * g}{2 * sin(\gamma)} \tag{2.13}$$

$$F_{friction} = \mu * F_{sled,N} \tag{2.14}$$

$$\mu = tan(\delta) \tag{2.15}$$

where:

$w_{wearing}$ = width wearing piece [m]
$h_{i,sled}$ = layer thickness of the sled layer [m]
q_{sled} = specific soil compaction force [kg/cm^3]
γ = visor angle [deg]
μ = friction coefficient [-]
δ = external friction force [-]

Hydraulic force [F,hydr,visor]: The hydraulic force is an extra force emerging at the upper part of the visor to push the visor down. This force may vary based on the contact with the bed layer and is operated by the dredging captain of the ship. If the desired visor angle is known or assumed based on soil conditions, the hydraulic force can be calculated by using a momentum balance around point C. The forces included in this formulas are explained above, the geometry explanation where the forces emerge on the visor is included in Appendix section A.3.

$$\begin{aligned} M_C = (F_{vac,visor,h} * sin(\gamma) + F_{vac,visor,v} * cos(\gamma)) * l_{vac} - (F_{cut,h} * sin(\gamma) \\ + F_{cut,v} * cos(\gamma)) * l_{cut} + F_{grav,visor} * l_{grav} \\ - (F_{sled,visor,h} * sin(\gamma) + F_{sled,visor,v} * cos(\gamma)) * l_{sled} + F_{hydr,visor} * l_{hydr,visor} = 0 \end{aligned} \tag{2.16}$$

$$\begin{aligned} F_{hydr,visor} = (-(F_{vac,visor,h} * sin(\gamma) + F_{vac,visor,v} * cos(\gamma)) * l_{vac} + (F_{cut,h} * sin(\gamma) \\ - F_{cut,v} * cos(\gamma)) * l_{cut} - F_{grav,visor} * l_{grav} \\ + (F_{sled,visor,h} * sin(\gamma) + F_{sled,visor,v} * cos(\gamma)) * l_{sled})/l_{hydr} \end{aligned} \tag{2.17}$$

Resultant visor force [Fc,visor]: are the vertical and horizontal reaction forces obtained by force balances of the visor.

$$F_{c,visor,v} = F_{vac,v} + F_{g,visor} + F_{cut,v} - F_{sled,v} + F_{fric,visor} + F_{hydr,v} \tag{2.18}$$

$$F_{c,visor,h} = -F_{vac,h} + F_{cut,h} + F_{sled,h} + F_{fric,h} + F_{hydr,h} \tag{2.19}$$

Now the horizontal and vertical resultant forces are calculated, the right side of the draghead can by analysed. The forces working on the visor apply at point C and are included in the force balance of this FBD (Figure 2.7).
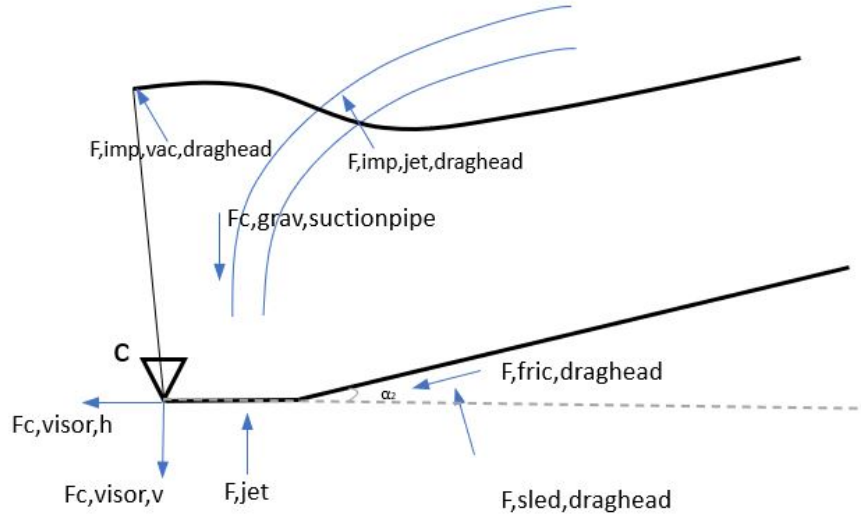

Figure 2.7: Free body diagram draghead, source (modified) (ter Meulen, 2018). Fc,visor = resultant force on visor | F,imp,vac,draghead = impulse force mixture on draghead | F,imp,jet,draghead = impulse force on jet pipe in draghead | Fc,grav,suctionpipe = weight of suction pipe and draghead | F,jet = reaction force jet | F,sled,draghead = reaction force soil on draghead | F,fric,draghead = friction force soil on draghead.

Impulse forces [F,imp,bend,jet and F,imp,bend,vac]: The excavated sand is turned into a sand mixture in the draghead and from there the mixture is accelerated into the direction of the suction pipe. The sand mixture is accelerated from almost standstill to the speed which the mixture reaches before entering the pump. The mixture (sand particles) are not directly transported in the right direction. The bends in the draghead and pipe makes it possible to lead the mixture in the direction of the pumps. These bends experience an impulse force for redirecting the mixture flow. This is also the case for the water moving through the jet pipe.

$$F_{imp,bend,jet} = \rho_w * Q_w * v_w \qquad (2.20)$$

$$F_{imp,bend,vac} = \rho_{mix} * Q_{mix} * v_{mix} \qquad (2.21)$$

where:

Q_w = water discharge [m^3/s]
Q_{mix} = mixture discharge [m^3/s]
v_w = water velocity [m/s]
v_{mix} = mixture velocity [m/s]

Jet force [F,jet]: The jet force emerging in the heel of the draghead is a reaction force of the jet which is penetrated in the ground. The jetting process will be explained in the next section and is based on the literature of Weegenaar and Cees van Rhee (Weegenaar et al., 2015). The jetting force is determined by the in house models of Van Oord based on literature of VOUW.

$$F_{jet} = \rho_w * A_n * u_0^2 * n_n \qquad (2.22)$$

where:

A_n = area of one nozzle [m^2]
n_n = number of nozzles [-]
u_0 = water jet velocity [m/s]

Gravity suction pipe [F,grav,suctionpipe]: the weight of the suction pipe acts on the draghead and results in an extra gravity force pushing downward. The weight of the draghead is also included in this force. Again the submerged weight is used as input, this method is described at the resistance working on the suction pipe.

Sled and friction force [F,sled,draghead and F,fric,draghead]: The heel of the draghead will also makes contact with the bed and results in a sled and friction force. These are estimated with a moment equilibrium around point C. The friction force is again calculated as described at equation Equation 2.14.

$$F_{sled,N,draghead} = -(F_{c,visor,h} + F_{imp,bend,visor,h} + F_{imp,bend,jet,h}) * sin(\alpha_2) +$$
$$(F_{c,draghead,v} - F_{jet} + F_{c,visor,v} - F_{imp,bend,visor,v} - F_{imp,bend,jet,v}) * cos(\alpha_2) \quad (2.23)$$

Resultant of draghead force [Fc,draghead]: are the vertical and horizontal reaction forces obtained by force balances of the draghead.

$$F_{c,draghead,v} = F_{c,visor,v} + F_{fric,draghead,v} + F_{c,grav,suctionpipe,v} - F_{jet}$$
$$- F_{fsled,draghead,v} - F_{imp,vac,draghead,v} - F_{imp,jet,draghead,v} \quad (2.24)$$

$$F_{c,draghead,h} = F_{c,visor,h} + F_{fric,draghead,h} + F_{sled,draghead,h}$$
$$+ F_{imp,vac,draghead,h} + F_{imp,jet,draghead,h} \quad (2.25)$$

2.1.2 Efficiency terms

Due to the different efficiency losses less power is available at the propellers. The efficiency terms can be split up into hydrodynamic efficiency and mechanical losses (Figure 2.8).

$$\eta_{tot} = \eta_g * \eta_t * \eta_o * \eta_r * \eta_h \quad (2.26)$$

Where:

η_g = gearing efficiency
η_t = transmissions efficiency
η_o = open water efficiency
η_r = relative rotative efficiency
η_h = hull efficiency
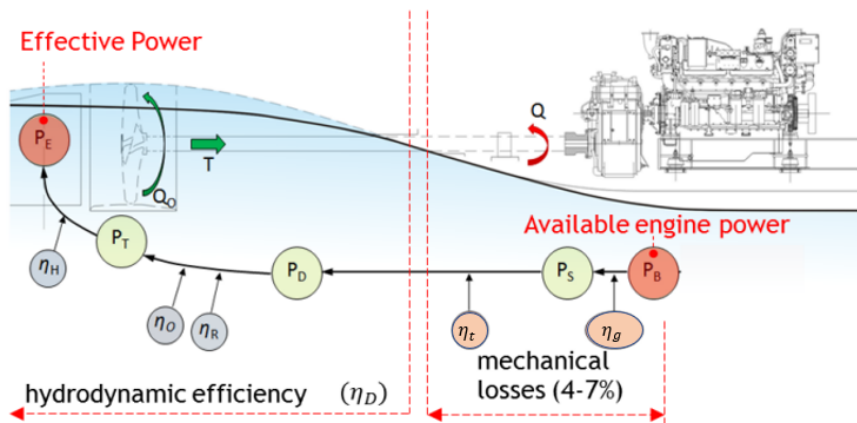
Figure 2.8: Hydrodynamic and mechanical efficiency terms, source (modified):(Simi and RadoDejan, 2013). Definition of the terms are described below.

The mechanical losses are due to transmissions efficiency (η_t) (losses in the shaft) and gearing efficiency (η_g) and lay normally around the (4 - 7 %).
The hydrodynamic efficiency (η_D) exist of the three terms ($\eta_o * \eta_r * \eta_h$). A research based on self-propelled inland waterway vessels has shown that the hydrodynamic efficiency will decrease for operating at a low vertical Froude number, i.e. the ratio of the inertial force divided by gravitational force (Simi and RadoDejan, 2013). This study shows that these efficiency terms are underestimated for low vertical Froude number and should therefore be adjusted for these cases.

Dredging activities operate in this 'lower Froude number area'. During the loading phase the vessel sails at low speed, which will result in a small vertical Froude number ($Fnh = \frac{v}{\sqrt{g*d}}$). The waterdepth is also less in restricted waters, however due to the square root the velocity term has a bigger impact. Figure 2.9 shows two test cases based on inland waterway vessels. The upper line could be used for matching a dredging activity since these are normally not width (and sometimes depth) restricted. When calculating the Froude number for the case study ($Fnh = \frac{3}{\sqrt{9.81*16.5}} \approx 0.02$), it shows that the vessel is operating at a low number. Therefore the lowest observed hydrodynamic efficiency term will be assumed which is 0.45 [-].
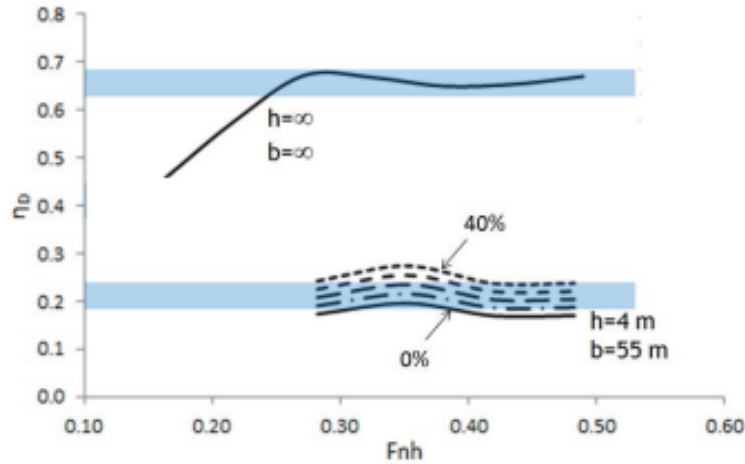
Figure 2.9: The vertical Froude number which determines the hydrodynamic efficiency. In this case it is chosen to use $\eta_D = 0.45$, based on upper line.

2.2 Jet pump

This section elaborates on the energy consumption of the jet pump system. The model to determine the power of the jet pumps is based on Van Oord in house models.

2.2.1 Energy consumption

The energy of the jet pump can be derived from the power of the jet and the active time of the jet (assumed as the loading time) and can be calculated with the familiar formula:

$$E_j = \int P_j dt \tag{2.27}$$

The loading time will be described in section 2.6. The jet power is determined by the jet discharge and the jet pressure of the pump Equation 2.28. The pump will always operate based on the working point of the pump, which is the point of intersection of the pump characteristics and the resistance curve based on the characteristics of the fluid and the pipe.

$$P_j = p_j * Q_j [W] \tag{2.28}$$

p_j = pressure at working point
Q_j = flow at working point

One way to change the power of the pump is by lowering or increasing rpm. Another way is to lower the discharge by squeezing the flow with a smaller nozzle diameter. Changing the nozzle diameter is widely used at TSHD's, as been seen on the HAM318 (Figure 2.10). The working point, which determines the pump pressure just behind the pump, will also change when changing the diameter of the nozzles.

Figure 2.10: Varying jet nozzles diameters of TSHD: HAM 318

In house model literature

The in house model of VO is used to calculate the pressure and the discharge of the jet pumps. This method is based on pump characteristics, resistance characteristics and active revolutions controlled by the dredge captain on board of the ship. The output of the model will show the working point of the pump and the power on which the pump runs. An example of this output is shown in Figure 2.11.
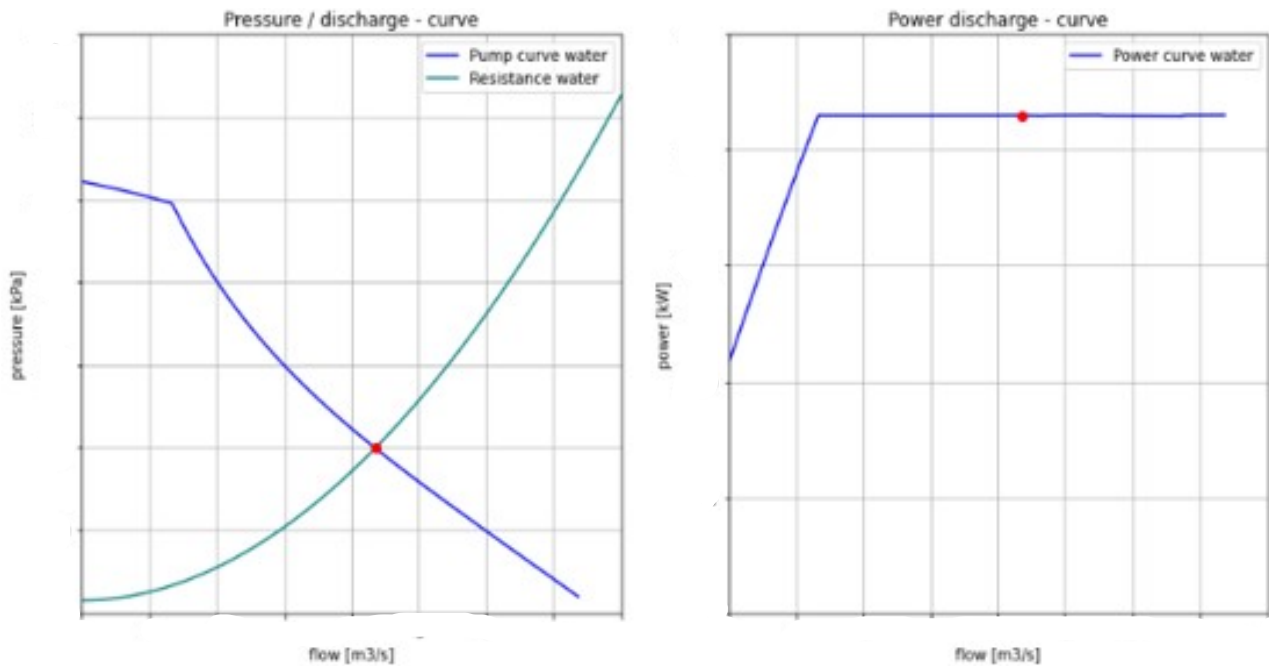
Figure 2.11: Output of in-house pump module of Van Oord. Left: pressure discharge curve, in which the working point of the pump can be recognised. Right: the pump power curve, the red point represents the working point and is used to determine the power consumption of the pump. (**Note: axis confidential**)

2.3 Dredge pump

The energy consumption of the dredge pumps is described in the same in house model, since both pumps are centrifugal pumps. The main difference between both processes is the fluid transportation, the jet pump transports water and the dredge pumps transport a mixture with a higher density. The suction process by the dredge pumps can be described as lifting the sand-mixture (created by the jets and cutting teeth) up from the seabed into the hopper. The mixture that is formed in the draghead is sucked upwards via the suction pipe into the hopper by the dredge pump(s). The dredge pumps are needed to overcome the potential energy and the friction losses that occur in the suction pipe. The pump configuration can exist of one or two pumps per suction pipe. The inboard dredge pump (IBP) is present in every TSHD. In addition to this pump an underwater pump (UWP) can be added between the lower and upper part of the suction pipe. The UWP is located underneath the water level close to the ground and the inboard dredge pumps are located in the vessel.

(a) IBP, centrifugal pump located in a TSHD, source = (RoyalIHC, 2022)

(b) UWP located between upper and lower suction pipe, source = (IADC, 2022)

Figure 2.12: IBP and UWP installed on TSHD

2.3.1 Energy consumption

The energy of the dredge pump can be derived from the power of the two installed dredge pumps and the active time (assumed as the loading time) and can be calculated with the familiar formula:

$$E_{DP} = \int P_{DP} dt [J] \tag{2.29}$$

The calculation of the power of the dredge pumps will be comparable with the jet pumps system. However, some TSHD's make use of an underwater pump which will increase the maximum power of the dredge pumps system.

$$P_{DP} = p_{DP} * Q_{DP} [W] \tag{2.30}$$

p_{DP} = pressure dredge pump at working point
Q_{DP} = flow dredge pump at working point

The pressure of the dredge pump (p_{DP}) is now based on the two dredge pumps installed per suction pipe. The underwater pump (UWP) located in between the upper- and lower pipe and the Inboard dredge pump (IBP). To calculate the new working point based on these two pumps, the manometric head should be added up and used as input to calculate the working point. The discharge flowing through the systems will stay the same.

Pumps which are set in series have in common that the discharge moving through the pumps remains constant. The new manometric head debit curve can be obtained by adding the two manometric pressure curves from the UWP and IBP (VOUB, 2010). This also means that power of the separate pumps can simple add up together. So when analysing the energy consumption of the dredge pumps system the combined power can be used. Figure 2.13 shows an example of the manometric discharge curve by adding two pumps together.
This method should also be applied to the in house model used to calculate the pump characteristics. By creating a new combined dredge pump based on characteristics of the UWP and IBP.
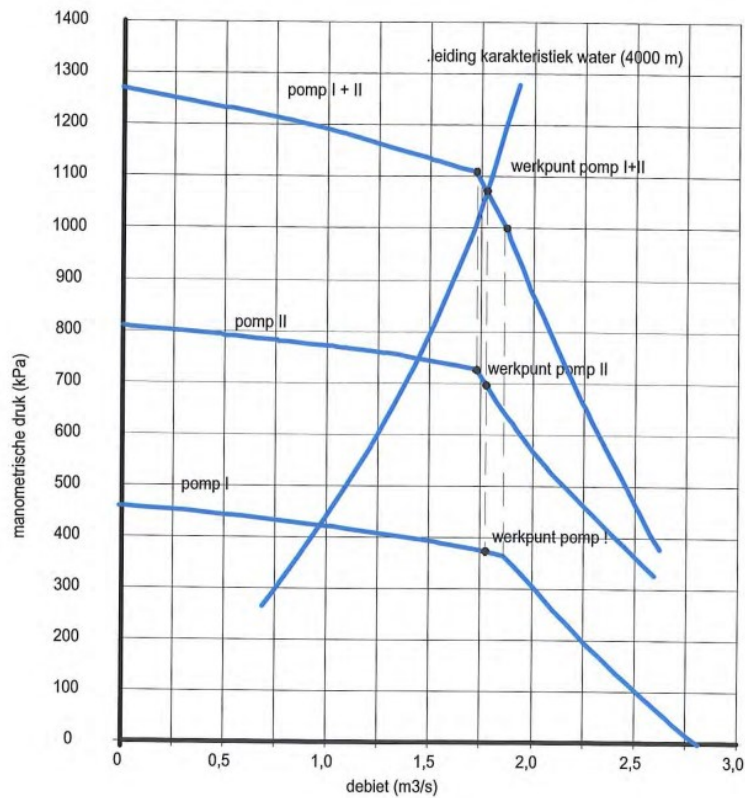
Figure 2.13: Example of two pumps in series, source: (VOUB, 2010). The manometric pressure of the two pumps can be added which results in a new pump curve

Input for in house model

The model will result in two pressure (power) discharge curves. One for the mixture moving through the pump and one for the water moving through the pump. Both will result in different working points. The input for the model is again, the pump and pipeline characteristics, revolutions (RPM) and the density of the mixture. The density of the mixture should be dependent on the situ production calculated at the jetting section.
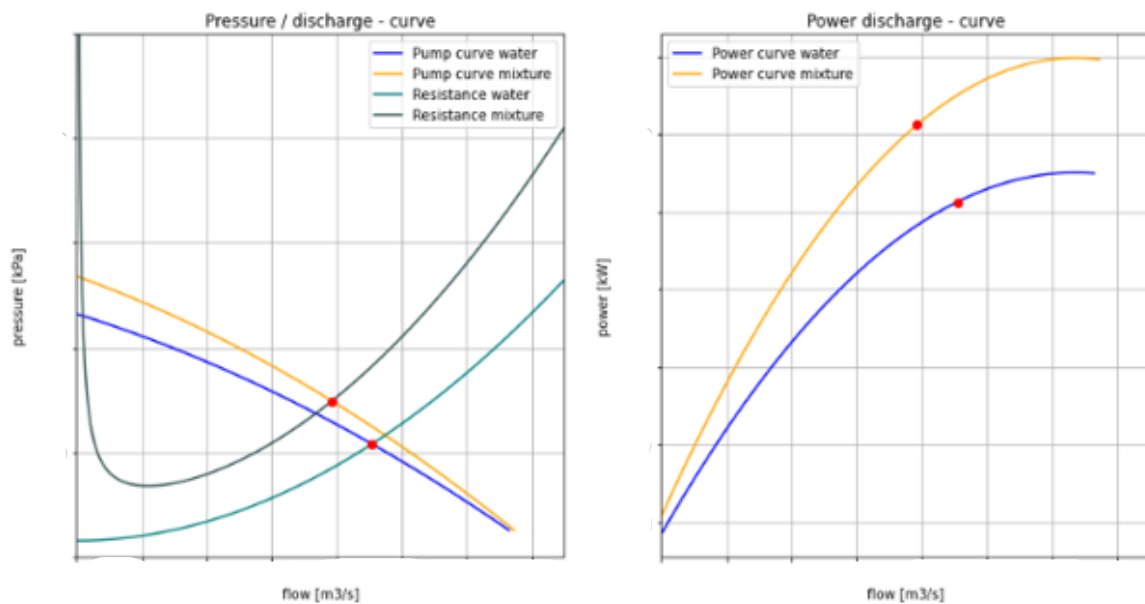
Figure 2.14: Output of the in-house pump module of Van Oord when two pumps are set in series. The blue curve represent water and the orange line represents a mixture. (**Note: axis confidential**)

2.4 Board net

The board net is the energy which is used for all the other non dredging power consumers on board. Marine insight has studied the so called hotel power on board for an inland water way vessel (Marine Insight, 2021b). Figure 2.15 gives an overview of the components included for this type of vessel and can be used as first approximation of the board net. This factor will deviate a bit for dredging vessels.

For this research the current Van Oord model is used as input for the model. The ratio of the maximum board net and the total installed power is calculated. This ratio can than be used to calculate the board net power for a particular TSHD.

Device	# inst.	# in use	MRP (kW)	Pinst (kW)	Sailing			Manoeuvring			Harbour		
					LF	UF	kW	LF	UF	kW	LF	UF	kW
Steering gear	2	1	24	27	0.8	0.8	17	0.8	0.8	17	0.8	0	0
Windlass	1	1	37	41	0.8	0	0	0.8	0.7	23	0.8	0	0
Baggage crane	2	1	14	16	0.8	0	0	0.8	0	0	0.8	0.6	7.5
Mooring winch	2	1	20	22	0.8	0	0	0.8	0.7	12	0.8	0	0
ER-crane	1	1	4	5	0.8	0.1	0.4	0.8	0	0	0.8	0.2	0.8
Provision davit	2	2	5	6	0.8	0.1	0.9	0.8	0.1	0.9	0.8	0.5	4.7
Galley equipmt	1	1	489	544	0.8	0.2	87	0.8	0.2	87	0.8	0.1	44
Laundry equipmt	1	1	85	95	0.8	0.2	15	0.8	0.2	15	0.8	0	0
Ventilation	1	1	110	122	0.8	0.8	78	0.8	0.8	78	0.8	0.4	39
Side thruster	2	1	250	280	0.8	0	0	0.8	0.7	289	0.8	0	0
Incinerator	1	1	14	17	0.8	0.2	2.6	0.8	0.2	2.6	0.8	0	0
Workshop	1	1	10	11	0.8	0.2	1.8	0.8	0.2	1.8	0.8	0.2	1.8
Welding equipmt	1	1	32	36	0.8	0.1	2.8	0.8	0.1	2.8	0.8	0.1	2.8
Starting air compr.	2	2	9	10	0.8	0.2	3.1	0.8	0.3	4.9	0.8	0.3	4.9
Control air compr.	1	1	3	4	0.8	0.4	1.1	0.8	0.4	1.1	0.8	0.3	1.1
Air drier	1	1	0.3	0.4	0.8	0.4	0.1	0.8	0.4	0.1	0.8	0.3	0.1
Total							**210**			**535**			**107**

Figure 2.15: Board net power for an Inland Waterway vessel, source: (Marine Insight, 2021b)

2.5 Bow thrusters

The bow thrusters are propellers which are installed on the front part of the ship (bow) and are used as extra manoeuvre medium to better sail at low speeds. These are primarily used during turning, moving in coastal waters or leaving a port facility (Marine Insight, 2021a). These bow thrusters are therefore especially used during the loading phase of a dredging cycle.

Compared to the other energy consumers on board it is assumed that the bow thrusters still contribute very little to the total energy consumption. The maximum power of the bow thrusters is bigger than for example the board net, but the limited time these bow thrusters are active during the loading phase, ensure that they have a small contribution to the energy consumption.

For this reason it is decided that the energy consumption will still be based on the actual data analysis. The duration these bow thrusters are active will be estimated based on the actual data even as the power which is used.
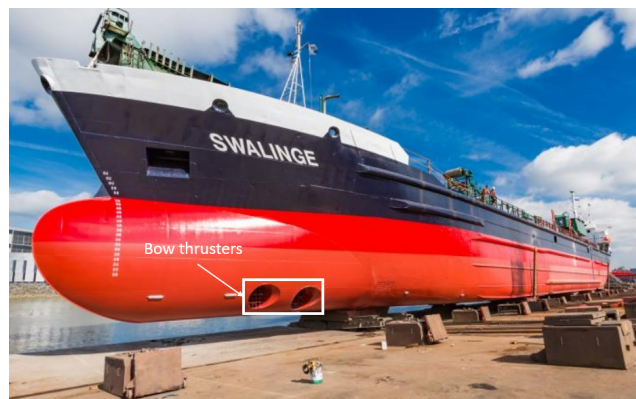
Figure 2.16: Bow thrusters installed on TSHD, source (modified): (DredgingToday, 2022)

2.6 Loading duration

The loading duration is the process of filling the hopper until a chosen hopper density. The loading duration of the dredging cycle can be split up into two parts. First the loading until overflow, followed by the non-linear process which is used to increase the density of the mixture in the hopper. This process is visualized with Figure 3.3, where the red parts shows the linear filling process and the purple part the settling process within the hopper.
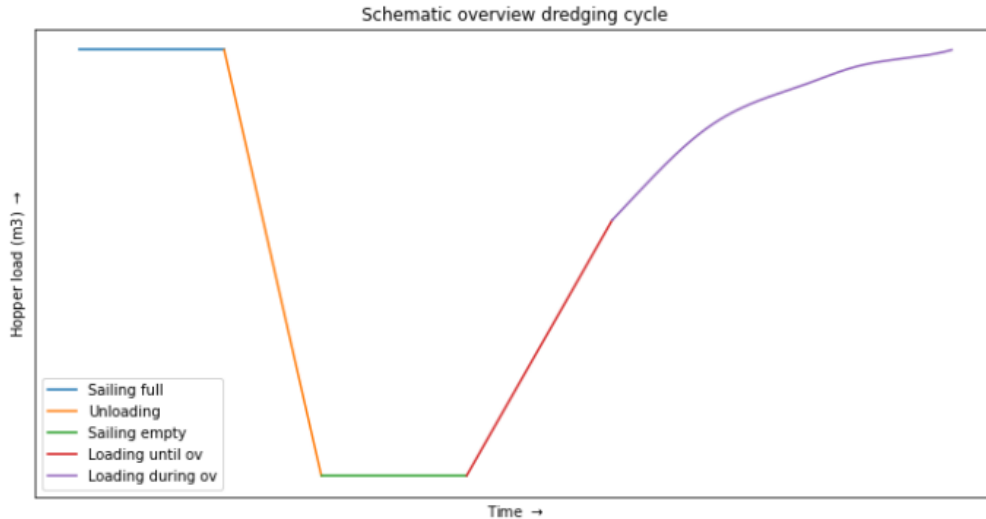

Figure 2.17: Schematic overview dredging cycle, the loading phase is represented by the red and purple line. Red line shows the linear loading curve and the purple shows the overflowing process.

At the start of the loading process the hopper is already filled with some water. The mixture is discharged into the hopper by the dredge pumps until it reaches the dredging mark, to this point the process is linear. The time it takes to reach this point is based on the excavation and suction production. The second part of the loading process is the settling process. The settling process determines the time for filling the hopper to a certain density and plays therefore an important role in the determination of the total loading time.

As the filling process of the hopper moves on, the water included in the mixture will be on top of the bed layer due to the difference in density, the sand (other soil type) will settle down and will form a bed. The water should be discharged out of the hopper to make more place for the material. New mixture can then be added to the hopper to increase the density of the material in the hopper. This process is controlled by the overflow system which can be designed in two ways. The overflow system can be put in a fixed position (a fixed allowed draught). The ship is loaded until it reaches its dredge mark after which the suction process is stopped. This method is called Constant Volume System (CVS). The overflow system can also be adjustable, this gives the captain the opportunity to lower the overflow to remove excessive water in the hopper. New sand-mixture can then be sucked up and which will increase the amount of sand in the hopper, this process will be repeated a couple of times until the total weight of the hopper remains constant. This method is therefore called Constant Tonnage System (CTS).
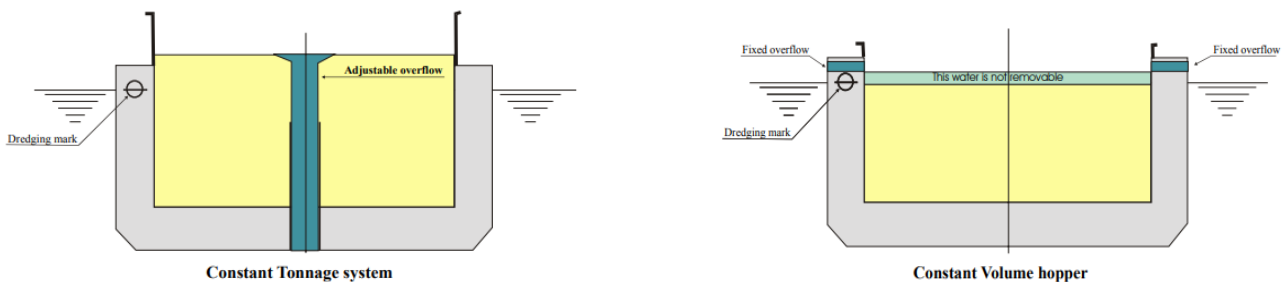
Figure 2.18: Two different hopper filling systems possible at a TSHD

Most modern TSHD's are designed with the CTS system. To minimize the mixture overflow (water + sand) the overflow system should be used that is far away from the loading system. This non-linear loading process is controlled by the captain of the ship and the mixture is distributed evenly over the hopper by T-shaped pipes. It depends on the soil type if the overflow system is used or not. In plastic soils as clay there is no settling process and overflow is often not allowed due to environmental policies, in this case the overflow is put in top position. In settling soils as sand the overflow is used to increase the hopper load.

The settling process elaborates on the time it takes for filling the total hopper and is the key element to estimate the time of the loading process. If the overflow is not used it is easy to calculate the duration to fill the total hopper since it is a linear process. If the overflow is used it gets more difficult to estimate settling time of the particles. Different models exist to describe the settling processes in the hopper, these will be elaborated in the next section.

2.6.1 Loading until overflow

The time to load until overflow is dependent on the hopper capacity and the suction production. The suction production is the sum of the excavation production and the created vacuum by the pumps. For this study it is assumed that enough vacuum is available to suck up the total excavation production. The studied TSHD makes use of an underwater pump and an inboard dredge pump, which will most likely result in a high enough vacuum to suck up all the excavated soil in low water depth situations.

Excavation production

A detailed explanation of the jetting process can be found in Appendix section A.2. This section elaborates on the formulas to describe the excavation production, which exists of the sum of the jet, cut and erosion production (Equation 2.31).

$$Q_{excavation} = Q_{jet} + Q_{cut} + Q_{erosion}[m^3/s] \tag{2.31}$$

Jet production

The jet production is the amount of loosened situ soil plus the jet water injected in the soil. The jet production can be derived from the Mass flux calculation done by Vlasblom (Vlasblom, 2003) and some soil characteristics as the porosity and the grain density. The description in formulas is as follows:

$$Q_{jet} = Q_{sand} + Q_{water} + Q_{jet,water} \tag{2.32}$$

$$Q_{water} = \frac{Q_{sand}}{(1 - n_0)} * n_0 \tag{2.33}$$

$$Q_{sand} = \frac{M_s}{\rho_s} \tag{2.34}$$

Where:

n = porosity of the soil [-]
M_s = Mass flux [kg/s]
ρ_s = grain density $[kg/m^3]$

The foundation to determine the mass flux of eroded sand (in situ sand) is laid by Vlasblom. This method is based on the momentum of the jet times a non-dimensionless empirical parameter α. It is not entirely clear how this empirical parameter is defined by Vlasblom, but the most plausible is that he defined it based on field data. The jet production of the eroded sand, referred to as mass flux [kg/s] by Vlasblom, is defined as:

$$M_s = \alpha * I = \alpha * \rho_w * Q_j * u_0 = \alpha * \rho_w * Q_j * \sqrt{\frac{2 * p_j}{\rho_w}}[kg/s] \tag{2.35}$$

Where:

α = empirical parameter by vlasblom [-]
p_j = jet pressure at working point [kpa]
Q_j = jet discharge at working point $[m^3/s]$

A typical value for α is 0.1, this method does not consider different soil characteristics and is based on a constant trailing velocity. However, it has turned out that the trailing speed has a major impact on the Mass flux and that is why van Rhee rewrote the mass flux definition into the penetration depth of the jet. The derivation of van Rhee can be described as follows (van Rhee, 2017):

$$M_s = \rho_s * (1 - n_0) * h_{i,jet} * w_c * v_t * n_n [kg/s] \tag{2.36}$$

Where:

$h_{i,jet}$ = jet layer thickness [m]
w_c = cavity width [m]
v_t = trailing speed [m/s]
n_n = number of nozzles [-]

Mass flux is converted into a density term $(\rho_s * (1 * n_0))$ and a volume term $(h_{i,jet} * w_c * v_t)$. By rewriting this equation and by using the mass flux definition of Vlasblom it is possible to calculate the penetration depth and to see how the visor makes contact with the ground.

$$h_{i,jet} = \frac{M_s}{\rho_s * (1 - n_0) * w_c * v_t * n_n} [m] \tag{2.37}$$

The penetration depth can be divided into soil-, draghead- and operational parameters. The cavity width is the only unknown left and can be approximated in multiple ways:

- $w_c = D_n$, cavity width equal to the nozzle diameter. This is the case for cohesive soils as clay layers

- $w_c = h_{i,jet}$, now the cavity width is based on the trailing velocity, nozzle diameter, jet pressure and soil characteristics (empirical value).

- $w_c = h_{i,jet} * \alpha$, the penetration depth times a length/width ratio (α). It has turned out that α is almost equal to the trailing velocity. However it is found that this is not the case for all trailing velocities and this statement should be analysed further.

The maximum cavity width can be obtained by dividing the visor width by the number of nozzles ($w_{c,max} = \frac{w}{n_n}$). If the cavity width become larger than maximum cavity width, the scour holes will overlap each other (see Figure 2.19). This larger cavity width will not contribute to a higher production since there is no extra sand to fluidize. Therefore an upper limit for the cavity width should be apprehended, which is expressed as follows:

$$w_c = \begin{cases} h_{i,jet} \text{ if } h_{i,jet} < w_{c,max} \\ w_{c,max} \text{ if } h_{i,jet} > w_{c,max} \end{cases} \tag{2.38}$$

This means that at low trailing velocities there will be a maximum jet production, due to the cavity width limitation. The production is underestimated at low trailing velocities (< 1 m/s) and overestimated at higher velocities (> 1 m/s). The optimum trailing velocity for jetting is found when the cavity width equals the optimal cavity width ($w_c = w/n_n$), at velocities higher than this maximum the production and jet mixture are set constant. At velocities below the optimum, the density increased steadily when the velocity is increased.
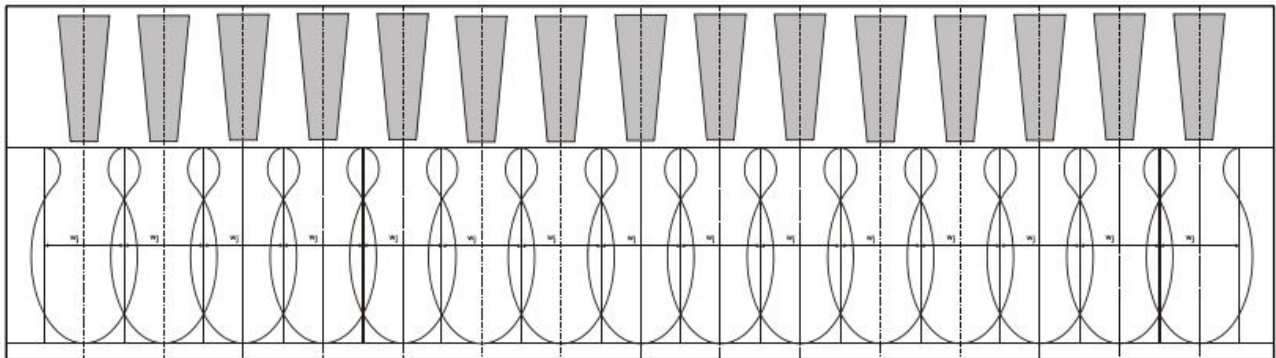
Figure 2.19: Overlapping scour holes. This overlap will not contribute to a higher production, source: (S. Miedema, 2019)

Cut production

The cutting production is described by the loosened soil production by the cutting teeth (de Jonge, 2017). This production is dependent on the jetting process and trailing speed as described in previous paragraph. The maximum volume that can be cut by the cutting teeth is dependent on the width of the teeth, the cutting layer thickness and the trailing speed. The following formula can be used to describe the cutting production:

$$P_{cut} = w * h_{i,cut} * v_t \tag{2.39}$$

where:

w = draghead width [m]
$h_{i,cut}$ = cutting layer thickness (defined at jetting process) [m]
v_t = trailing speed [m/s]

Erosion production

The last term to estimate the excavation production is the erosion production. There will always be a supply of ambient water within the visor, since the gap between the visor and the ground will not always be fully closed. The pressure difference within the draghead created by the dredge pumps will suck extra water/sand into the draghead. However, it is almost impossible to estimate the supply of ambient water in the visor. Therefore it is chosen to neglect the supply of ambient water to the excavation production. It is recommended to study the quantity of the erosion term for later research.

2.6.2 Settling process

The duration of this settling process can be calculated in different ways. A predefined loading curve can be used, but it is even more accurate to describe this process by a model. Different models are available to describe the loading process like analytical models (de Groot, 1981) and numerical methods based on the Camp model. Cees van Rhee developed the 1DV model which is a one-dimensional model, but in contrast with the other one-dimensional models this one is used in vertical direction (Van Rhee, 2002). A 2DV model was also derived by Cees van Rhee, which look at the two dimensional array of the hopper. Sape Miedema made some adjustments to the Camp model. The modified model of Miedema gives results that match the method of van Rhee, with a higher speed of calculation (S. Miedema, 2008).

For now, it is chosen to represent the settling phase based on the loading curve estimations due to a lack of time. Non of the described models will be used in this research. Is is recommended for later research to include a loading model and it is especially recommended to study the improved method of the Camp model by S. Miedema, since this model has higher speed of calculation.

2.7 Simulation tool

To bring all energy consumer together to estimate the energy consumption of the total loading phase a tool is needed. This section provides a background on the simulation package, OpenCLSim, which has been utilized in prior research. As the current study builds upon these previous works, OpenCLSim will be employed in this thesis as well.

OpenCLSim is a Python package for discrete event simulation of logistics systems (van Koningsveld, 2019). It provides a framework for modeling and simulating logistics systems, including container terminals, ports, and transportation networks. The package is built on top of the SimPy library, which is a popular simulation library for Python. OpenCLSim allows users to define logistics objects such as cranes, vehicles, and shipping containers, and to simulate the interactions between these objects as they move through the logistics system. This can be useful for analyzing and optimizing logistics operations, and for testing the impact of different scenarios and policies on logistics performance. The dredging cycle can be seen as a discrete event, since it can be split up into the four different stages. This makes it suitable to be simulated by the OpenCLSim python package. Within these discrete events there are continues events which should be simulated as discrete events to be able to use this software. Section 4 will elaborate how this simulation tool can be used to simulate the energy consumption of the loading phase.

A plugin in the OpenCLSim Python package is a way to extend the functionality of the package and add new features or capabilities. Plugins are separate Python modules that can be imported and used in a simulation, and they allow users to customize or enhance the behavior of the simulation objects. There are several types of plugins that can be used in OpenCLSim, for this study it is chosen to create a plugin where power function are included. By using these functions in combination with the described excavation production (time indicator) it is possible to calculate energy.

2.8   Summary: Literature

The literature section presents the answer to the sub-research question:

Which methods are available to quantify the energy consumption during the loading phase based on physics?

There are five main energy consumers on board of a TSHD. The energy consumption will be calculated by multiplying the estimated power with the estimated time that the consumer is active (Equation 2.40). The different power terms are either approached by studied literature, in-house Van Oord methods or are based on empirical values and are described below per energy consumer.

$$E = \int P dt \tag{2.40}$$

Propulsion system
The propulsion power is calculated by analysing the resistance terms on the vessel, suction pipe and draghead. These resistance terms are estimated by analysing all separate forces working on the different components via free body diagrams. The propulsion power can be calculated by multiplying the resistance terms with the trailing velocity and efficiency terms. The developed method should be validated with a case study to check the reliability of the estimation.

$$P_{prop} = (R_{vessel} + R_{suction-pipe} + R_{draghead}) * v_{trail} * \frac{1}{\eta_{tot}} \tag{2.41}$$

Dredge pumps
In order to estimate the required power for the dredge pumps, an in-house Van Oord model will be used. The TSHD under investigation is equipped with an underwater pump and an inboard dredge pump, which are installed in series. To simplify the analysis, the consumed power of both pumps will be treated as a single pump.

Jet pumps
The required power for the jet pumps will be estimated using an in-house Van Oord model. A crucial parameter in calculating the jet pump power is the jet discharge. This parameter can either be assumed on pump characteristics or more precisely from the actual sensor data of the vessel.

Board net
The board net power is the power which is consumed on board of the vessel for daily use. Think of power which is consumed by the crew, taking a shower etc. The board net power consumption is based on the current assumption of Van Oord. Different tables exist to estimate the board net power on an IWT vessel. The approach of Van Oord matches the tables, but will probably give a more accurate estimate for now.

Bow thrusters
In order to estimate the energy consumption of the bow thrusters, data analysis is used. The power and active time of the bow thrusters during the loading and unloading phases are analyzed, and this information is used to calculate the energy consumption. The active time will be included as percentage of the total loading duration.

Loading duration
The loading duration will be based on the excavation production and the the hopper capacity. For now, only loading until overflow will be estimated which is represented by a linear curve. The settling process is recommended for later study.

The different methods will be brought together in an plugin for the OpenCLSim python package. This plugin will be run during a dredging process and will make it possible to estimate the energy consumption during a dredging cycle. The OpenCLSim software will then enable to simulate the energy consumption of dredging process based on operational parameters. The energy consumption can thereafter easily be transferred into fuel, emissions and costs.

3 | Propulsion model

To simulate the total energy consumption during the loading phase of a dredging cycle a physics based model is needed to describe the energy consumption of the propulsion system. This model can then be added to the other energy estimation methods to calculate the energy consumption for the total dredging cycle. This brings the thesis to the second research question:

How to develop and calibrate a physics-based energy estimation model with a real case study?

To answer this sub-research question, the materials and methods to form a propulsion model are described. Thereafter the results of the model are shown whereafter these results are discussed. Finally, a conclusion is made which answers this sub-research question.

3.1 Materials and method

The following generic Experiment Plan to develop the propulsion model is defined and is represented in Figure 3.1. It exists of the following steps:

- ■ EST: defining a semi-empirical physic based model
- ■ ACT: selecting measured data that can be used to calibrate the model
- ■ Calibration: evaluation of the set boundaries for which the model is assumed valid
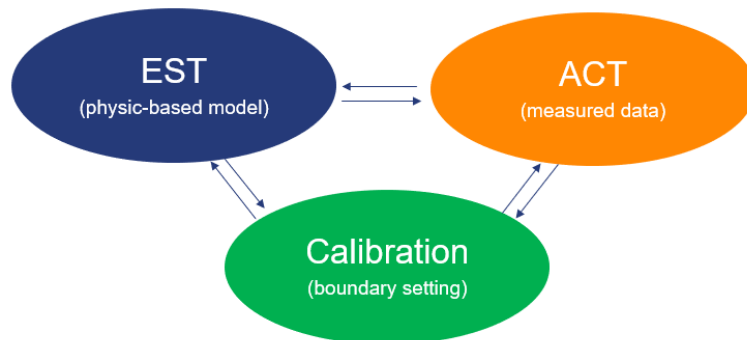
Figure 3.1: Generic experiment plan on calibration of the power calculation of the propulsion system. EST represent the estimation model to calculate the power consumption. ACT represent the analysis of the data and calibration represent the testing of EST based on ACT and set boundaries

The structure of the Materials and Method section will follow the generic Experiment Plan. Starting with the section of developing the physics-based model (EST) for the propulsion system. The section focuses on the model development based on the literature study. It gives an overview of the stationary input parameters and shows the limitations of the model.

The Actual Data section (ACT) explains the method used to analyse the measured data from a case study for which the estimation model will be calibrated. It starts with the description of the case study itself to understand the context of the case study. Thereafter filters/selection procedure have been described to obtain project input parameters (data) for the estimation model and to eventually calibrate the estimation model.

The calibration section (calibration) compares the propulsion power output of the estimation model with the "filtered" actual data. It defines the set boundary conditions on which the estimation model is valid to be included in the simulation tool and if not which steps should be taken to improve the estimation model and/or measured data.

3.1.1 Estimation model

This section describes the model to estimate the power consumption of the propulsion system during the loading phase of the dredging process. The section includes three main subsections: Physics (formulas), Boundary Conditions and Stationary parameters.

The Literature summary summarizes the estimation method (physics) described in the literature study, a detailed explanation can be found in the literature study. The Boundary Conditions section explains the conditions under which the model is valid. The stationary Parameters section describes the constant values which are used in the estimation method, these are parameters that are based on literature values and vessel characteristics. This section also describes how a sensitivity study could be performed to understand the effect of parameter variation on the estimation results.
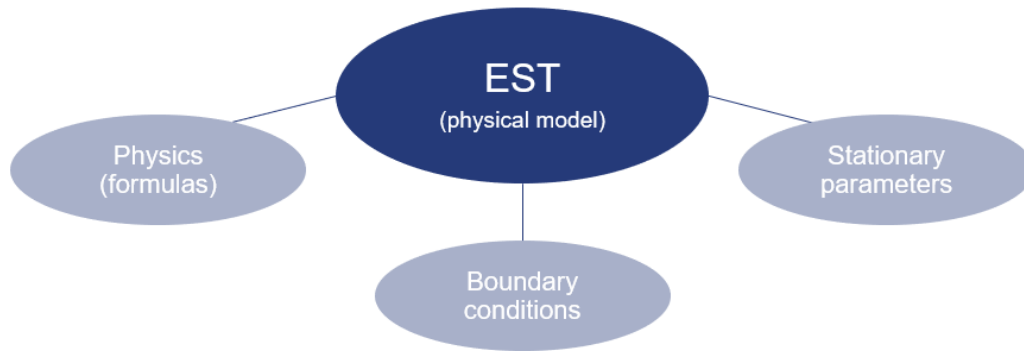
Figure 3.2: Overview of estimation method subsections

Physics (formulas)

The physics behind the estimation model is described in the literature section section 2.1. To summarize, the propulsion power is calculated by the following formula:

$$P_{prop} = R_{tot} * v_{trail} * \frac{1}{\eta_{hydr} * \eta_{mech}} \tag{3.1}$$

Where:

R_{tot} = Total horizontal resistance [kN]
v_{trail} = Trail speed of vessel [m/s]
η_{mech} = Hydrodynamic efficiency = 0.94 [-]
η_{hydr} = Mechanical efficiency = 0.45 [-]

The total resistance force exists of all resistance factors working on the draghead, suction pipe and vessel (Equation 3.1). The method to calculate these resistance forces have been described in the literature section (section section 2.1).
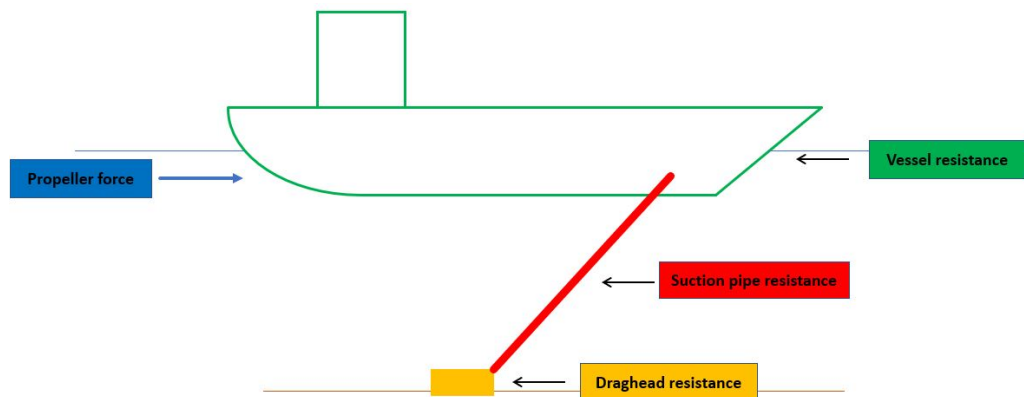
Figure 3.3: Schematic overview of the forces during dredging, the propulsion force should overcome the three resistance terms.

Boundary conditions

The boundary conditions refer to the constraints or limitations for the use of the estimation model and the input parameters which are held constant during the calibration of the model. The methods described to estimate the propulsion power are based on resistance forces working on the vessel, the suction pipe and the draghead. For now the estimation model will be calibrated for all resistance terms, this means that the draghead should stay on the ground, contact with the bed should be made and the suction pipe angles remain constant. The resistance factors are analysed in two dimensions only(x and z plane), this means that the vessel should dredge in one constant line. The resistance working on the vessel during turning is therefore excluded. The trailing velocity input does not consider environmental conditions as trailing speeds and waves. This can cause the model to under/over-estimate the needed power to sail on a particular speed. If the vessel is moving with the current less power is needed to reach a certain velocity and more power is needed when it is moving against a current. The Model also includes soil conditions as the permeability and porosity of the soil. During dredging these values are not exactly known. At most, only a few samples have been taken before the dredging works start. These soil conditions are now set based on a saturated sand soil and are the input for the cutting model of Sape Miedema. Other soil types are excluded for this research and it is recommended to add these methods later on.

- The Draghead will remain on the bed
- Water will be stationary with respect to the bed (Currents and other environmental conditions are excluded)
- The loading will be along a straight line (turning etc. excluded)
- Only saturated sand soils will be dredged
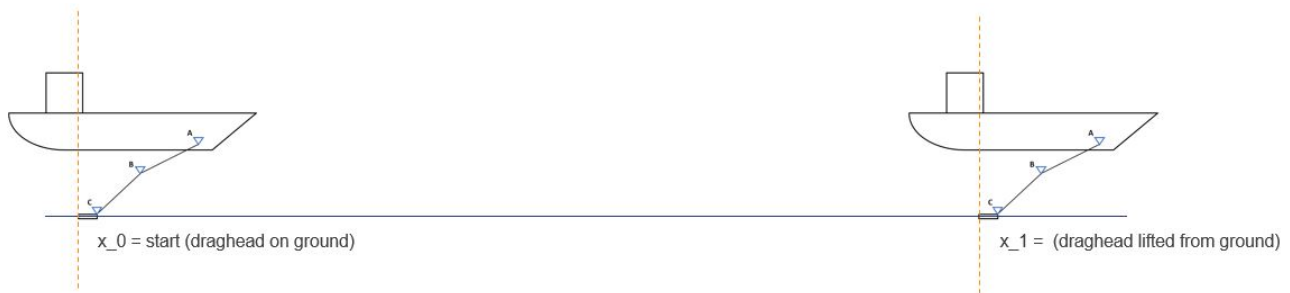
Figure 3.4: Visualization EST model boundary conditions

Stationary parameters

The stationary parameters refer to values or variables that are set constant during the calibration of the estimation method. These parameters are determined prior to the data analysis and are based on drawings of the TSHD and the literature study. It has been assumed that during the project these parameters remain constant and they provide a baseline for the comparison with the data analysis. These parameters are therefore seen as part of the total physical estimation method and will be held constant during the calibration of the model.

In reality, certain parameters may vary from one project to another or even during a project, such as soil conditions (permeability and porosity). As these precise conditions are not always known for different projects, they are currently held constant based on a literature study (S. A. Miedema, 2014). Other parameters (Table 3.6) that can be obtained via project analysis will be treated in the actual data analysis.

The following tables will give an overview of all input parameters with the indication where the parameter value is based on. Some parameters are not valuated, since these are dependent on project characteristics and operational conditions (project data), which are analysed in section Figure 3.1.2.

Parameter	Definition	Value	Unit	Assumed
γ	Visor angle	-	deg	Sensor data
l_{visor}	Length visor	1.5	m	Dummy
l_{vac}	Length point C to F_{vac}	1.0	m	Dummy
l_{grav}	Length point C to F_{grav}	1.0	m	Dummy
l_{cut}	Length point C to F_{cut}	1.3	m	Dummy
l_{sled}	Length point C to F_{cut}	1.5	m	Dummy
l_{hydr}	Length point C to F_{hydr}	1.5	m	Dummy
L_b	Length cutting teeth	0.2	m	Dummy
w_{teeth}	Width cutting teeth	0.3	m	Dummy
n_{teeth}	Number cutting teeth	40	m	Dummy
m_{visor}	Mass of visor	9000	kg	Dummy
V_{visor}	Volume of visor	0.40	m^3	Dummy
$l_{visor,op}$	Length visor opening	1.5	m	Dummy
w_{in}	Width visor opening	5.8	m	Dummy
$w_{wearing}$	Width wearing part visor	0.2	m	Dummy
B_{visor}	Width of single visor	3.0	m	Dummy
γ_2	Cutting teeth angle	45	deg	Literature
β_{shear}	Shear angle	20	deg	Literature
δ	Soil/steel interface friction angle	27	deg	Literature
ϕ	Internal friction angle	42	deg	Literature

Table 3.1: Stationary parameters for Visor input (**Note: Dummy values have been used due to confidentiality.**)

Parameter	Definition	Value	Unit	Assumed
L	Length of vessel	240	m	Dummy
L_{wl}	Length of vessel at waterline	170	m	Dummy
B	Width of vessel	35	m	Dummy
T	Draught of vessel	15	m	Dummy
x_{pipe}	Number of suction pipes	2	-	Dummy
x_{screw}	Number of propellers	2	-	Dummy
BB	Bulbous bow [yes or no]	yes	-	Dummy
C_b	Block coefficient	0.85	-	Literature
$(1 + k_2)$	Appendage resistance factor	2.5	-	Literature
η_0	Efficiency term	0.65	-	Literature
η_r	Efficiency term	0.98	-	Literature
η_t	Efficiency term	0.98	-	Literature
η_g	Efficiency term	0.96	-	Literature

Table 3.2: Stationary parameters for Vessel input (**Note: Dummy values have been used due to confidentiality**)

Parameter	Definition	Value	Unit	Assumed
$Q_{j,wp}$	Jet discharge at working point	-	m^3/s	Sensor data
D_j	Jet pipe diameter	0.80	m	Dummy
$\beta_{bend,jet}$	Bend of the jet pipe	45	deg	Dummy
D_n	Nozzle Diameter	0.060	m	Dummy
n_n	Number of nozzles	28	-	Dummy
c_d	Contraction coefficient jet	0.85	-	Literature

Table 3.3: Stationary parameters for Jet input (**Note: Dummy values have been used due to confidentiality**)

Parameter	Definition	Value	Unit	Assumed
α_1	Upper pipe angle	-	deg	Sensor data
α_2	Lower pipe angle	-	deg	Sensor data
β_1	Upper pipe cable angle	-	deg	Sensor data
β_2	Upper pipe cable angle	-	deg	Sensor data
L_1	Upper pipe length	45	m	Dummy
L_2	Lower pipe length	36	m	Dummy
$D_{pipe,out,upp}$	Outer diameter of upper pipe	1.4	m	Dummy
$D_{pipe,out,low}$	Outer diameter of lower pipe	1.4	m	Dummy
$c_{d,pipe}$	Drag coefficient pipe	0.9	-	Literature

Table 3.4: Stationary parameters for Suction pipe input (**Note: Dummy values have been used due to confidentiality**)

Parameter	Definition	Value	Unit	Assumed
z	Water depth	-	m	Sensor data
n_i	initial porosity soil	0.44	-	Literature
n_{max}	Porosity soil on cutting teeth	0.50	-	Literature
k_i	Initial permeability soil	5e-5	-	Literature
k_{max}	Maximum porosity soil on cutting teeth	4.5e-4	-	Literature
q_{soil}	Soil compaction force	6	kg/cm^3	Literature
α	Vlasblom coefficient Mass flux	0.1	-	Literature
g	Gravitational acceleration	9.81	m/s^2	Literature
ρ_w	Density of water	1025	kg/m^3	Literature
ρ_s	Density of soil particle	2600	kg/m^3	Literature
μ	Viscosity water	0.000001	-	Literature

Table 3.5: Stationary parameters for Project input

Parameter	Definition	Value	Unit	Assumed
α_1	Upper pipe angle	-	deg	Sensor data
α_2	Lower pipe angle	-	deg	Sensor data
β_1	Upper pipe cable angle	-	deg	Sensor data
β_2	Upper pipe cable angle	-	deg	Sensor data
z	Water depth	-	m	Sensor data
$Q_{j,wp}$	Jet discharge at working point	-	m^3/s	Sensor data
γ	Visor angle	-	deg	Sensor data
v_t	Trailing speed	-	kn	Sensor data

Table 3.6: Parameters based on actual data analysis, these will be analysed in the next section

To study the effect on the output of the model when these parameters are modified, a sensitivity study has been applied. A parameter sensitivity study is a method used to understand how the output of a model or system is affected by changes in its input parameters. The goal of a sensitivity analysis is to identify which parameters have the greatest impact on the output of the model, and to understand the range of values over which the model's behavior is most sensitive (Saltelli et al., 2008).

The results of the sensitivity analysis will be visualized by a sensitivity plot, which shows the relationship between the input parameters and the output of the model or system. The input parameters are plotted on the x-axis and the output of the model will be plotted on the y-axis. The sensitivity of the output to each input parameter is then represented by a curve on the plot. If the output of the model or system is highly sensitive to changes in a particular input parameter, the curve for that parameter will be steep, indicating that even small changes in the input parameter can have a large impact on the output. On the other hand, if the output is less sensitive to changes in the input parameter, the curve will be shallower, indicating that larger changes in the input parameter are needed to affect the output.

The parameters of the starting point of the analysis are called the 'base case' parameters, summarized in the stationary parameter tables. It is chosen to variate the base case parameter with a standard deviation of [-20, 20]. with steps of 10%. An example of the visualization is shown in Figure 3.5. The figure shows that parameter 2 is the most sensitive parameter, represented by the steep curve.
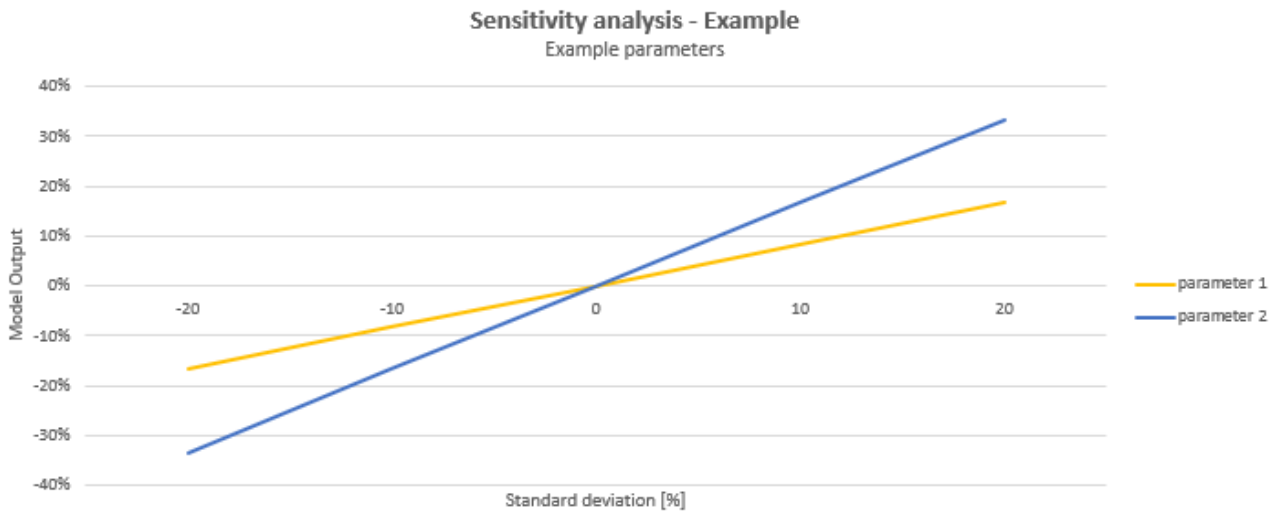
Figure 3.5: Example of sensitivity analysis result, the model output is represented on the y-axis and the parameter variation is shown on the x-axis by standard deviation. A steeper slope indicates a higher sensitivity

3.1.2 Actual data

This section presents the actual data analysis which has been done to obtain the non-stationary (project) input parameters for the estimation model and to create a dataset for which the estimation model can be calibrated. The section is divided into several sub-sections, each focusing on a different aspect of the data. The first sub-section is the Raw sensor data. This is where the data of the case study is described and background information of the case study is provided to understand the context of the data. The next sub-section is about filtering the data. This is where the process of cleaning and pre-processing the data is described. This includes removing outliers, dealing with missing data, and performing any other necessary data cleaning steps. This sub-section is important for ensuring that the data is accurate and reliable for the calibration of the estimate. The final sub-section is the project parameter data analysis. This is where the data is examined and interpreted to extract relevant information through, for example, statistical analysis and visualization of the data.
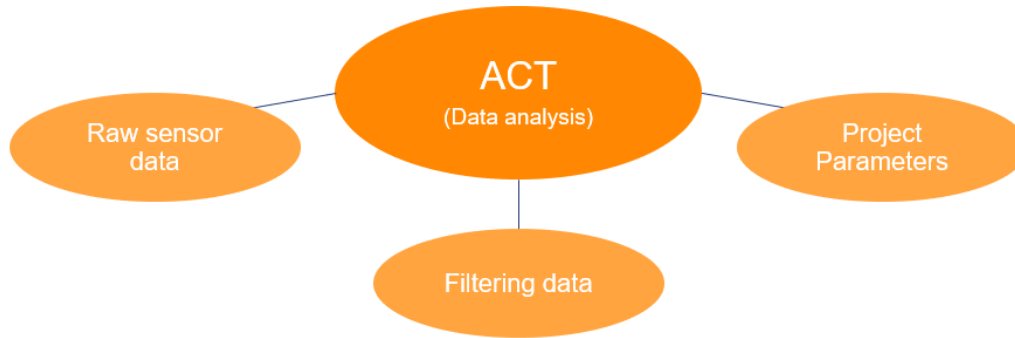
Figure 3.6: Actual data section overview

Raw sensor data

Case description - Karachi
The project that is chosen to calibrate the Estimation model is located in Karachi, Pakistan. The project was executed in 2017 and consisted of the deepening of an access channel for a new constructed deep sea container terminal. This was the final phase before completion of the total port project of the PWDCP project (Pakistan Deep Water Container Port) [TET, 2017].This case study was suitable to calibrate the estimation model because mostly straight loading lines have been used when dredging and the soil is mainly saturated sand. Also enough trips are made to have a sufficient amount of data (+/- 500 data points). Some background information of the project is summarized below:

- Deepening and widening of approach channel
- Channel width: $\approx 300m$, length: $\approx 8000m$
- Overflow allowed
- Dredged material to be dumped offshore
  - Edge dump area at 7.5km from end Approach
  - Dimensions $\approx 2400x2400m$
- Soils existed of medium dense fine sandy silt and moderately weak silt-stone (extra information is stated below)

(a) Location port Karachi, source = Google, 2022   (b) Karachi terminal, source = (TET, 2017)

Figure 3.7: Case study dredging of access channel Karachi, Pakistan

Data description

The data analyzed in this research is obtained from sensor data. Since 2012, Van Oord has been using sensors to measure various signals during the dredging process. These sensors are installed on many different parts of the vessel and can be used to measure and interpret numerous signals. The signals are already transferred into NetCDF (Network Common Data Form) data, which is a file format for storing multidimensional scientific data, such as arrays of data. The data is defined to be self-describing, so that it is easy to understand. Therefore, the NetCDF files can be read and written using various programming languages and software libraries. During this research it is chosen to run the NetCDF files in the programming language: Python. Jupyter Notebook it is than used to visualize and filter the data. The focus of this study was the biggest TSHD of Van Oord, HAM 318. The data obtained is only from this vessel, however the same method of data analysis can be used to run and calibrate an estimation model for other vessels.

Filtering data

Not all recorded data of the case study is being used in this study. There are several reasons why the sensor data of the vessel should be filtered (cleaned). These reasons are first given whereafter the selection of data (filtering) is visualized. The reasons to filter the data set are:

1. Removing unnecessary data: Filters are applied to remove the unnecessary data and to focus on the calibration of the estimation model. The boundary conditions of the estimation model are described in section Figure 3.1.1. The filters that are applied to make calibration of the estimation model possible are summed up below. The focus of this research is the loading phase of the dredging cycle. The other phases will therefore be removed. This will help to make the data more manageable and easier to work with.

   - Dredging status signal: loading
   - Draghead filters:
     - Draghead depth port side /star board < -16m
     - Difference between depth port side/star board < 2m
   - Heading: the difference of the heading should not be to big to ensure vessel is sailing in one direction instead of turning.
   - To filter out the turning points and the power difference between both propellers should not be to big: [-300 kW < Difference propulsion power sb/ps < 100 kW]
   - The estimation model calculates the total propulsion power needed to overcome all the resistance, the sb and ps propulsion power should therefore be summed up: [propulsion power sb + propulsion power ps]
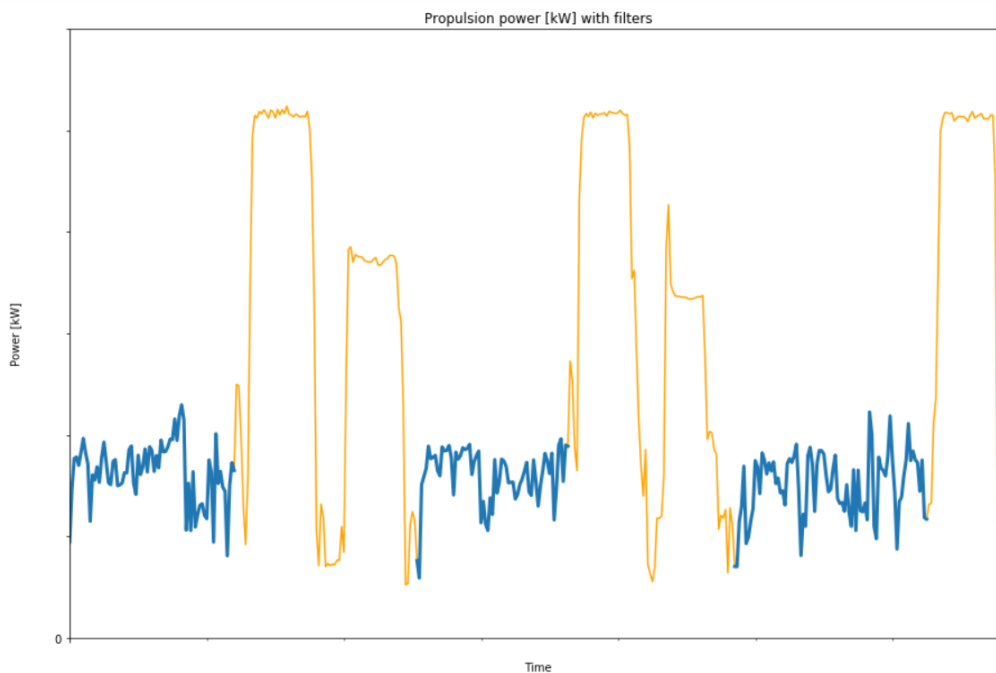
Figure 3.8: Representation of the propulsion power on the y-axis and the time on the x-axis. The yellow line represents the total power propulsion. The blue line represents the power propulsion during loading, which is obtained by applying filters to the dataset. (**Note: axis confidential**)

2. Improving data quality: in a large data set as the current, it is almost impossible not to have small errors and noise. These errors can exist of zero valued data or non-explainable outliers. Filters can be used to identify and remove errors in the data set, this will improve the overall quality of the data set which can improve the overall quality and make the analysis more accurate.

- Resample data size. The data set retrieved from the sensor data is data per second. This is very sensitive to errors or outliers. By resampling the data size with a bigger timestep 1 sec / 1 min you will decrease the amount of errors.
- Remove by visualization of data. Enormous outliers which are not possible to describe based on physical definition can be removed by hand. It can be hard to describe where some outliers come from, but based on physical knowledge it is possible to remove these outliers.
- Applying multiple filters will also help to remove errors in dataset. Sometimes a status signal could be wrong or non-explainable. By applying multiple filters most of these non-explainable signals will automatically removed. An example of a status error is visualized in Figure 3.9.
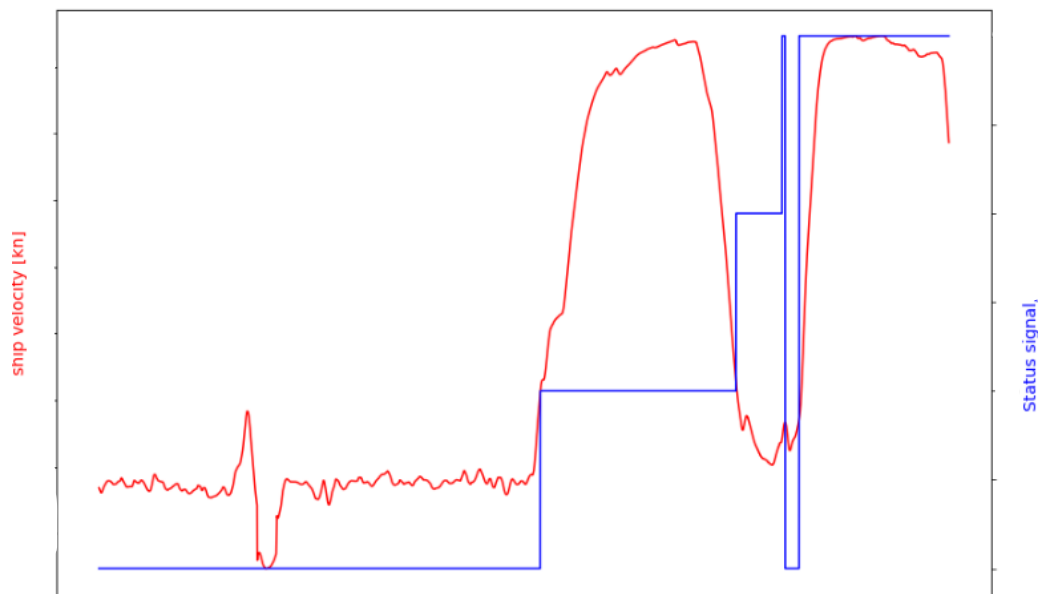
Figure 3.9: The ship velocity [kn] is represented by the red line on the left y-axis. The blue line represents the status signal, which is an integer number, and its value is shown on the right y-axis. However, due to this integer representation, incorrect status signals may occur. (**Note: axis confidential**)

3. Focusing on specific subsets: Filtering is used to look at specific subsets of the data. Due the enormous amount of data, different sets of parameters, subsets have been created to calibrate the estimation model. The creation of the subsets has been based on the most important parameters, which can be related to the sensitivity analysis. This can help to narrow the focus and make the analysis more targeted and relevant. The sensitivity study will be performed on the project parameters on which the most important parameters on the estimation output will remain. The focus will lay on these parameters during the calibration of the estimation model.

4. Identifying patterns and trends: The above filters are used to identify patterns and trends in the dataset that may not be apparent when looking at the entire data set. This can help to optimize the non-stationary (project) parameters in the estimation model. An example of the visualization of patterns and trends is shown in Figure 3.11.
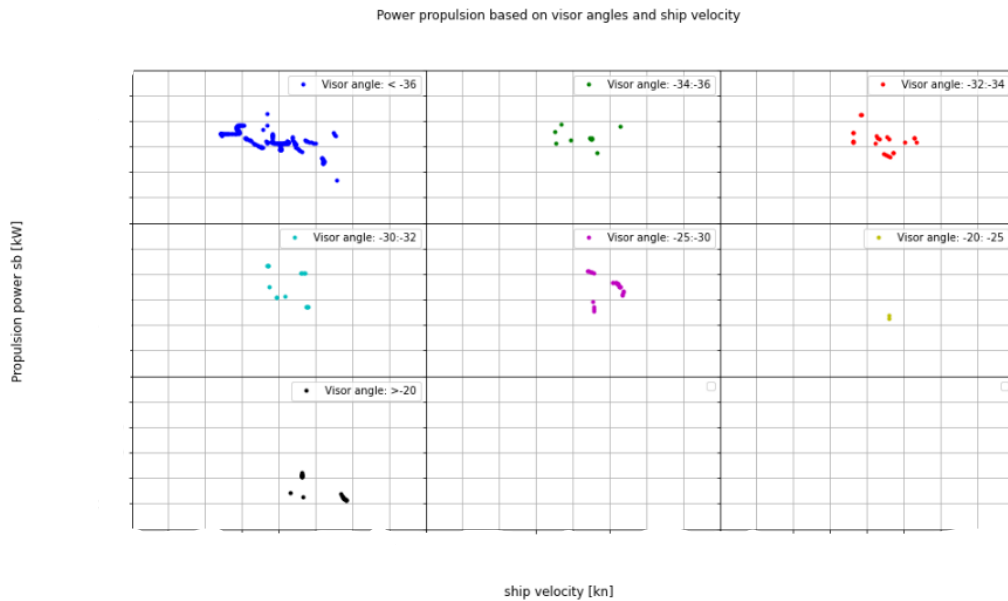
Figure 3.10: Visualization of identifying patterns and trends by the operational parameters, trailing speed and visor angle and total power output. The visor angle is subdivided into different bins and plotted per image, for fluctuating trailing speed. The y-axis represents the total power output which is the sum of the sb and ps propulsion power (**Note: axis confidential**).

To calibrate the estimation model an operational parameter will be analysed with corresponding propulsion power. By applying a non-linear regression line through this data the correlation between the operational parameter and the propulsion power can be found. The non linear regression line is the mean value of the described dataset. A prediction band and a confidence region can be plotted when this equation is known. The prediction band is the area in which x% of the data is expected to fall. The x% confidence region is the area that has a x% chance of containing the true regression line.

As a first step only the prediction band will be used during the calibration of the estimation model, the confidence region can be used to optimize the estimation model.
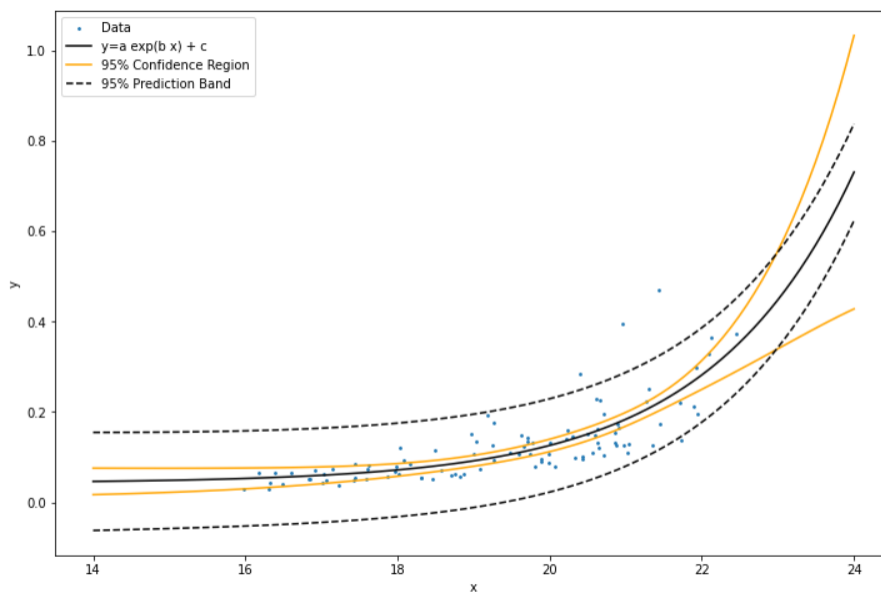
Figure 3.11: A regression line on a random dataset. The x and y axes represent the values of the dataset. The black line represents the regression line, the black dotted line shows the prediction band, and the yellow line indicates the confidence region.

Project parameters

The (non-stationary) project parameters which are based on project characteristics will vary based on project but also during a project. These parameters are set equal to a chosen case study to set the estimation model equal to the dataset. This subset of eight parameters is chosen since they can be obtained via the tender phase or are parameters which can be retrieved from sensory data in contrast to the stationary parameters (Table 3.5) which will not change during a project (vessel characteristics) or are not always known during a project (exact soil characteristics). Since not all parameters can be retrieved directly some calculation or conversions will be elaborated.

If the sensitivity analyses have shown that the variation of the parameter does not impact the output of the estimation model a lot, than these project parameters can be set constant. Setting a parameter constant can be done by taking the mean of the specific parameter based on the filtered data. The standard deviation can still be an interesting value, this to exclude that the applied filters are correct. The standard deviation of the dataset can be calculated with the following formula:

$$std = \sqrt{\frac{\sum(X - \overline{x})^2}{n - 1}} \tag{3.2}$$

where:

X = The value in the data distribution
$\overline{x}$ = The sample mean
n = Total number of observations

If the sensitivity analysis has shown that the project parameters does influence the output of the estimation a lot and there is a high standard deviation within the dataset, than these parameters cannot be set constant within the estimation model. These parameters should be analysed to find correlation between certain project conditions. To spark the imagination a flowchart of the described process is visualized below:
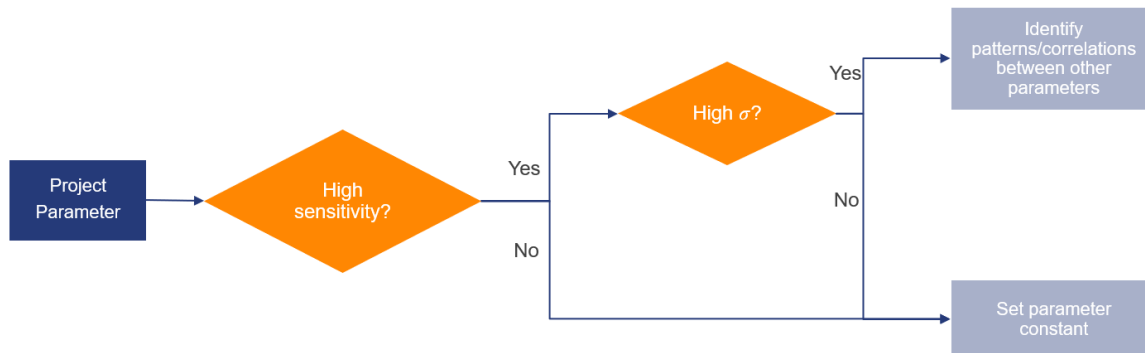
Figure 3.12: Project parameters analysis plan

The project parameters which should be obtained from the data analysis are shown in table Table 3.7. Some parameters cannot immediately be retrieved from the dataset and should be derived from other signals and estimation models. The methods and sensor data to obtain the correct project parameters are described below per parameter.

Parameter	Definition	Unit	Sens	Std	Value
α_1	Upper pipe angle	deg	-	-	-
α_2	Lower pipe angle	deg	-	-	-
β_1	Upper pipe cable angle	deg	-	-	-
β_2	Upper pipe cable angle	deg	-	-	-
z	Water depth	m	-	-	-
$Q_{j,wp}$	Jet discharge at working point	m^3/s	-	-	-
γ	Visor angle	deg	-	-	-
v_t	Trailing speed	m/s	-	-	-

Table 3.7: Parameters based on actual data analysis, these will be analysed in the next section

$Q_{jet,wp}$: **Jet discharge at the working point**

The jet discharge can directly be obtained from the dataset. This obtained parameter can then be used to check the resistance from the in-house pump method. Input for this in house pump module will be sensor data and the output of the pump module will be compared to pump sensor data to validate that the pump module makes an accurate estimation. The rpm and the pump power on which the jet pump worked will be retrieved from the sensor dataset.

By tuning the input of the in house pump module to the sensor data of the Karachi project the discharge of the jet at the working point can be calculated. Through the intersection point of the resistance line and the analysed pump power the jet discharge can be found. This process is visualized in Figure 3.13.
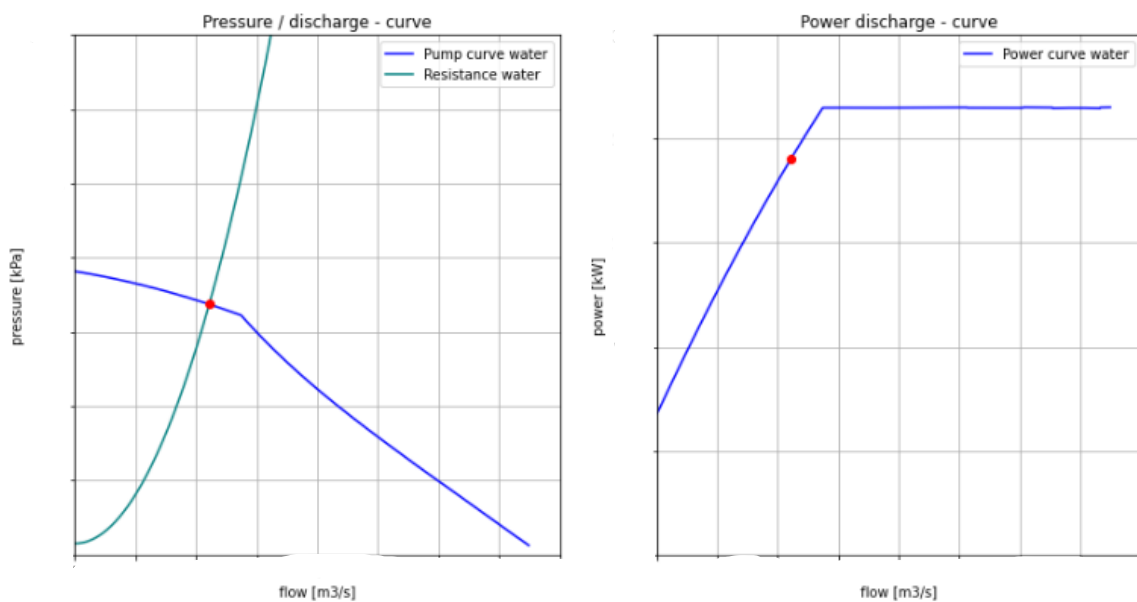
Figure 3.13: Output of the in-house Van Oord model results in working point jet with corresponding power (**Note: axis confidential**).

γ: **Visor angle**

The starboard and portside visor angle can be directly retrieved from the filtered dataset.

z: **Water depth**

The water depth is obtained via the portside and starboard draghead depth. Both draghead depths are analysed since it is than possible to filter out the turning of the vessel. During this process sometimes one draghead remains on the bed while the other is lifted up. By analysing both sensor it is possible to filter out these movements.

v_t: **The trailing speed**

The ships velocity which is retrieved from the dataset is the speed on which the vessel is moving forward. This ship velocity cannot directly be used as input for the estimation model since this model does not include currents and other environmental aspects and is based on still water. It is therefore likely that the estimation model will under- or over estimate the needed propulsion power. To cope with this problem the ship velocity input for the estimation model should be analysed per cycle, to include all different environmental aspects.

For now, this mean ship velocity per cycle has been used to analyse the estimation tool. If in the future the model needs to be improved, a more accurate estimation per smaller time step should be used.

α_1, α_2: **The upper and lower pipe angle**

The suction pipe angles can directly be retrieved from the filtered dataset. If the water depth is known, a check based on this data can easily be applied by filling in the following equation:

$$\text{Water depth} = sin(\alpha_1) * \text{length upper pipe} + sin(\alpha_2) * \text{length lower pipe} \tag{3.3}$$

β_1, β_2: **The upper and lower cable angle**

The upper and lower cable angle has been derived from the obtained pipe angle data. By using the dimensions of the pipe and the vessel it is possible to calculate the angles of the cables. The equations to determine the cable angles and the schematized dimensions of the vessel are summed up below.

$$\delta = \arctan \frac{L_5 - L_4}{H_{IW} + H_{UP2}} \tag{3.4}$$

$$\gamma = \arctan \frac{L_6 - (L_3 + L_2)}{H_{CW} + (H_{UP2} + H_{LP2})} \tag{3.5}$$

$$\beta_1 = 90 - \delta \tag{3.6}$$

$$\beta_2 = 90 - \gamma \tag{3.7}$$
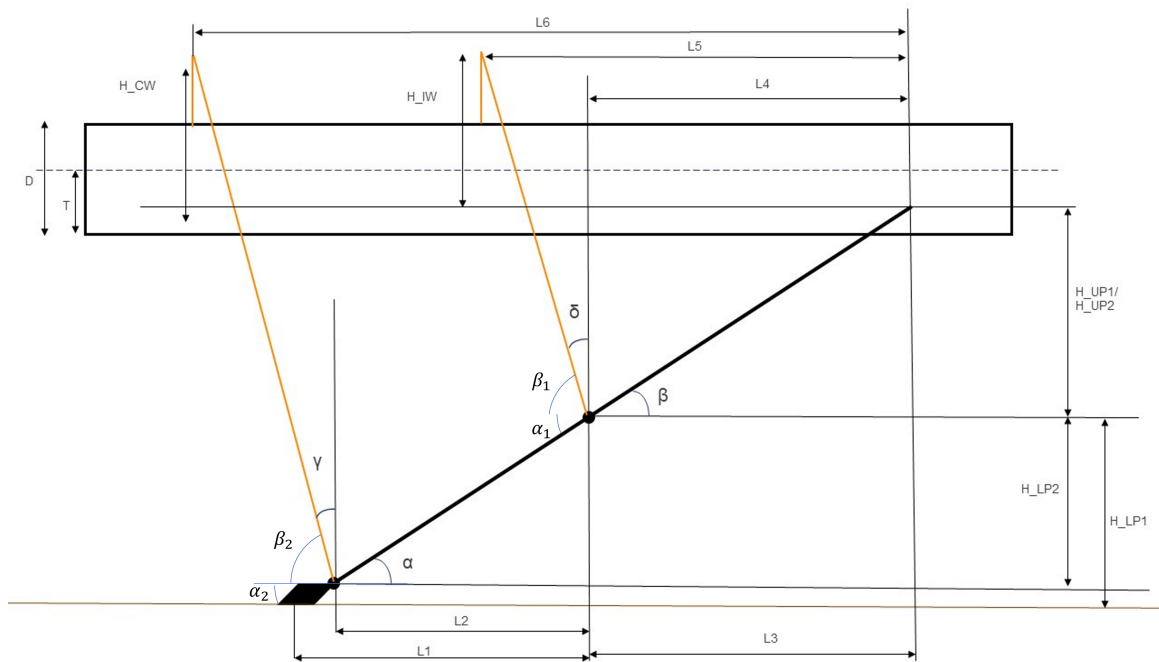
Figure 3.14: Schematization of vessel dimensions to determine the upper and lower pipe angles for a TSHD, source (modified): (**Mihir**)

3.1.3 Calibration

The calibration is the last step of the experiment plan. It is an iterative process in which the calibration of the estimation model is described based on the desired accuracy of the model. The process is shown in Figure 3.15 and is described in this section.

The requirements of an accurate prediction are described below. When the requirements have been matched the propulsion power system can be used in the simulation tool to simulate the energy consumption during the total loading phase (section chapter 4). When the model does not match the set requirements the calibrating steps to create a more accurate estimate are described:

- $EST \neq ACT$, the comparison of the EST output with the ACT data reveals that the estimation model falls outside the prediction band of the filtered dataset. The calibration indicates a fundamental issue (for certain area) with the estimation model as the estimate is extremely inaccurate. The estimation model needs to be re-examined, starting with the (non-stationary) project parameters, where correlation/patterns between different parameters can be identified. If this does not lead to a higher accuracy, then the stationary parameters should be checked, after which the physics of the estimation model should be re-examined.
- $EST \approx ACT$, the EST fits completely within the prediction band (85%) of the dataset. While the EST provides a good first estimate, it should be improved to better match the confidence region of the dataset. To achieve this, the dataset should be expanded with data from similar dredging projects and multiple filters should be applied to better examine specific dredging strategies.
- $EST = ACT$, the EST completely fits within the confidence region of the dataset. The estimation model is ready to be used in the current Van Oord methods to estimate the required power of the propulsion system during set boundaries.

The calibration of the model is presented in the results section. This section also elaborates on the iteration steps to optimize the estimation model based on the improvement of the filters and input parameters. This calibration process can be repeated until an exact match has been achieved, but for this research it is chosen to show the calibration steps to be able to implement the propulsion model in the simulation tool defined in the next section.
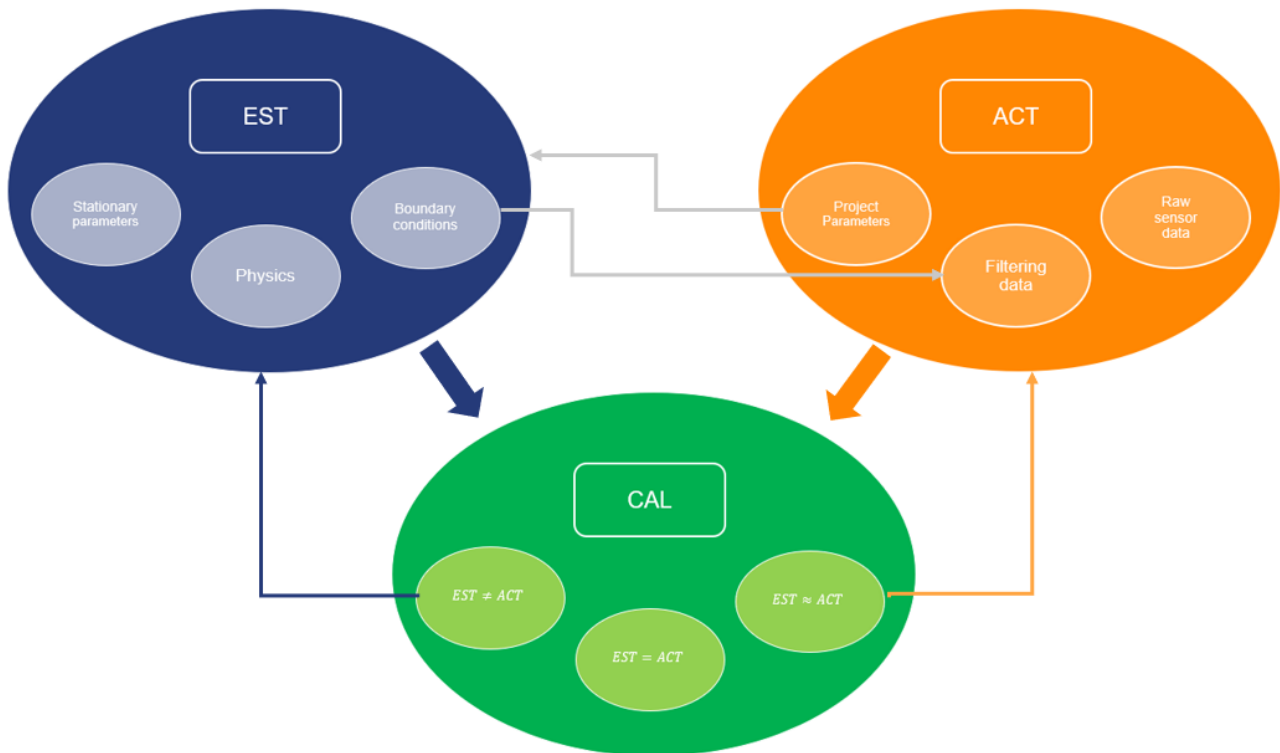
Figure 3.15: Schematization of experiment plan for the calibration of the estimation model

3.2 Results

This section follows the structure of the Experiment Plan as described in the materials and method section. It first describes the results of the physics based model. Thereafter the results of the data analysis are shown in which the input and sensitivity of the project parameters are defined. The total propulsion power is also extracted from the data and is displayed so it can be used during the calibration of the estimation method. The final section elaborates on the results of the calibration steps, discusses the outcome and concludes if the estimation model can be integrated in the simulation tool.

3.2.1 Estimation model

Stationary parameters

The analysis of the project parameters show that especially the initial porosity (ni) has a big influence on the propulsion power output. This parameters is now based on literature of (S. A. Miedema, 2014). A deviation of 10% will have a significant impact ($>20\%$) on the output of the estimation model.
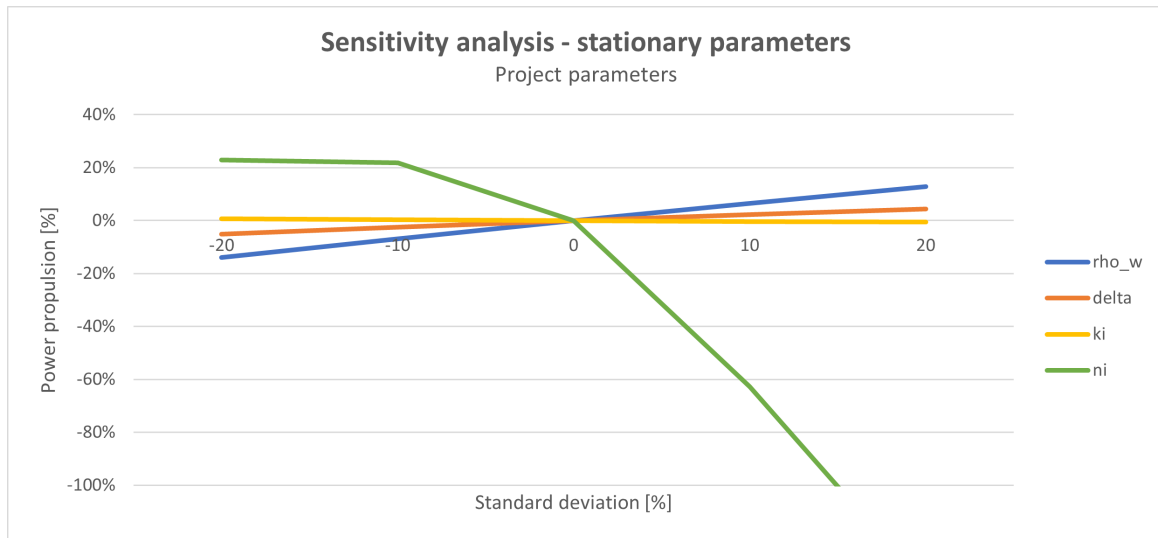
Figure 3.16: Sensitivity study of the stationary project parameters of the estimation model. ρ_w = water density [kg/m^3], k_i = initial permeability [-], n_i = initial porosity [-], δ = soil/steel friction angle [deg]

The analysis of the vessel parameters show less influence on the propulsion power output. When the number of teeth is increased from 32 to 38 it will result in a increase of 20% of propulsion power. The other parameters show less influence on the output of the model.
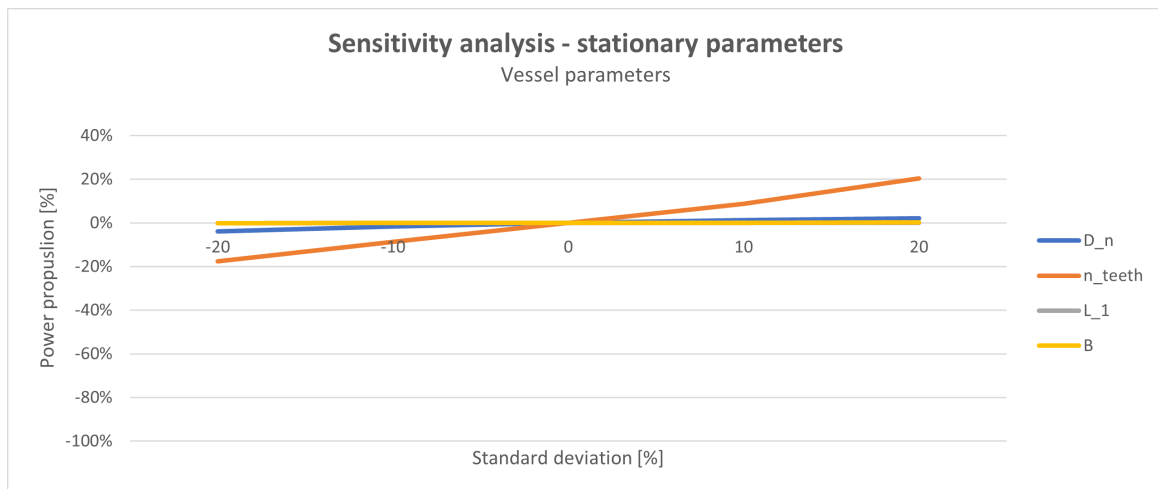
Figure 3.17: Sensitivity study of the stationary vessel parameters of the estimation model. D_n = jet diameter [m], n_{teeth} = number of teeth [-], L_1 = upper suction pipe length [m], B = width of the vessel [m]

Output model

The different resistance terms working on the draghead vessel and suction pipe have been analysed. As can be observed in Figure 3.18 the draghead is the primary resistance term. A more detailed result of the forces that create this high draghead force have been plotted for different trialing speeds and are included in Appendix section B.1.
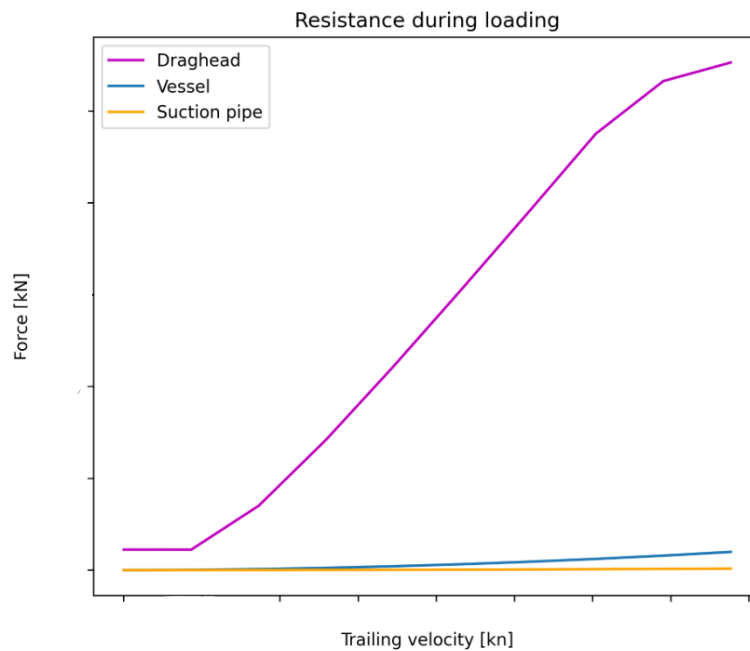
Figure 3.18: Resistance working vessel, suction pipe and draghead. Draghead resistance is the main resistance term.

The propulsion power and the EHP power (power without efficiency terms) are plotted for increasing trailing speed. The total resistance exist of two dragheads and suction pipes and one vessel. The efficiency terms that are used can be found in section Figure 3.1.1.
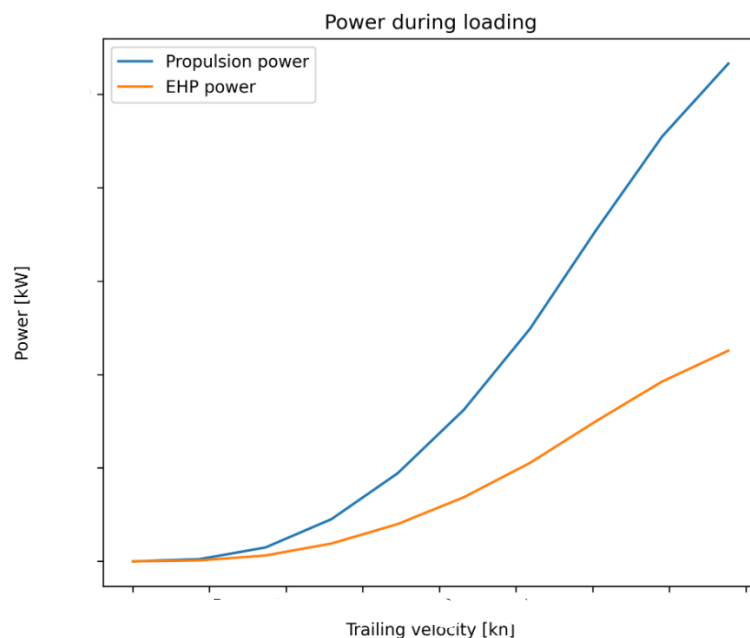
Figure 3.19: End result of estimation model, delivered propulsion power by the engine and the effective horse power, which is the power without efficiency factors. The blue line will be used during the calibration of the estimation model with the case study.

3.2.2 Actual data

Non stationary parameters

The results of the non-stationary (project) parameter sensitivity analysis are shown in Figure 3.20. The water depth, suction pipe- and cable angles will be set constant on their mean value due to their low sensitivity. The visor angle (gamma), trailing speed (v_t) and jet discharge ($Q_{j,wp}$) will be analysed further to visualize the variation during a project.

Parameter	Definition	Unit	Sens	Value
α_1	Upper pipe angle	deg	Low	15
α_2	Lower pipe angle	deg	Low	15
β_1	Upper pipe cable angle	deg	Low	95
β_2	Upper pipe cable angle	deg	Low	95
z	Water depth	m	Low	20

Table 3.8: Project parameters with low sensitivity which are set constant in estimation model (**Dummy values are used due to confidentiality**)
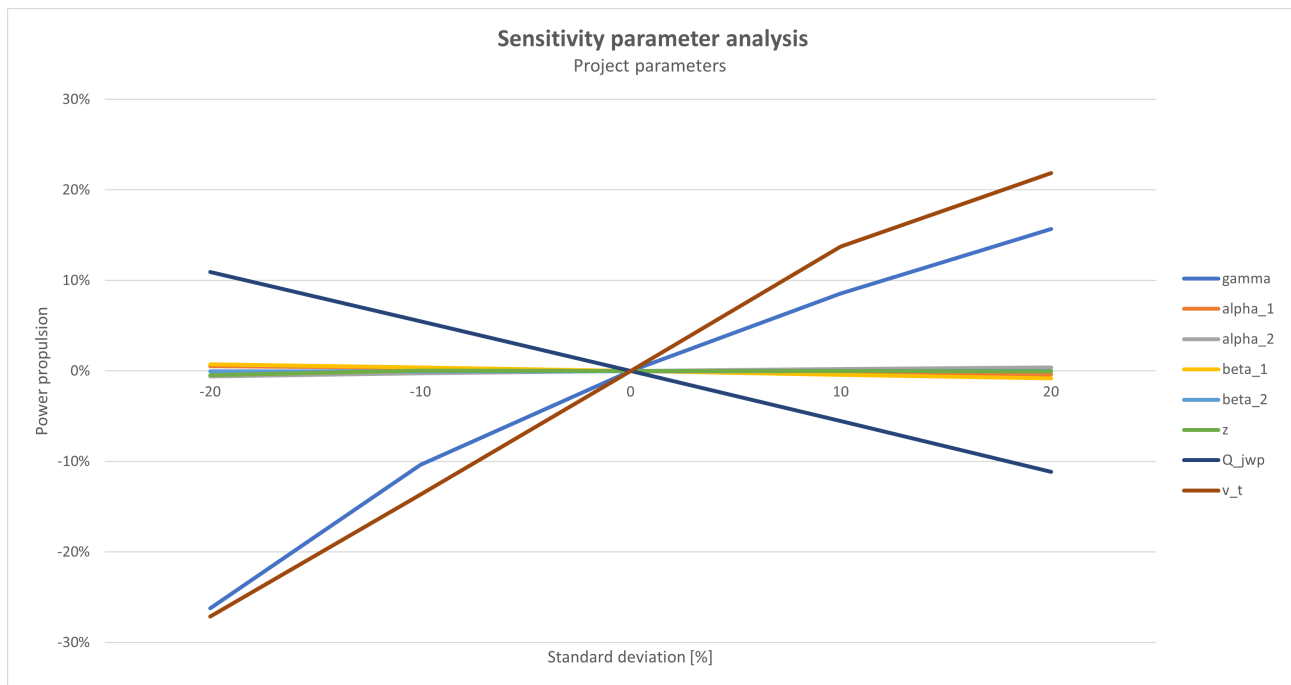
Figure 3.20: Sensitivity analysis on the non stationary parameters retrieved from the data analysis. γ = visor angle [deg], $\alpha_{1,2}$ = suction pipe angles [deg], $\beta_{1,2}$ = cable pipe angles [deg], z = waterdepth [m], Q_{jwp} = Jet discharge at working point [m^3/s], v_t = trailing speed [kn]

The results of the standard deviation analysis are shown in Table 3.9. The figure shows that the standard deviation of the jet discharge is low (3.62 %), which means that this parameter will be set constant (on its mean value) and can be included by the other estimation parameters. The other two parameters do have a high standard deviation and cannot directly be included in the estimation model.

Parameter	Definition	Unit	Sens	Std	Value
$Q_{j,wp}$	Jet discharge at working point	m^3/s	High	5.0%	3.0
γ	Visor angle	deg	High	30%	-
v_t	Trailing speed	kn	High	30%	-

Table 3.9: Project parameters with high sensitivity, next step is to retrieve standard deviation (**Dummy values are used due to confidentiality**)
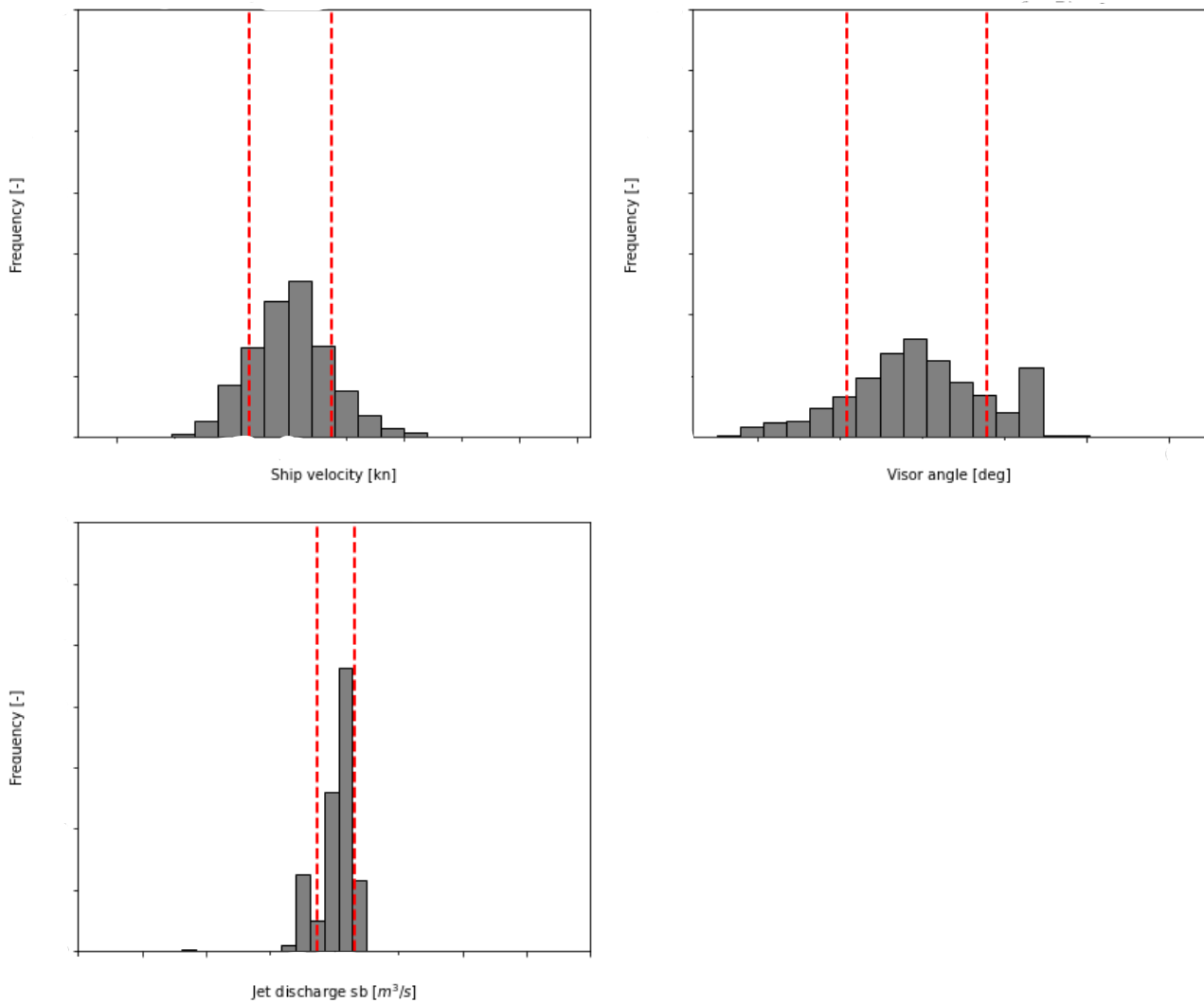
Figure 3.21: Standard deviations of high sensitivity parameters (**Note: axis confidential**)

The total results of the correlation and pattern identification research are included in Appendix section B.2. This section shows the main insight of this research.

The figure shows that the cloud of data is shifting to the right with decreasing visor angle. This correlation of certain visor angles per trailing velocity can be included in the estimation model. This means that per trailing velocity a visor angle is used. The different boundary setting are as follows:

$$\gamma = -35[deg] \qquad \text{for, } [v_t \leq 1.4[kn]]$$
$$\gamma = -33[deg] \qquad \text{for, } [1.4[kn] \leq v_t \leq 1.55[kn]]$$
$$\gamma = -31[deg] \qquad \text{for, } [1.55[kn] \leq v_t \leq 2.0[kn]]$$
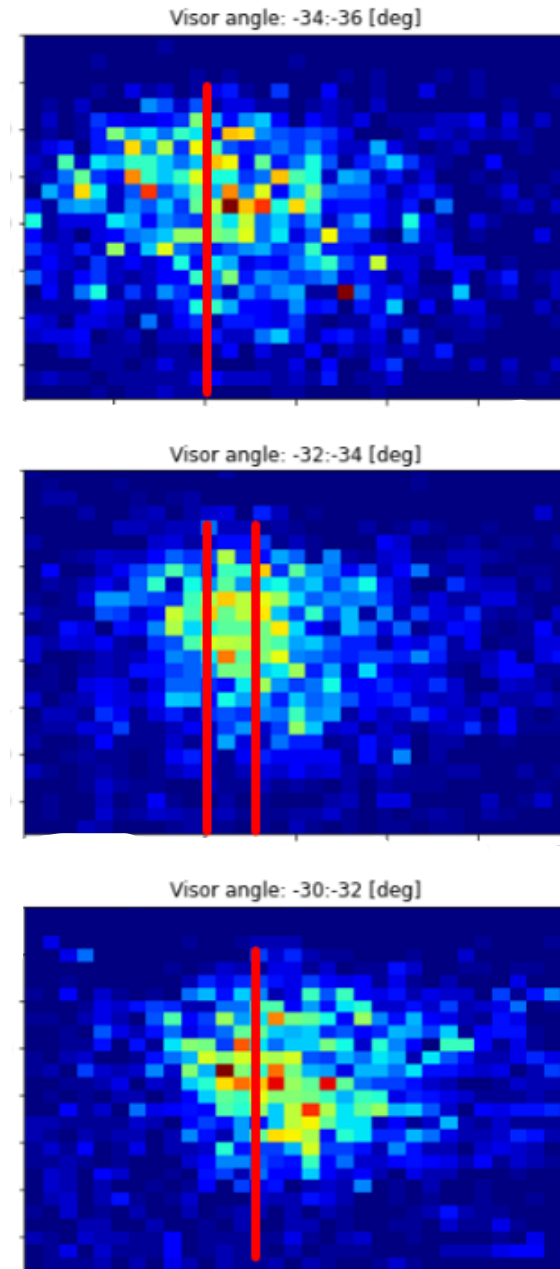
Figure 3.22: The visor angle sections move from left to right with decreasing visor angle. Limits have been set on the trailing speed per visor angle section (**Note: axis confidential**).

Output data analysis

The non-linear regression line that is used during the calibration of the estimation model is show in Figure 3.23. The mean trailing velocity per loading cycle is plotted on the x-axis and the corresponding propulsion power on the y-axis. An increase of the propulsion power can be seen by increasing trailing velocity. This result will be used in the steps to calibrate the model.

The figure shows that much data falls outside the confidence region interval. This means that it is very hard to predict the output of the dataset. That is why the decision is made to use the prediction band as indicator for the calibration steps. A follow up study should first focus on creating a better filtered dataset to create a more accurate prediction whereafter the confidence region could be used as validation method.
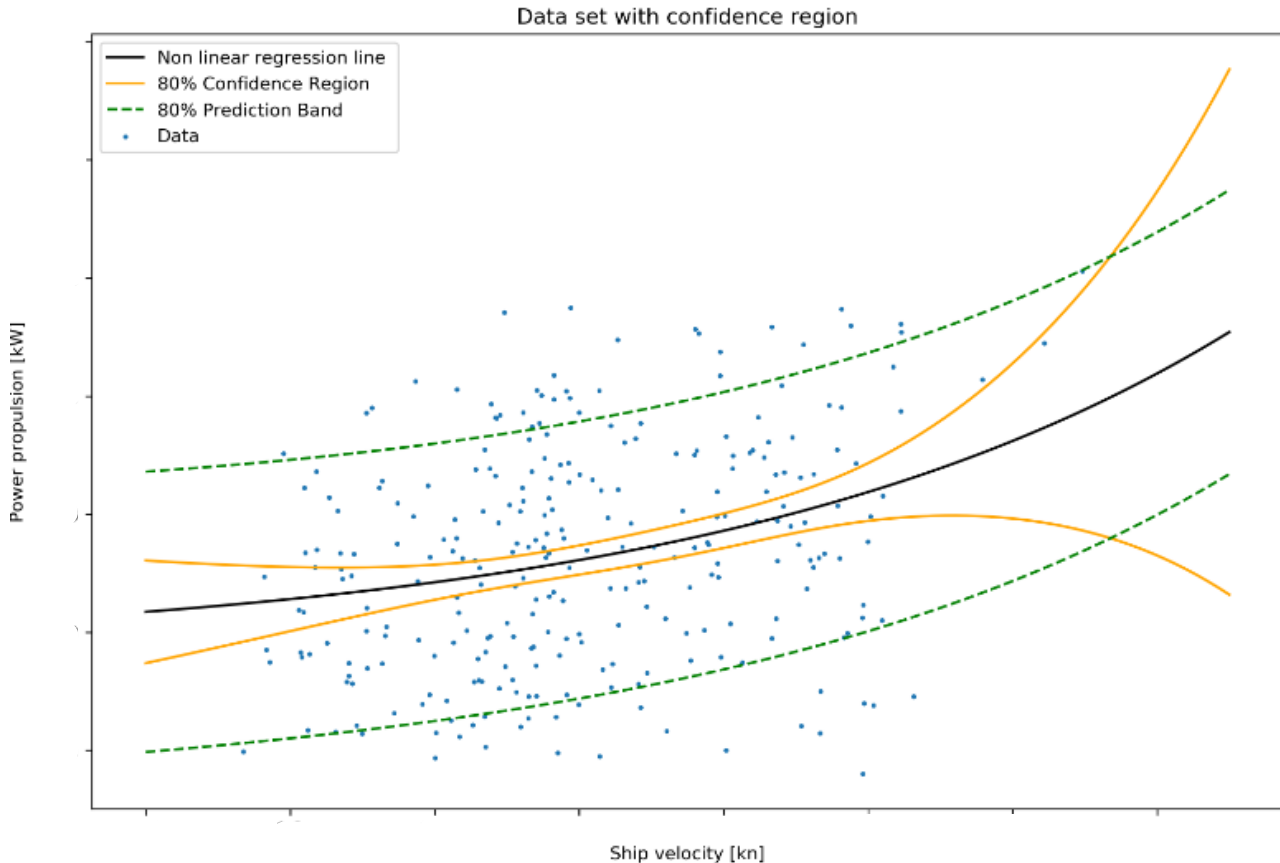
Figure 3.23: The non linear regression line on the retrieved sensor data. The non linear regression line is the mean value of the described dataset. The 80% prediction band is the band in which 80% of the data is expected to fall (**Note: axis confidential**).

3.2.3 Calibration

This section provides the results of the different calibration steps that have been taken to compare the estimation model with the case study data. Thereafter it is elaborated if and how the estimation model can be integrated in the simulation tool to run the energy consumption during the loading phase.

Calibration step 1

The first calibration is done by plotting the estimation model with a visor angle of 33 [deg] in the dataset. The estimation model falls within the prediction band for trailing velocities $\approx$ 1.5 - 1.9 [kn]. An underestimation is made for low trailing velocities and the model overestimates at high trailing velocities. The slope of the estimation model does also not match the regression line.

The calibration check indicates that $EST \neq ACT$ since the estimation model does not fully fit within the prediction band for all cases. The calibration step defined beforehand is to improve the non-stationary parameters in order to optimize the estimation model. This process is described in calibration step 2.
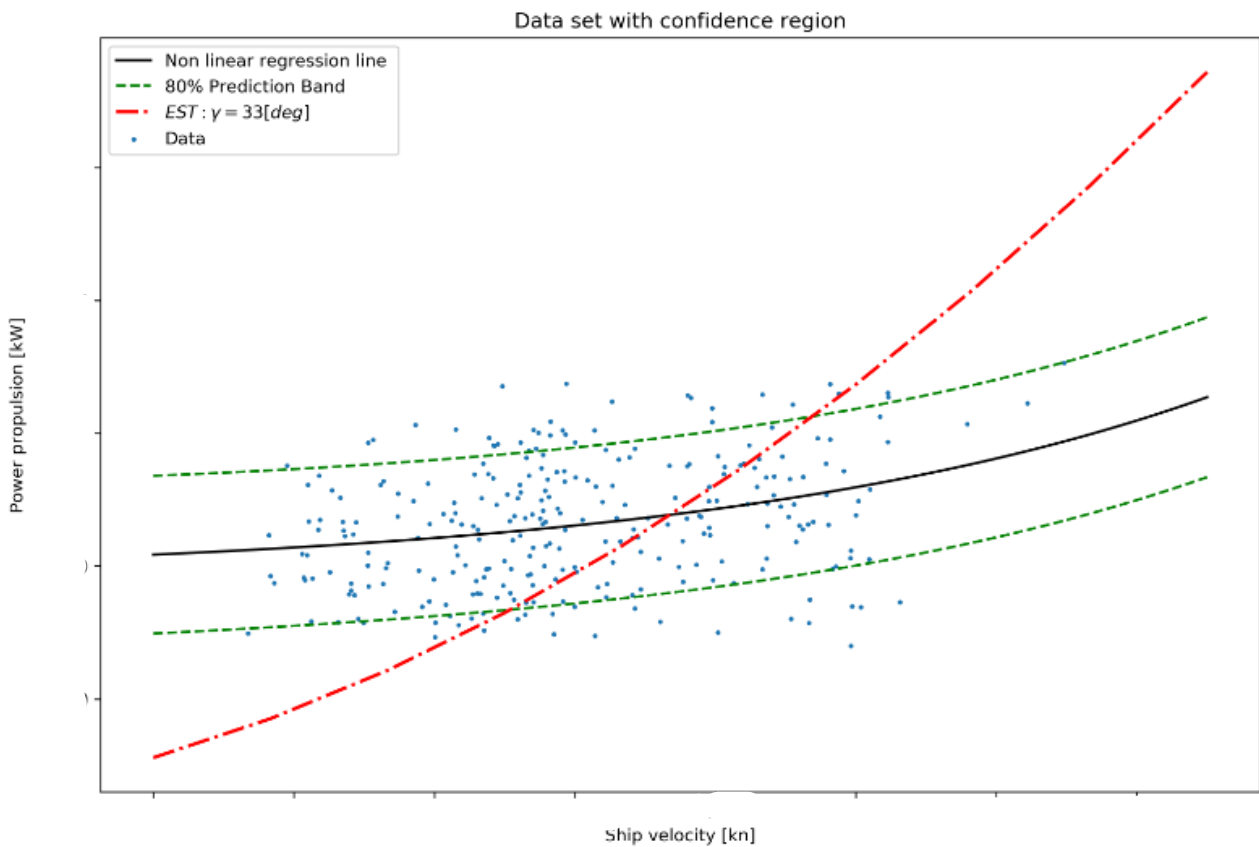
Figure 3.24: The estimation model with a visor angle $\gamma = 33[deg]$ in the actual data (**Note: axis confidential**).

Calibration step 2

The estimation model is optimized by using different visor angles per trailing velocity. The correlation between the two non-stationary parameters is found via the research described in section 3.1.2. The estimation at lower trailing velocity will shift upwards and the trailing velocity at the higher trailing velocities will shift downwards. The change in the output of the estimation model is small, but will lead to a better fit. The propulsion power at higher trailing velocities ($v_t > 2.0[kn]$) is not changed and will still result in an overestimation. The mismatch in the slope of the estimation model is still present.

The predefined calibration check will still result in $EST \neq ACT$. The next calibration step will give a first approach to optimize estimation model for higher trailing velocities.
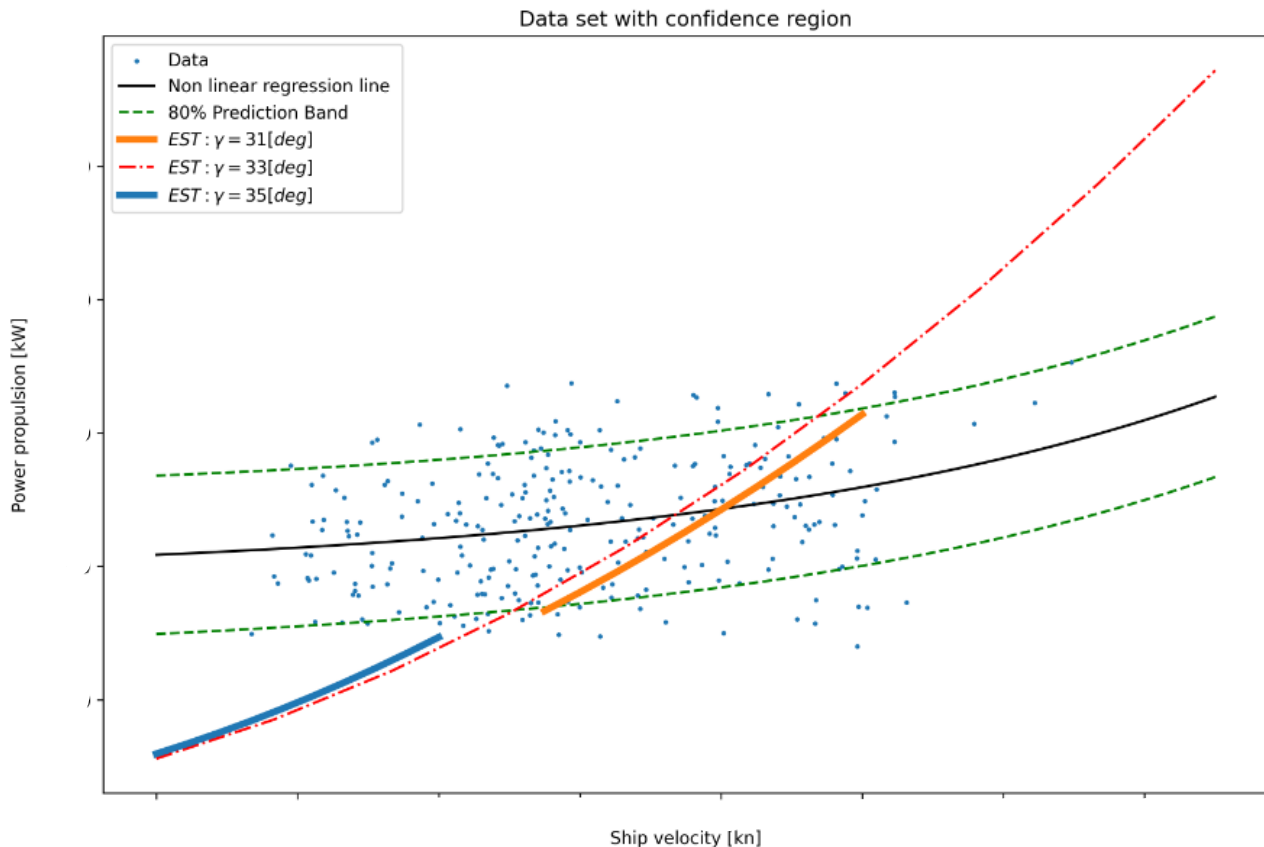
Figure 3.25: The estimation model with a variating visor angle per trialing speed. The blue line represents the estimation model with a visor angle of 35 [deg] and the orange line a visor angle of 31 [deg]. The red dotted line is the output of the estimation with visor angle 33 [deg] (**Note: axis confidential**)

Calibration step 3

The last calibration step can be seen as a first outline for future research. The correlation analysis of the visor angle and trailing velocity (included in Appendix section B.2) have revealed that at higher trailing velocities a rather small visor angle is used ($\gamma = -20 : -25[deg]$). Using a visor angle of 23 [deg] at higher trailing velocities will result in a big decrease in propulsion power (Figure 3.26).

The plot also shows that there are very few data points located at trailing velocity $v_t > 2.0[kn]$. Also the research included in Appendix section B.2 shows different propulsion power output for these range of visor angles. Since not all parts fall within the prediction band the calibration check still indicates $EST \neq ACT$.
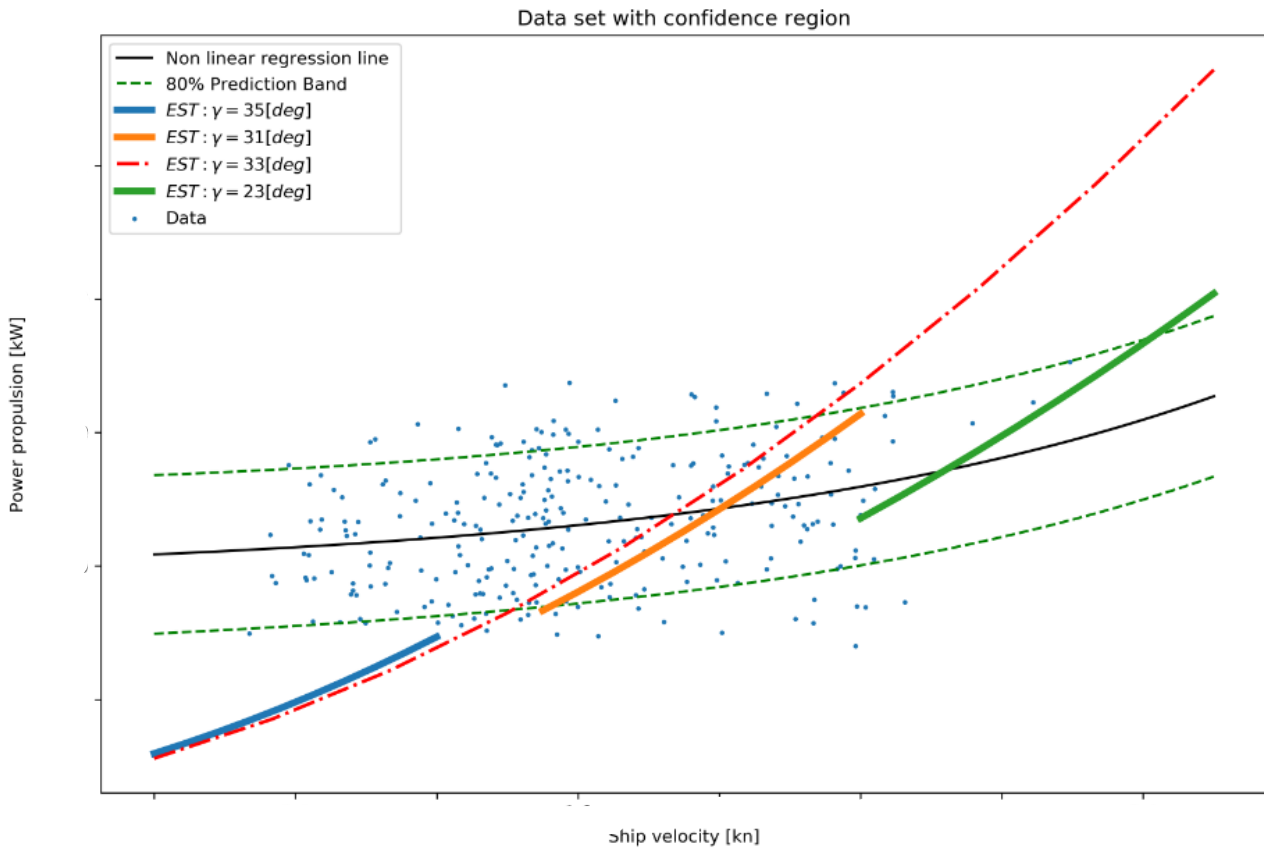
Figure 3.26: The output of the estimation model with an angle of 23 at high trailing speeds. The estimation better fits within the prediction band (**Note: axis confidential**).

3.3 Discussion

This section elaborates on the interpretation of the results provided in the previous subsection. The structure of this section will follow the results section. First, the estimation model results are discussed. Second, the data analysis results are elaborated, whereafter the calibration steps are discussed.

3.3.1 Estimation model

The sensitivity analysis is done by calculating the output of the model based on difference parameter input. During this process all the parameters are hold constant and one parameters is being changed. A problem during this research is that the assumption is made that all parameters are independent and can therefore be adjusted separately. In reality there is a dependence between some parameters. This is the case for the porosity of the soil working on the cutting teeth (n_{max}) and the initial porosity (n_i) of the soil. This study only focused on variating one parameter, where in reality these parameters are dependent. This could be an explanation of the enormous sensitivity of the initial porosity parameter shown in Figure 3.16.

In this research it is decided to exclude environmental conditions as currents and winds. The decision is made to get an initial estimate of the propulsion power on a more global level, namely per loading cycle. Despite this exclusion, it is acknowledged that the importance of the currents do play an important role when trying to describe the trailing speed on smaller scale, different time periods within the loading cycle. The assumption that is made for now is that the currents working on the vessel/suction pipe and draghead will cancel each other in respect to the total loading cycle. The actual movement of the vessel during the loading phase should however better be checked before making this assumption. If the dredging vessels sails only in one direction per loading phase the currents working on this vessel will not cancel out and can have an impact on the propulsion power.

The waterdepth is used as a stationary input parameter within the model. This makes it possible to equally model the resistance working on the starboard and port side of the vessel. In reality the behaviour of these systems is seen as independent based on deviating waterdepth and other environmental parameters. With the same reason the draghead have been modelled as a draghead with one visor, whereas in reality a double visor is used at the HAM318 which can move up and down separately. This could again have an impact on the force calculations within the draghead since the visor angle is normally different at both compartments. To more accurately estimate the needed power to overcome all resistance terms, the structure and other soil characteristics of the bed should be known. Which can then be implemented in the estimation model.

The cutting force included in the visor force model is based on the cutting of saturated sand model of Miedema (S. A. Miedema, 2014). This model include a pore pressure model which describes dislocation of the grain structure of sand. Due to this effect a pressure difference in the pores arises, which forms increased grain stresses and higher cutting forces. This model is used to calculate the cutting forces within the Karachi project. However, a small deviation of the soil characteristics (such as porosity, permeability and soil compaction) could already result in a difference cutting force output. Especially the porosity of the soil is an important input, due to missing soil characteristics of the Karachi project, assumptions made by Miedema are used as input for this model.

To convert the EHP power in the propulsion power certain efficiency terms are used. The hydrodynamic efficiency terms that are used in this research are based on a study on inland waterway vessels. When the dredging vessel moves in shallow waters there are many comparisons that can be made between those two vessels. However, the assumption that is made does have a great influence on the outcome of the model $\eta_{old} = 0.64$ and $\eta_{new} = 0.45$ (for hydrodynamic efficiency terms). The assumption that the efficiency term is much lower at sailing slow should therefore be double checked if this is also true at dredging vessels.

The pump forces working within the visor and draghead are not linked to the exact pump forces calculated by the pump models. For now these forces as the vacuum force and the impulse forces make use of a stationary mixture velocity and mixture density. In reality this mixture will fluctuate during the dredging process and the impact of the force on the pipes and visor will therefore also change. This affect have been left out of this research.

3.3.2 Data analysis

The calibration of the propulsion model and the obtained non-stationary (project) input parameters are based on the analysis of data from a case study. It is always good to question the reliability of this data. If the analysis has shown that the visor angle was at a certain angle, then in reality it may deviate from this. This applies for all obtained data and filtered data and can be seen as a more general note of discussion.

The identified correlation and patterns based on the visor angle and trailing speed are now determined by visualization of the amount of data points. It is visualized that the cloud of data is moving from left to right for approximately the same power output. This visualization process will only give a rough estimate of the particular visor angle with corresponding trailing speeds.

The R-squared value of the regression line, in which is represented how well the model fits the observed data, is still very low ($R^2 = 0.1$). This value presents the proportion of the variation in the dependent variable (propulsion power) that is explained the independent variable (trailing speed) in the model. This means that the trailing speed is not explaining much of the variation in the propulsion power variable. The observed dataset is based on the mean trailing velocity per loading cycle with corresponding power term. The sample size of the dataset is now based on 2 month of data of one project. By adding more data of similar dredging projects the comparison and the calibration will be more accurate. In addition, better filters should be applied to increase the R^2 value. This will also make it possible to use the calculated confidence region based on the regressions line to validate the estimation model.

Different filters have been applied to the dataset to mimic the limitations of the developed model as closely as possible. In this way a as good as possible comparison can be made between the output of the model and the propulsion power obtained from the dataset. It should be noted that these filters never fully filter out all incorrect data. Therefore, it is possible that a higher power consumption during the sailing phases is still inadvertently included.

The filtering of the data to mean velocity and mean propulsion power will decrease the reliability of the data analysis. A large amount of data is combined and an average is taken from this group of data. However, the duration of a loading cycle is that long that ground conditions and other effects can vary greatly from cycle to cycle. These effects are currently not included in the analysis.

3.3.3 Calibration

From the first calibration step, it has been found that the model underestimates for low trailing speeds and overestimates for high trailing speeds. By finding correlations between project parameters and using these as new input parameters the model will improve only a small bit. It comes down to the fact that the developed model makes an imprecise estimation of the power consumption based on the trailing speed, especially for high-($v_t > 2.0$ [kn]) and low trailing speeds ($v_t < 1.6$ [kn]). Possible reasons for this mismatch are discussed below.

Underestimation

As been seen during the calibrating steps, the underestimation of the model cannot be solved by finding correlations/patterns in the non stationary parameters. This means that their is a fundamental problem in the estimation model for low trailing velocities. A possible explanation of this effect could be due to excluding the static friction in the estimation model. The static friction should be overcome to start moving the object. This friction is higher than the friction during movement (kinetic friction). The model does not include this higher static friction force. The estimation model shows that low trailing velocities will result in a low propulsion power, but in reality a high propulsion power is needed to start the movement of the draghead.

The movement of the draghead along the ground can be seen as an anchor moving over the ground. When starting at rest an extra force is needed to start the movement of this 'anchor'. Once the draghead is in motion the power could be expressed by the estimation model. A representation of the static versus kinetic force is shown in Figure 3.27.
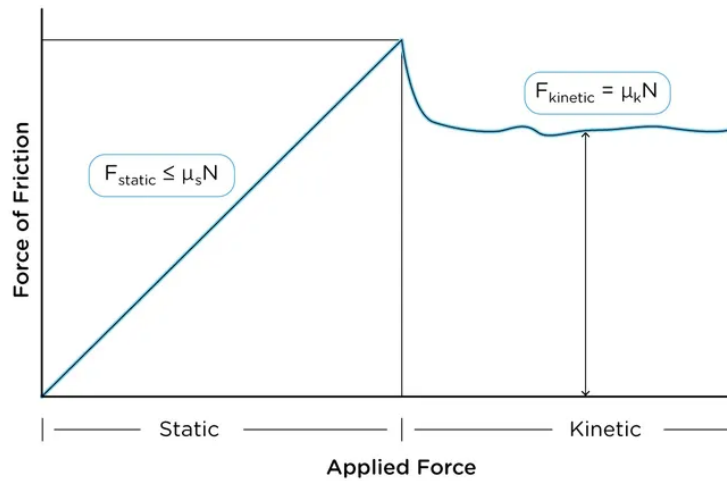
Figure 3.27: Static friction vs kinetic friction. The static friction is the friction which should be overcome to start moving the object. This friction is higher than the friction during moving (kinetic friction). Source: (Westin, 2023)

Overestimation

Three possibilities of the overestimation of the model are discussed:

1. The overestimation at higher speeds could possibly be solved by finding a correlation between visor angle and trailing speed. The third validation step shows an outline of the possible approach. However their is still to little data available to validate this approach as the plots have shown It seems that the green line will make a better fit, but this could also be a coincidence.
2. The overestimation at this region could also be due to the exclusion of the total power distribution during the loading phase. There are several other energy consumers active during the loading phase which means that there is less power available for the propulsion system. The estimation model does now only look at the power needed to overcome the resistance terms, but should also look at the power available.
3. The different forces working on the draghead are analysed to explain the overestimation at higher trailing speed. Zooming in on the visor component of the draghead it can be seen that the cutting force is the main contributor to the resistance at higher trailing velocities. The cutting force is based on the cutting model of saturated sand of (S. A. Miedema, 2014). A sensitivity study on this cutting force is included in the Appendix Figure A.2 to show which parameters will impact the cutting force the most. It can be observed that the porosity of the sand layer is a very sensitive parameter. Further analysis of the cutting force should determine whether a change in this force results in the propulsion model providing a better estimate at higher trailing speeds.
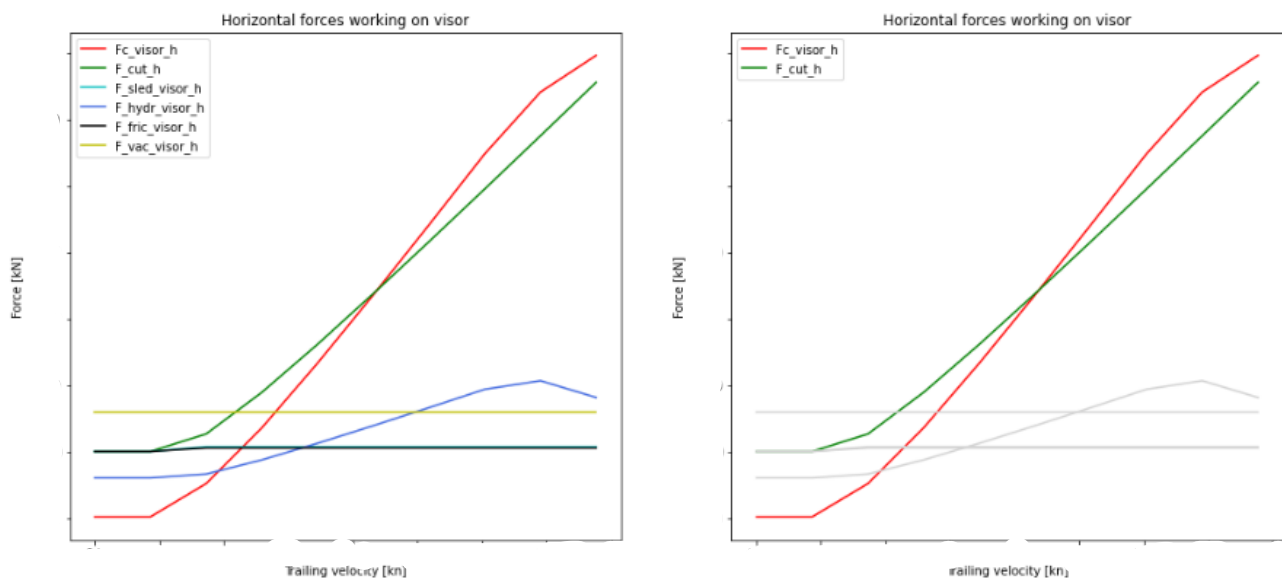
Figure 3.28: Left: all resistance terms working on the visor. Right: cutting force is highlighted since it is the main resistance term working on the visor

3.4   Conclusion

The conclusion of this section answers the second sub research questions:

How to develop and calibrate a physics-based energy estimation model with a real case study?

An experiment plan have been created to develop and calibrate an estimation model to estimate the energy consumption of the propulsion system. This experiment plan exist of the estimation model, actual data analysis of a case study and the calibration of the model.

The model which have been developed is a semi-empirical physics-based estimation model. The physics behind the model describe the different resistance terms on vessel, suction pipe and draghead in which the draghead is the main resistance term. All separate forces working on the components are analysed via FBD's. An important force working on the visor is the cutting force which is described by the cutting model of Sape Miedema (S. A. Miedema, 2014). For now, this model is based solely on cutting sand. Further research will need to incorporate other types of soil. The estimation model was compared and calibrated with a case study. The data has been obtained from sensor data of the HAM318 based on a saturated sand project, which ensures that the cutting model can be applied. Via this data analysis the propulsion power output is analysed based on the set limits of the estimation model. In addition, the non-stationary (project) parameters are analysed so that they can be used as input for the estimation model.

As a final step the output of the estimation model has been compared to the data during the calibration phase. Three pre-defined outcome have been described. The estimation model made a mismatch, does approximately matched, or fully matched the propulsion power output defined within the case study. The first calibration step identified that the model did approximately matches the actual data for some trailing speeds. Because of this, it was chosen to find certain correlations between the visor angle and trailing speed to optimize the model. By finding certain correlations and by applying them in the estimation model it can be seen that the estimation model improved for certain trailing speed ranges. It is also seen that that their is still a mismatch for trailing at low and high velocities. It was identified that this mismatch was because of a fundamental problem in the estimation model and other improvements on the data analysis showed no improved results.

It is concluded that the created semi-empirical physics-based model makes a first estimation of the propulsion power for trailing speed ranges 1.6 [kn] to 1.9 [kn] and that it should be further improved and validated. An important issue in the propulsion model is the static friction term, which accounts for the additional force that must be overcome prior to initiating the movement of the draghead. This exclusion will result in an underestimation of the propulsion power, especially at low trailing speeds. Furthermore the propulsion model tends to overestimate at high trailing speeds, this can probably be related to the high cutting force, in which the porosity parameter seemed to have the greatest effect. It is concluded that the propulsion model can be used, with the set limitations, as a first impression of the propulsion power and it should be improved and validated on other sand cases before implementing it in VO registered estimation models.

4 | Simulation tool

The developed estimation model is compared and calibrated with a case study (section 3) and will now be integrated in a simulation tool to estimate the total energy consumption.
This section answers the third and fourth sub-question:

How to integrate the developed model to estimate the energy consumption during the total loading phase?

How can the energy consumption among different dredging strategies be compared?

The structure of this section is as follows: first the materials and method to develop the plugin for the simulation tool is described. An imaginary case study will be described to test the simulation tool and demonstrate how the different strategies can be compared. The results of this simulation are shown, whereafter a discussion will take place and some conclusions will be made.

4.1 Materials and method

This section elaborates on the development of the plugin for simulation tool and the integration of the developed propulsion model. As a result the developed simulation will be run for an imaginary case study: Project Barachi, which is described in the last subsection.

4.1.1 Plugin

The plugin will be developed to run in a simulation tool which is based on the OpenCLSim python package described in the literature (section 2.7). The energy consumption of the five consumers will be simulated based on different input parameters. The structure of the simulation tool is shown in figure 4.1.

The input for simulating the loading cycle is divided into four boxes. The TSHD input based on input parameters for running the estimation methods, like vessel characteristics and pump characteristics. The Sites parameters, which elaborates on the dredging project as the location of the dredged material. The dredging strategy represented by the operational parameters and the data which is used to estimate the energy of the bow thrusters and the board net.

The calculation box represent the energy plugin where the developed functions are included. The developed functions describe the power needed by the propulsion system, dredge- and jet pumps. In addition the loading duration is also calculated. This loading duration is determined by the excavation production and the size of the hopper (input of TSHD). For now the loading duration is only based on the excavation production, a complete loading model does also need to look at the suction production and settling process. The (highlighted) propulsion model is included in the simulation tool but can only be used based on the defined limits in section 3.4.

The output of the simulation will then show the consumed power, energy, project duration, fuel, emission and corresponding project costs. This can be simulated for one loading cycle but also for the total dredging project.
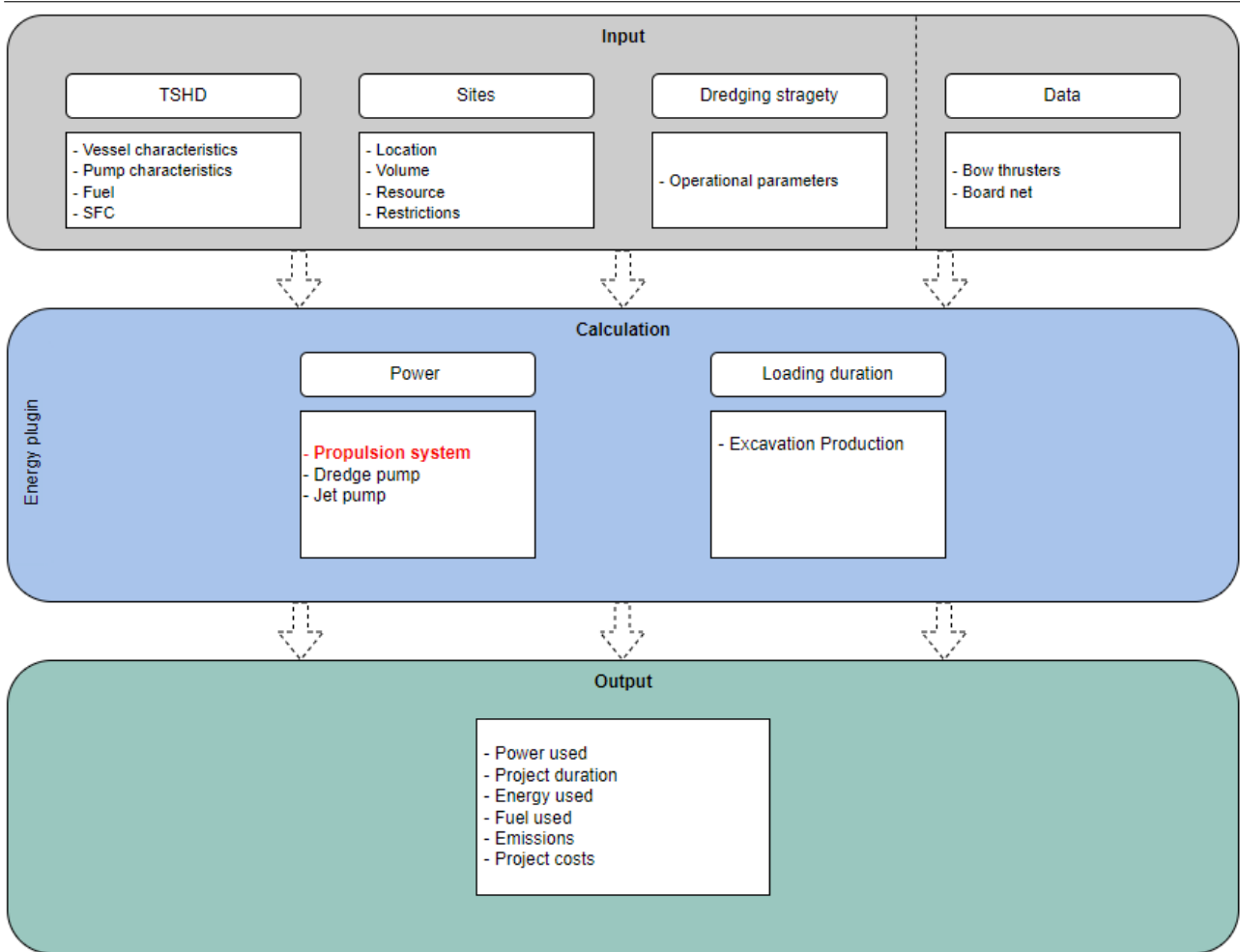
Figure 4.1: The simulation model structure overview

The plugin enables to run the physic based functions during the simulation of the dredging activities. The calculation of the required power and the duration of the loading process is calculated with this energy plugin. Those two terms can be transferred in to energy consumption by the following equation:

$$Energy = \int P dt \tag{4.1}$$

After this, the fuel consumption can easily be calculated when the specific fuel consumption (SFC) of the input fuel is known. The SFC indicates how efficiently a power plant converts chemical into mechanical energy.

$$\text{Fuel consumption} = \text{SFC} * \text{Energy} \tag{4.2}$$

When the fuel costs and vessel costs are known, a first approximation of the project costs can be made by the using the next formula:

$$\text{Costs} = €_{fuel} * fuel + €_{vessel} * t_{project} \tag{4.3}$$

To calculate the emissions, the fuel emission factor can be used. This factor is used to transfer the fuel into emissions.

$$\text{Emission} = \text{Factor} * \text{Fuel} \tag{4.4}$$

The tool is developed as a generic tool in which different dredging phases can be simulated by adding other estimation functions. This study focus on the loading phase, but previous research have already looked at the sailing phases. The description to simulate the total dredging phase is added in Appendix C.1. This study will solely focus on the simulating the results for the loading phase.

4.1.2 City of Barachi

The imaginary city of Barachi is created to make a test run with the simulation tool to show the capabilities of the tool. The case study is the dredging work of an access channel. Two different areas within this access channel should be dredged to a required depth of 18[m]. Dredging area [BC1] is located far offshore and can be seen as a normal dredging area with no limitations. Dredging area [BC2] is located nearby a diving area, which means that several limitations are set during this dredging process. Firstly, to protect the coral reef nearby the dredging area overflow is not permitted. Secondly, due to an environmentally sensitive area, an emission tax is applied. The dredging work will be executed by the biggest TSHD of Van Oord, HAM 318.

The input parameters will be described and listed per input category. The results will show the output of the simulation based on two dredging strategies for the dredging of area BC2.
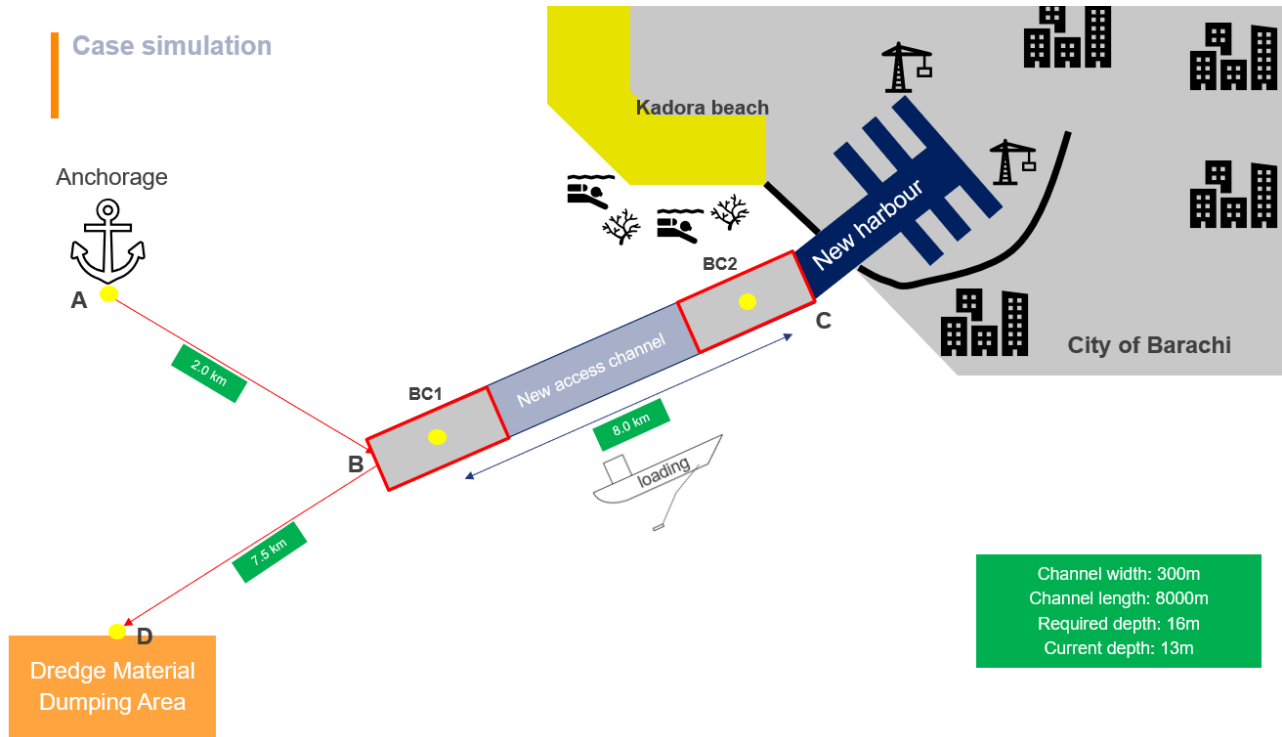
Figure 4.2: Imaginary city of Barachi. Dredging area [BC1]: no limitations. Dredging area [BC2]: overflow not permitted and emissions should be reduced

Sites

The Sites input is based on the project specific characteristics. The location of the loading area, the total amount of material to be dredged (capacity) and the amount of material present during the loading process (resource). Next to these site specific characteristics the environmental limitations should also be described, which could have an impact on the dredging strategy.

Parameter	Value	Unit	Note
Area name	BC2	-	
Location	(24.8; 67.0)	(Lat; Long)	
Capacity	1.8E6	m^3	
Resource	1.8E6	m^3	
Overflow	no	-	
Emission tax	200	€/ton	

Table 4.1: Site characteristics of dredging area BC2

TSHD

The input that is part of the TSHD are the vessel-, pump characteristics and the fuel properties. The vessel characteristics are the stationary parameters based on the dimensions of the vessel, suction pipe and draghead. The pump characteristics describe the input of the dredge- and jet pump calculation models. These are pump data based on pump type and dimensions. The fuel properties include fuel type, caloric value and emissions factors. Some of the parameters are included in table 4.2. The other parameters can be found at section 3.1.1 or via a link to the code archive included in Appendix D.

Parameter	Value	Unit	Note
Type of TSHD	HAM318	-	
Volume hopper minimum overflow	18000.0	m^3	Dummy
Volume hopper maximum overflow	40000.0	m^3	Dummy
Fuel type	VLSFO	-	
Caloric value	50	GJ/t	Dummy
Emission factor CO2e	0.9	t/t	WTT/Dummy
Emission factor CO2e	3.5	t/t	TTW/Dummy
Vessel costs	1 Mil	€/week	Dummy
Fuel costs	1000	€/t	Dummy
Operational hours eff	90	%/week	Dummy

Table 4.2: A selection of the input parameters based on vessel characteristics. Two possibilities to calculate emissions are: WTT (Well-to-tank) and TTW (Tank-to-wheel) (**Note: dummy values have been used due to confidentiality**).

Dredging Strategy

The dredging strategy is based on operational parameters of the dredging vessel. There are many different operational parameters which can be changed to optimize the dredging project. This study will focus on one of them, the trailing speed (v_t).

The vessel wants to sail at highest cost efficiency if no other restrictions are present. This often means that trailing on high velocity is preferred to reduce the loading time, since the vessel operation cost are normative (table 4.2).
Other dredging strategies can be more applicable when restrictions are present. Restriction rugulations on emissions may result in a change of dredging strategy. Trailing at low speed will decrease the power consumption, but will increase the loading time. The question is therefore what the optimal ratio will be to reduce the consumed energy (emissions), to lower the impact of the emission tax.

The developed propulsion model is represented in section 3 and the conclusion is made that the developed model could only be used between trailing velocity 1.6 [kn] and 1.9 [kn]. The outer limits will be used to compare the dredging strategy on trailing slow ($v_t = 1.6[kn]$) and fast ($v_t = 1.9[kn]$).

- Strategy 1: $v_t = 1.6[kn]$
- Strategy 2: $v_t = 1.9[kn]$

Data

The data input is based on the data analysis of a similar dredging project (Karachi) and is used to determine the power consumed by the bow thrusters and board net. The board net is assumed to be active during the total loading phase and the active time of the bow thrusters is analysed per loading cycle. The result of this analysis can be found in Appendix C.3. This analysis have shown that the activity duration of the bow thrusters during the loading phase is around 10% of the total loading time.

System	Retrieved data	value	unit
Bow thrusters	Power	1400	[kW]
	Time	10% loading duration	[min]
Board net	Power	2050	[kW]
	Time	loading duration	[min]

Table 4.3: Data retrieved via case study analysis and current Van Oord assumptions (**Note: dummy values have been used due to confidentiality**)

4.2 Results

This section will present the simulation results for two dredging strategies ($v_t = 1.6[kn]$ and $v_t = 1.9[kn]$) in the imaginary case study of Barachi. The exact values shown for each category are mainly intended to provide an impression of the tool's capabilities. Due to the limitations of the physics-based models and the global assumptions regarding emissions and costs, the exact values are not critically important.

The simulation tool will provide estimates of project duration, project characteristics (such as required power, energy consumption, fuel usage, and emissions), and project costs. One of the primary capabilities of this simulation tool is the ability to predict time- and location-specific emissions based on dredging strategies. This means that an emission pattern can be created based on the dredging strategies, indicating where, for example, fine emissions will be present in the air. Therefore, it is possible to make a choice to limit these emissions at a certain location, such as near a sensitive area.

The next subsection will give an overview of the simulation results per category.

4.2.1 Project duration

The excavation production will increase with increasing trail speed with 27 m^3/min. The loading time until overflow will therefore decrease by 5 min. With respect to the dredging of the total area BC2 this means a decrease of $\approx 18[hrs]$. Dredging with the higher trailing velocity shows therefore a decrease in project duration of approximate 9%.

Dredging stragety	Calculated	value	unit
$v_t = 1.6[kn]$	Loading rate	289	$[m^3/min]$
	Loading time	54	[min]
$v_t = 1.9[kn]$	Loading rate	316	$[m^3/min]$
	Loading time	49	[min]

Table 4.4: Data retrieved via case study analysis and current Van Oord assumptions
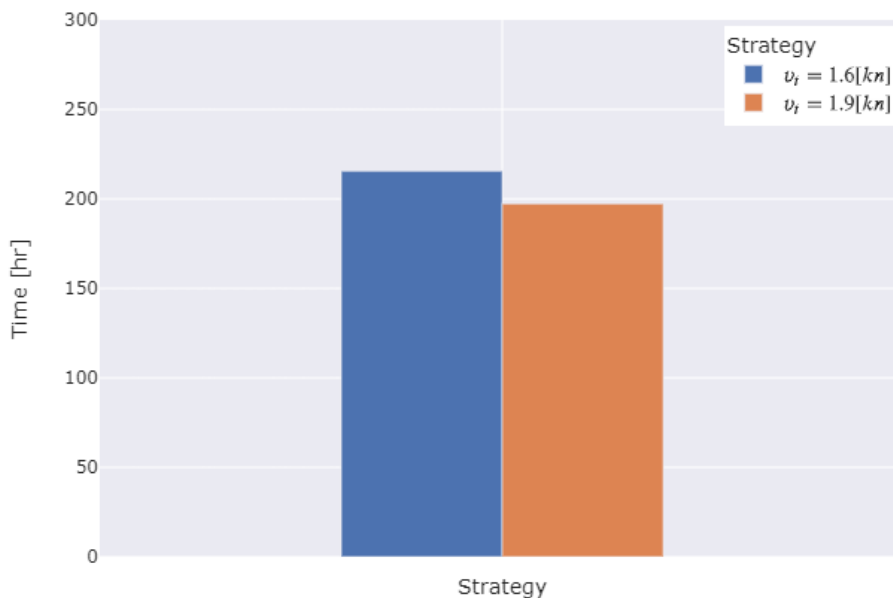
Figure 4.3: Project duration for two dredging strategies

4.2.2 Project characteristics

The project characteristics which results form the output of simulation are power, energy, fuel and emissions. The required power per system is plotted in Figure 4.4. It can be observed that by changing the trailing velocity only the propulsion power will increase and the rest of the systems will remain constant. The propulsion power will increase by approximate 2000 [kw] which means that the total power consumption will increase with approximate 17 %.
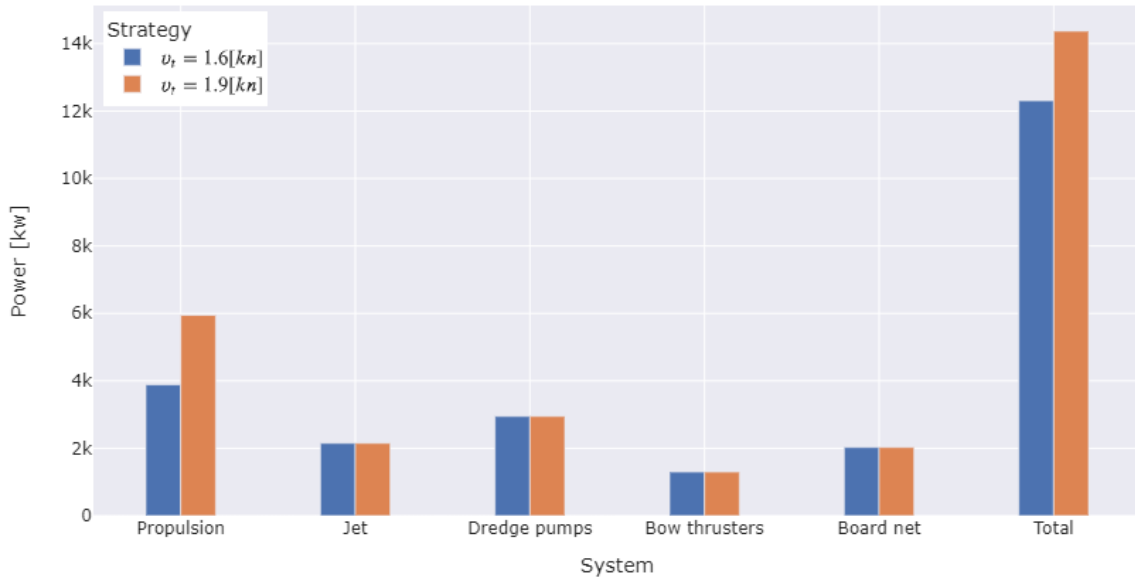
Figure 4.4: Required power per system for two dredging strategies

The energy consumption per system is shown in figure Figure 4.5. The project duration (subsection 4.2.1) is used to calculate the energy consumption of the systems. The bow thrusters are only 10% active during the loading phase which can be observed in the energy consumption in respect to the other consumers. The result of the energy consumption shows that the increase in power has a greater effect on energy consumption than the decrease in project duration. The total energy consumption will increase with approximate 8%.
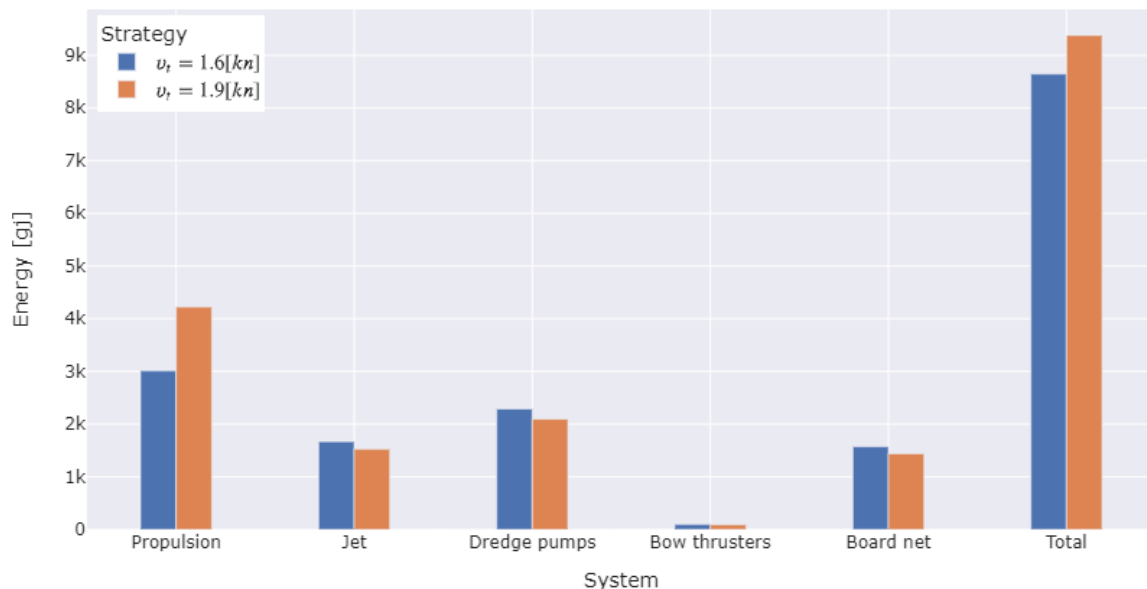
Figure 4.5: Consumed energy per system for two dredging strategies

The ratio observed for energy consumption is also seen in fuel use and emissions per system. Quantitatively, increasing the trailing speed from $v_t = 1.6[kn]$ to $v_t = 1.9[kn]$ results in a total fuel consumption increase of 18 tons. The fuel used in this result is VLSFO, other fuels can also be used as input.
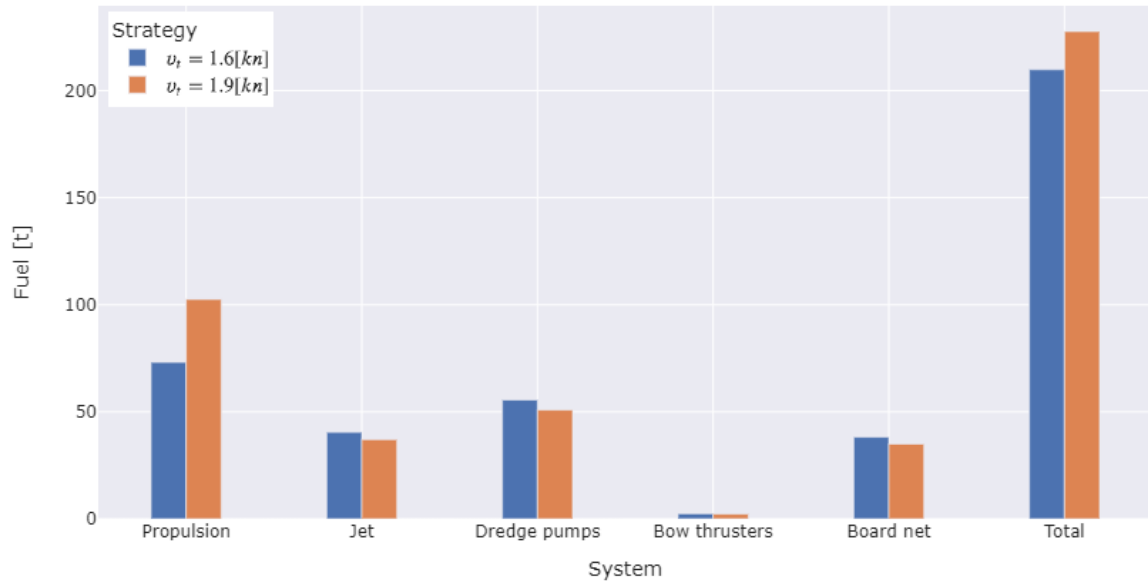
Figure 4.6: Consumed fuel per system for two dredging strategies

The difference in emissions is shown in Figure 4.7. The tool can predict the emissions per system as well as the total emissions. When other emission factors are known, the tool can also estimate other greenhouse gas emissions corresponding to certain fuels and determine the location of the emitted emissions. These capabilities could be very useful in predicting the quantity of fine particles in sensitive areas.
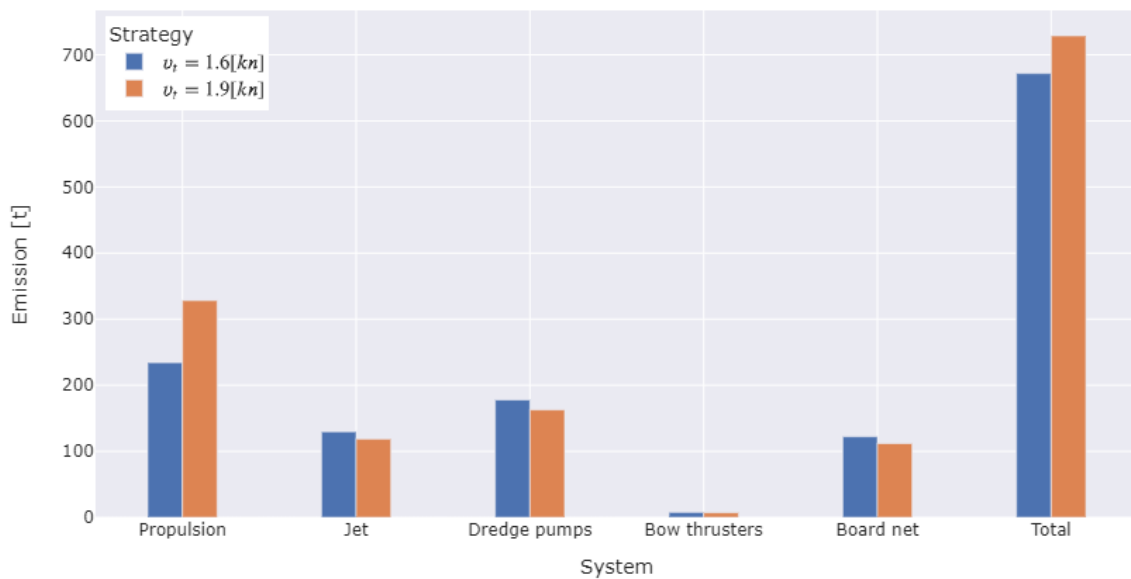
Figure 4.7: Emissions (CO2e) per system for two dredging strategies

4.2.3 Project costs

The simulation tool shows a first estimation of three different project costs based on the two dredging strategies: the vessel operation costs, the fuel costs and the emission tax which is applied on this project.

The results show that dredging at the high trailing speed of 1.9 [kn] will be the most cost efficient dredging strategy (Figure 4.8). Because the ship's operating costs are governing, in this case, faster trailing is the most cost-efficient (6.5%), even if an emission tax of 200 euros/ton is applied. Fuel costs and emission costs are both cheaper at sailing slow.

The break even point on the emission tax can be found by solving Equation 4.5. The dredging strategy will change if the emission tax will be higher than approximate € 1580/ton CO2.

$$1.28 + 0.21 + 671.80 * tax = 1.17 + 0.23 + 728.7734 * tax \tag{4.5}$$
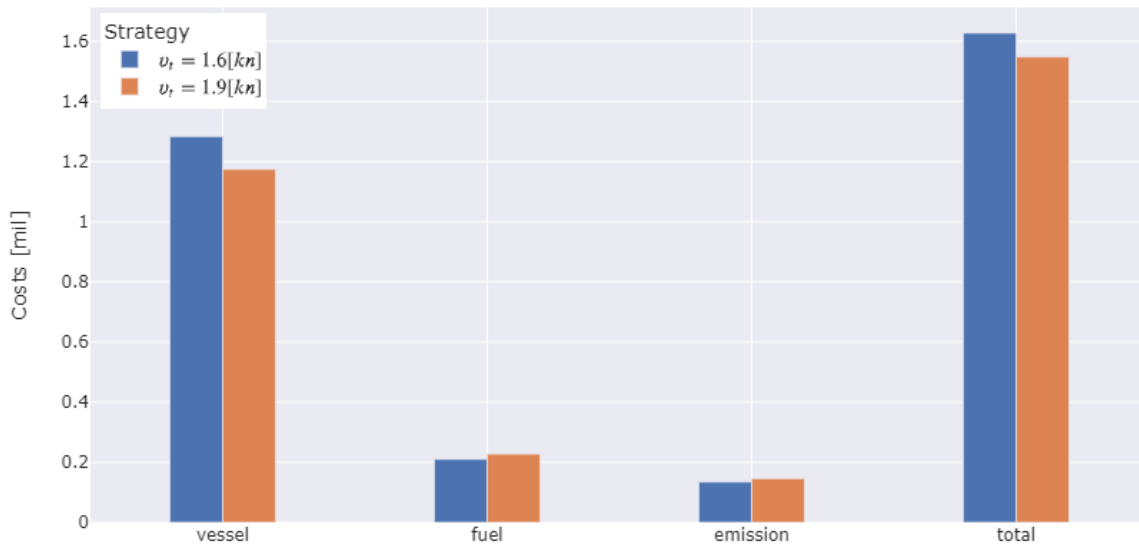
Figure 4.8: The costs of the project, including: vessel, emission tax and fuel

Dredging stragety	Calculated	value	unit
$v_t = 1.6[kn]$	Vessel	1.28	Mil €
	Fuel	0.21	Mil €
	Emission	0.13	Mil €
$v_t = 1.9[kn]$	Vessel	1.17	Mil €
	Fuel	0.23	Mil €
	Emission	0.15	Mil €

Table 4.5: Overview of the estimated costs of the project, it can be observed that the operating costs of the vessel are normative

4.3 Discussion

The current integrated propulsion model is only applicable for trailing speeds within the range of 1.6-1.9 knots, and has not yet undergone any validation procedures. As a result, utilizing this model in the developed plugin may lead to an inaccurate estimation of power, which will in turn affect the estimation of other project factors such as fuel consumption, emissions, and costs. In order to ensure the accuracy of the power estimation, it is necessary to first improve the propulsion model, based on the points discussed in the previous section. Only then can the model be used with confidence in the developed plugin.

Focusing exclusively on the loading phase results can lead to a distorted view of the entire dredging process. It is important to consider the entirety of the dredging cycle when creating a plan for a dredging project, as decisions based solely on the loading process can have significant impacts on the dredging cycle. A dredging strategy that appears to be cost-efficient during the loading phase may not necessarily be the most efficient approach when considering the entire dredging cycle. Therefore, it is critical to take the entire dredging cycle into account when making decisions regarding dredging strategy.

Power consumption of the dredge- and jet pumps are based on an in house Van Oord physics based model. This model does calculate the power consumption of the pumps based on operational parameters. However, the correct power consumption still needs to be established by adjusting the friction factor in the model, as observed by comparisons with actual data. Therefore, in order to apply this model more widely, these factors must first be clearly established for each vessel and installed pump.

The plugin developed for the vessel does not account for the total installed power, which can potentially result in an excessive power consumption by all five power consumers on board. If operational parameters are modified such that 80% of the total power consumption is attributed to the propulsion system, only 20% of the available power will be allocated to the other power consumers onboard in practice. This phenomenon assumes critical significance during the loading phase, when all power consumers are simultaneously operational.

The energy consumption estimates for two of the energy consumers in the current model are still based on empirical data. In order to provide more accurate estimations based on operational parameters, these models must be updated to semi-empirical physics-based models. Furthermore, the estimation for energy consumption by the bow-thrusters is currently based solely on data from one dredging project (Karachi), resulting in a lower accuracy of predictions for future projects. Finally, the board net energy consumption is still assumed based on empirical data utilized by Van Oord.

The simulation tool currently has limited applicability, as it can only be utilized for dredging projects involving saturated sand (due to the propulsion model) and loading duration is calculated solely based on excavation production. This can result in inaccuracies as the suction production should also be included to calculate loading duration until overflow. Currently, it is assumed that the suction production equals the excavation production, as vacuum is generally not a limiting factor in dredging projects at shallow water depths. Additionally, the excavation production could be increased by including an erosion term, which is currently set to zero. To expand the applicability of the simulation tool, the settling process duration should be incorporated into the model to enable its use in dredging projects involving overflow.

4.4 Conclusion

The conclusion of this section provides an answer to the following two sub-research questions:

How to integrate the developed model to estimate the energy consumption during the total loading phase?

How can the energy consumption among different dredging strategies be compared?

A plugin have been developed based on the OpenCLSim python package to simulate the energy consumption during the total loading phase based on operational parameters. The developed semi-empirical method to estimate the propulsion power is integrated in this plugin, together with the four other methods which are described in the literature. In addition, the excavation production is used to calculate the loading duration of filling the hopper until overflow. The time and power term can then be used to calculate the energy consumption per consumer ($E = \int P dt$).

To compare the energy consumption of two dredging strategies, the plugin has been integrated into the Open-CLSim Python package. The simulation tool runs based on four input characteristics: vessel parameters (TSHD), site characteristics, dredging strategy, and data describing the bow thrusters and board net. The output of the plugin after running the simulation includes required power, duration, and consumed energy. Additionally, the plugin can estimate fuel usage, emissions, and project costs associated with energy consumption.

The main result of the simulation is the tool's ability to visualize energy consumption (and emissions) based on dredging strategies and location. This enables the prediction and potential reduction of emissions in sensitive areas, such as fine dust emissions near cities. By using this simulation tool, a dredging plan can be created based on dredging strategies (trailing speed) to reduce emissions in these sensitive areas. To better demonstrate the other capabilities of the developed plugin within the OpenCLSim Python package, the simulation tool is applied to an imaginary project called Barachi. This project has strict regulations that prohibit overflow and apply emission taxes. Two dredging strategies are compared based on the limitations of the developed propulsion model: trailing speeds of 1.6 [kn] and 1.9 [kn]. By increasing the trailing speed from 1.6 [kn] to 1.9 [kn] the simulation tool shows the following results:

- A decrease in project duration: The filling of the hopper will decrease with 5 [min], for the entire project duration this means a decrease 8% or 18 [hrs].
- An increase in required power: The required power of the propulsion system will increase with approximate 2000 [kW], in respect tot the total power consumption this means a increase of 17%. The other power consumers remain constant.
- An increase in energy consumption: The increase in power has a greater effect on he energy consumption than the decrease in project duration. The total energy consumption will increase with approximate 8%.
- An increase of fuel consumption and emissions: The corresponding fuel consumption and emissions will increase corresponding the energy consumption. Quantitatively, this means that the total fuel consumption increases by 18 tons and the CO2e emissions increases by 57 tons.
- A decrease of total project costs: The vessel operation costs are normative and thus it is observed that faster trailing is most cost-efficient (6.5%), even if an emission tax of 200 euros/ton CO2e is applied.

In conclusion, the propulsion model has been successfully integrated (with set limits) into a plugin for the Open-CLSim python package, which includes other energy consumers and a time estimator to enable the estimation of energy consumption during the loading phase of a dredging cycle. The main result of the simulation tool is the ability to visualize energy consumption (and emissions) based on dredging strategies and location. The simulation tool has been tested using an imaginary case study, where two dredging strategies based on trailing speed were studied. The energy consumption of each strategy was compared, and with a simple conversion, the fuel consumption, emissions, and costs of the project could also be estimated. As a result, this simulation tool provides a potential useful tool for dredging strategy planning. When the tool is improved based on the discussion points the tool can be utilized to make informed decisions regarding energy consumption, fuel usage, and cost estimates for future dredging projects.

5 | Discussion

This section provides an overview of the main discussion points related to both the propulsion model and the simulation tool. A comprehensive discussion of these topics is presented in the respective sections.

Regarding the propulsion model, the main discussion points are the limited range of trailing speeds for which the model gives an estimate of the energy consumption and the need for further validation of the model. The model is currently limited to trailing speeds between 1.6-1.9 [kn], outside this range the accuracy of the energy consumption prediction is inaccurate. Therefore, to improve the model's accuracy and increase its range of applicability in different soil types, further research is needed.

An important issue in the propulsion model is the exclusion of the static friction term, which accounts for the additional force that must be applied prior to initiating the movement of the draghead. The current propulsion model output start at zero, which means that by increasing the power the vessel can immediately start moving. In reality, a higher power input is necessary to initiate vessel movement. As a result, the model significantly underestimates the power consumption of the propulsion system.

Furthermore, the propulsion model tends to overestimate the power consumption at higher trailing speeds. An analysis of the forces acting on the draghead and visor revealed that the cutting force is the primary source of the high resistance force at high trailing speeds. Additionally, a sensitivity analysis has demonstrated that the soil conditions, specifically the porosity of the sand, play a crucial role in estimating the resistance force.

For the simulation tool, the main discussion points include the limitations of the tool and the importance of considering the entire dredging cycle when using this tool in the decision making. The tool is currently limited to dredging projects in saturated sands, and the loading duration is only based on excavation production, which inaccurately predicts the loading time until overflow. Furthermore, the current integrated propulsion model is only applicable for trailing speeds within the range of 1.6-1.9 knots, and has not yet undergone any validation procedures. As a result, utilizing this model in the developed plugin may lead to an inaccurate estimation of power, which will in turn affect the estimation of other project factors such as fuel consumption, emissions, and costs.

The plugin does not account for the total installed power, which can potentially result in an excessive power consumption by all five power consumers on board. If operational parameters are altered such that 80% of the total available power is consumed by the propulsion system, then only 20% of the available power will be allocated to the other power consumers onboard. This phenomenon is critical during the loading phase, when all power consumers are simultaneously operational.

Additionally, the tool only estimates energy consumption during the loading phase. A dredging strategy that appears to be cost-efficient for the loading phase may not necessarily be the most cost-efficient approach when considering the entire dredging cycle. Therefore, it is important to consider the entire dredging cycle when making decisions regarding dredging strategies.

6 | Conclusion

The dredging industry is expected to face stricter regulations on greenhouse gas (GHG) emissions in the future. To minimize costs associated with high GHG footprints, it is essential for contractors to accurately estimate their energy consumption based on different dredging strategies. Currently, the estimation method used by Van Oord can accurately estimate energy consumption for the majority of dredging projects based on empirical data. However, for more complex dredging activities, the empirical data may result in a less accurate estimation. Previous research has focused to improve this estimation for the sailing phases of the dredging process. This study focuses on the loading phase and the main objective of this research is:

To quantify the energy consumption of different TSHD dredging strategies based on physics for the loading phase.

To achieve this research objective multiple sub-questions were formulated. The answers to these sub-questions are answered step-wise.

1. Which methods are available to quantify the energy consumption during the loading phase based on physics?
A literature study was conducted to investigate the available methods and literature to quantify the energy consumption during the loading phase based on physics. The study identified five main energy consumers and presented a method for calculating the required power of each. In combination with the loading duration the energy consumption can be calculated. The power required for the dredge and jet pumps is estimated using an in-house Van Oord model. The board net power is calculated based on current assumptions, and the energy consumption of the bow thrusters is estimated based on data analysis. The literature study revealed that no suitable model was available to estimate the required power of the propulsion system of the THSD of Van Oord. Previous studies have demonstrated a method for calculating the resistance terms on the vessel, suction pipe, and draghead system. The aim of this research was to develop a physics-based method to calculate the required power of the propulsion system based on these resistance terms. Additionally, a method was missing which could combine the five different power calculation methods to estimate the total energy consumption during the loading phase.

2. How to develop a semi-empirical physics-based energy estimation model and calibrate with a real case study?
In order to accurately quantify the required power of the propulsion system during the loading phase, an experiment plan has been developed to create and calibrate an estimation model. This plan includes the development of a semi-empirical, physics-based estimation model, as well as actual data analysis from a case study and calibration of the model. The estimation model is based on the physics of the different resistance terms on the vessel, the suction pipe, and the draghead, with the draghead being observed as the primary resistance term. At present, the model is only based on cutting sand, and further research will be necessary to incorporate other types of soil. The model has been compared and calibrated using actual data from a case study. During data analysis, the propulsion power output was examined based on the boundaries set by the estimation model. Non-stationary project parameters (trailing speed, visor angle) were also analyzed for use as input in the estimation model. Finally, the estimation model was compared to the data during the calibration phase. Based on the filtered dataset, three possible outcomes were described, namely a mismatch, an approximate match and a full match between the estimation model and the data. The calibration phase thus served to show the accuracy and reliability of the estimation model.

It is concluded that the created semi-empirical physics-based model makes a first estimation of the propulsion power for trailing speed ranges 1.6 [kn] to 1.9 [kn] and that it should be further improved and validated. An important issue in the propulsion model is the exclusion of the static friction term, which accounts for the additional force that must be overcome prior to initiating the movement of the draghead. This exclusion will result in an underestimation of the propulsion power, especially at low trailing speeds. Furthermore the propulsion model tends to overestimate at high trailing speeds, this can probably be related to the high cutting force, in

which the porosity parameter seemed to have the greatest effect. It is concluded that the propulsion model can be used, with the set limitations, as a first impression and it should be improved and validated on other sand cases before implementing it in Van Oord registered estimation models.

3. How to integrate the developed model to estimate the energy consumption during the total loading phase?
To estimate the total energy consumption during the loading phase, a plugin has been developed for the Open-CLSim python package. The developed semi-empirical method to estimate the propulsion power has been integrated in this plugin (with the set limitations) together with the four other methods which have already been described in the literature. In addition, the excavation production was used to calculate the loading duration of filling the hopper until overflow. This plugin enables the user to make a first estimate of the energy consumption during the loading phase. It should be noted that the plugin does not account for the total installed power, which can potentially result in an excessive power consumption by all five power consumers on board. This phenomenon is especially important during the loading phase, when all power consumers are simultaneously operational. Additionally, the integrated calculation methods should be further improved to provide a more accurate estimation.

4. How can the energy consumption among different dredging strategies be compared?
To compare the energy consumption of dredging strategies, the plugin has been integrated into the OpenCLSim Python package. The simulation tool runs based on four input characteristics: vessel parameters (TSHD), site characteristics, dredging strategy, and data describing the bow thrusters and board net. The output of the plugin after running the simulation includes required power, duration, and consumed energy. Additionally, the plugin can estimate fuel usage, emissions, and project costs associated with energy consumption.

The main result of the simulation is the tool's ability to visualize energy consumption (and emissions) based on dredging strategies and location. This enables the prediction and potential reduction of emissions in sensitive areas, such as fine dust emissions near cities. By using this simulation tool, a dredging plan can be created based on dredging strategies (trailing speed) to reduce emissions in these sensitive areas. To better demonstrate the other capabilities of the developed plugin within the OpenCLSim Python package, the simulation tool is applied to an imaginary project called Barachi. This project has strict regulations that prohibit overflow and apply emission taxes. Two dredging strategies are compared based on the limitations of the developed propulsion model: trailing speeds of 1.6 [kn] and 1.9 [kn]. By increasing the trailing speed from 1.6 [kn] to 1.9 [kn] the simulation tool shows the following results:

- A decrease in project duration: The filling of the hopper will decrease with 5 [min], for the entire project duration this means a decrease 8% or 18 [hrs].
- An increase in required power: The required power of the propulsion system will increase with approximate 2000 [kW], in respect tot the total power consumption this means a increase of 17%. The other power consumers remain constant.
- An increase in energy consumption: The increase in power has a greater effect on he energy consumption than the decrease in project duration. The total energy consumption will increase with approximate 8%.
- An increase of fuel consumption and emissions: The corresponding fuel consumption and emissions will increase corresponding the energy consumption. Quantitatively, this means that the total fuel consumption increases by 18 tons and the CO2e emissions increases by 57 tons.
- A decrease of total project costs: The vessel operation costs are normative and thus it is observed that faster trailing is most cost-efficient (6.5%), even if an emission tax of 200 euros/ton CO2e is applied.

The simulation tool currently has limited applicability, as it can only be utilized for the loading phase of a dredging project. Dredging strategies decisions made solely based on this could have a significant impact on the overall dredging cycle. Therefore, it is important to consider the entire dredging cycle when making decisions regarding dredging strategies. In addition, the loading duration is solely based on the filling until overflow and the model can only be applied on sandy soils.

All in all, the plugin developed for the OpenCLSim software has demonstrated the ability to quantify the energy consumption of various TSHD dredging strategies during the loading phase. This plugin is used in combination with the OpenCLSim software and makes use of different input parameters (vessel, site, data and dredging strategy) to compare dredging strategies on the energy consumption for the loading phase of a dredging project. The main tool's ability is to visualize energy consumption (and emissions) based on dredging strategies and location, which can help during the planning of a dredging project. More research is needed to improve the accuracy of the energy estimations made during the loading cycle, especially the propulsion model which is integrated in the plugin should be further developed and validated.

7 | Recommendations

In this section some recommendations are provided for the future directions of this study. These are based on the discussion and conclusion from section 5 and 6 respectively.

1. The static friction component should be included in the propulsion model which could potentially solve the underestimation at lower trailing speed. The first approach would be to add an extra force on top of the friction term of the draghead, equation 7.1. The quantity of this force could be observed via data analysis.

$$F_{c,draghead,h} = F_{c,visor,h} + F_{fric,draghead,h} + F_{sled,draghead,h}$$
$$+ F_{imp,vac,draghead,h} + F_{imp,jet,draghead,h} \quad (7.1)$$

2. The cutting force is observed as the primary contributor to the high resistance forces at trailing speed ($v_t > 2.0[kn]$). Inclusion of the static friction term is expected to further increase these resistance forces. However, since the cutting forces are solely predicted on the cutting of sand and are already based on averaged soil conditions (S. A. Miedema, 2014), the option to adjust the cutting force based on actual data can be explored. This would entail determining a coefficient per soil type through data analysis, to improve the estimation model to better match within the confidence region of the data set. While this would convert the model into a semi-empirical one, it would still be physics based on dredging strategies. If the model is improved and better matches the actual data, it should be validated by comparing it with new comparable datasets. The model should fall within the confidence region of the dataset. Figure 7.1 shows the idea on tuning the estimation model to fall within the confidence region of the dataset. For now, this line is adjusted by adding 3200 [kW] for the static friction and by transferring the visor angle to a very low value.
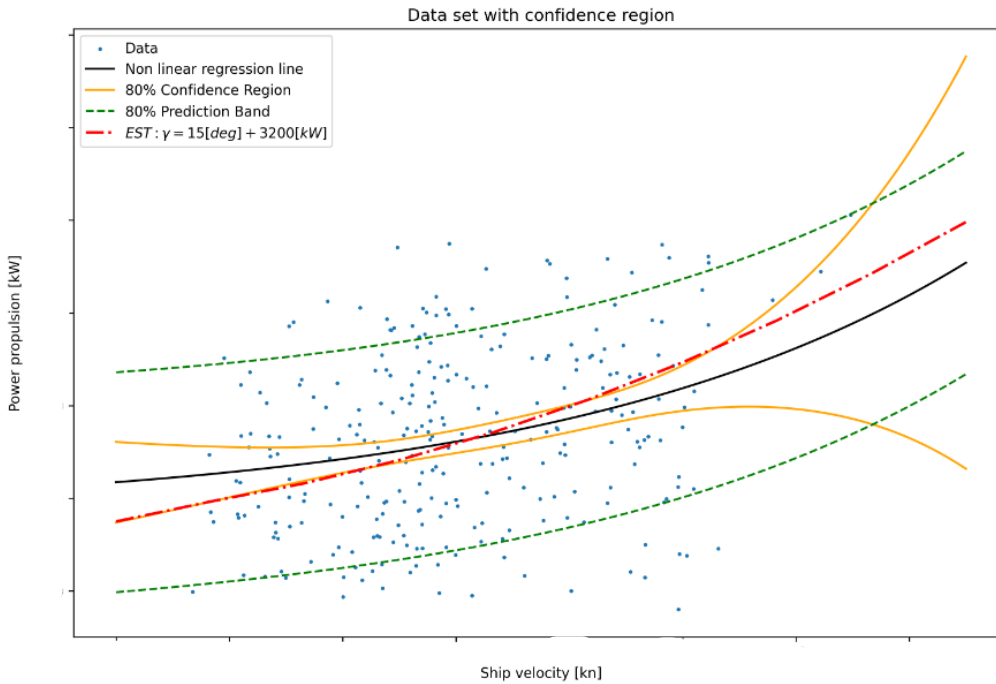
Figure 7.1: A first outline of the approach of tuning the cutting force. By adding a static friction force and by changing the visor angle the estimation model can be fit within the confidence interval of the dataset (**Note: axis confidential**).

3. The sample size of the dataset used for actual data analysis should be increased to improve the reliability of the results. This can be done by adding data of similar dredging project (waterdepth, soil conditions). Furthermore, additional filters should be added to focus more specifically on the dredging part of the loading phase. Currently, the dataset includes a significant amount of data that does not accurately reflect the forces present during dredging. Filters are applied such as a threshold on the draghead depth, but this does not particularly reflect if the material is really dredged. By implementing a filter based on the density of the material being dredged, a threshold can be established above which data will be included in the analysis. This approach is expected to improve the accuracy of the analysis. This will also effect the analysis of the non-stationary project parameters for the estimation model.

4. The plugin should be modified to account for the total installed power of the vessel. During the loading phase, all five power consumers are simultaneously operational, which can result in excessive power consumption. Therefore, it is important to consider the total installed power to ensure that the energy estimations will not pass this maximum power. There are different ways of implementing this set limit. A power limit can be implemented in the estimation functions based on maximum power available per dredging phase. Or, it can be chosen to implement limits in the simulation tool based on operational parameters. For example, when trailing the power consumption of the propulsion system cannot pass x [kw]. An equation can be implemented, in which is calculated how much power is left for the propulsion system based on the other consumers. Thereby, a maximum power is attributed to the propulsion system based on other power consumption. The maximum power will in this way also limit the trailing speed of the vessel.

5. The use of the tool is limited to dredging projects where overflow is not allowed. For now, the excavation production, which is determined by the propulsion model, is used as predictor for the loading time until overflow. However, the suction production should also be added to this equation since it can have an effect on the production, especially when dredging in deep waters, where vacuum can be limited. In addition, to widen the capabilities of the tool the settling process in the hopper should also be added. As result, the simulation can also be used in dredging project where overflow is allowed. There are several models available to calculate the settling process. A 2DV model is derived by Cees van Rhee, which takes the two dimensional array of the hopper into account and Sape Miedema made some adjustments to the Camp model. It is recommended to use the modified model of Miedema, since it gives results that match the method of van Rhee, with a higher speed of calculation S. Miedema, 2008.

6. To be able to estimate the energy consumption for the entire dredging project, it is essential to implement methods for the unloading phase. While various power consumption estimation techniques such as the in-house Van Oord pump methods, the board net, and the bow thrusters can already be utilized to determine the energy consumption during this phase, it is crucial to include the various unloading strategies, including dumping, pumping, and rainbowing, in the calculations.The in-house Van Oord methods can be adjusted to estimate these consumers and by analysing actual data these models can validated.

7. As for now the loading area is visualized by one point. The vessel sails to this point and the power of the different consumers is calculated based on the loading duration. The simulator will therefore calculate the propulsion energy based on the duration of the loading cycle, but during the simulation the vessel remains at one place. In reality the vessel will sail during loading and will finish the loading phase at another location, either further away or closer to the dumping area (Figure 7.2). This difference will have an effect on the sailing distance to the dumping area and therefore on the energy consumption of the sailing phases.
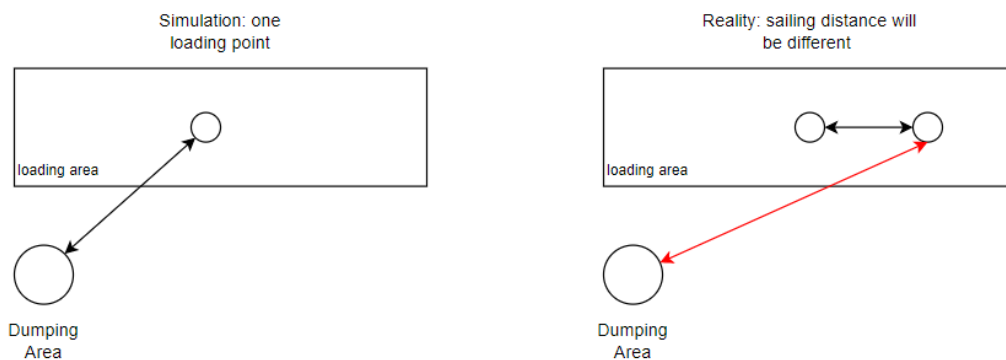
Figure 7.2: The loading phase is currently visualized by one point. In reality the distance to the dumping area will be different as the vessel is moving while it is loading. This location change will have an impact on the sailing distance to the dumping area.

To make a more accurate simulation of the loading process in respect to the total dredging cycle some adjustments should be made to the OpenCLSim Activities. The loading of a vessel is simulated by the ShiftAmountActivity. This activity is developed based on the loading of a container vessel, which remains at one location near the quay wall. To include the movement of the TSHD during loading the ParallelAcitivity can be used where the ShiftAmountActivity and the MoveActivity can be run at the same time. However as for now, this gives an error in logging the location of the vessel. The ShiftAmountActivity is programmed to remain at one location. It is recommended to adjust the location tracker in the ShiftAmountActivity to enable moving while loading. The first adjustments to the ShiftAmountActivity code are already done and will be included in Appendix D, Code Archive.

In addition, the loading area should be visualized by many different points based on the center of gravity of the loading area. The vessel should sail from point to point and grab material from the point where it started to move. When arrived at the next point the vessel should check its hopper capacity, if full than start sailing to the dumping area, if not, keep on moving to the next point and start grabbing material from this point. This process is visualized in figure Figure 7.3,
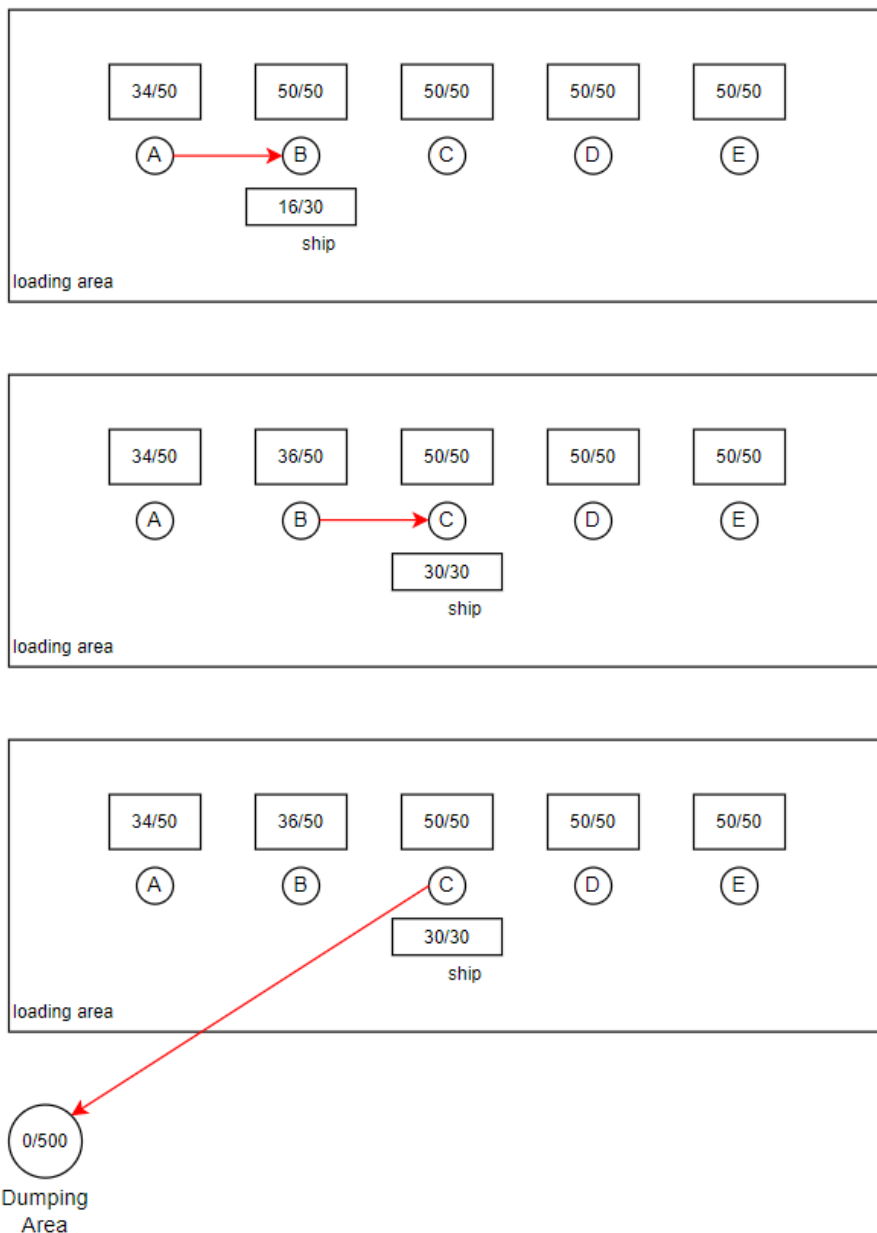
Figure 7.3: The visualization of including extra sailing distance in dredging cycle. The points represent the center of gravity of the material in the loading area. The vessel sails from point A to B and grab material from the point of origin (A). When arriving at point B the vessel will do a hopper capacity check, if not full than keeps on moving to the next point (C). Again a check, if full than start sailing to dumping area.

Bibliography

Castro, B. G., Ooijens, S., & Van Ingen, L. (2014). Approaching emissions in dredging. *Terra et Aqua, 137*, 19–26.

de Groot, J. (1981). *Rapport beunbezinking (in dutch) [master thesis]*. Delft University of Technology.

de Jonge, K. (2017). A trailing suction hopper dredge draghead production model [master thesis].

DredgingToday. (2022). Tshd swalinge deliverd and ready for action [figure]. https://www.lib.sfu.ca/help/cite-write/citation-style-guides/apa/tables-figures

Google. (2022). Port of karachi [figure]. https://www.google.nl/maps/place/Karachi+Port/@24.8221914,67.0027448,11.67z/data=!4m5!3m4!1s0x3eb315e31e0c631d:0xfb799c0236d87108!8m2!3d24.835865!4d66.9831639

Holtrop, J., & Mennen, G. (1982). An approximate power prediction method. *International Shipbuilding Progress, 29*(335), 166–170.

IADC. (2022). Uwp centrifugal pump [figure]. https://www.iadc-dredging.com/wp-content/uploads/2022/04/Equipment-TSHD.pdf

Jacoby, M. (2022). The shipping industry looks for green fuels. https://cen.acs.org/environment/greenhouse-gases/shipping-industry-looks-green-fuels/100/i8

Lamers, S. (2022). Evaluation and improvement of energy consumption estimation methods specified on sailing activities with the use of actual data.

Marine Insight. (2021a). Bow thrusters: Construction and working. https://www.marineinsight.com/tech/bow-thrusters-construction-and-working/

Marine Insight. (2021b). How the power requirement of a ship is estimated? https://www.marineinsight.com/naval-architecture/power-requirement-ship-estimated/

Mestemaker, B., van den Heuvel, H., & Gonalves Castro, B. (2020). Designing the zero emission vessels of the future: Technologic, economic and environmental aspects. *International Shipbuilding Progress, 67*(1), 5–31.

Miedema, S. (2008). An analytical approach to the sedimentation process in trailing suction hopper dredges. *Terra et Aqua, 110*.

Miedema, S. (2019). Production estimation of water jets and cutting blades in drag heads, dredging summit expo '19 proceedings.

Miedema, S. A. (2014). *The delft sand, clay and rock cutting model - pore pressure model*. IOS Press.

RoyalIHC. (2022). Ibp centrifugal pump [figure]. https://www.dutchwatersector.com/news/ihc-to-deliver-double-walled-onboard-dredging-pumps-to-jan-de-nul-group

RVO. (2023). Hollandse kust (west) wind farm zone. https://english.rvo.nl/sites/default/files/2023/01/Beoordelingssystematiek-ecologie-Hollandse-Kust-west-kavel-VI.pdf

Saltelli, A., Ratto, M., Andres, T., Campolongo, F., Cariboni, J., Gatelli, D., Saisana, M., & Tarantola, S. (2008). *Global sensitivity analysis: The primer*. John Wiley; Sons.

Simi, A., & RadoDejan. (2013). On energy efficiency of inland waterway self-propelled cargo vessels. *FME Transactions, 41*(2), 138–145.

ter Meulen, G. (2018). Draghead analysis: An analysis of the draghead's physical processes to determine the trailing forces and the production.

TET. (2017). Pakistan's first deep-water terminal to be ready in april. https://tribune.com.pk/story/1294318/karachi-port-pakistans-first-deep-water-terminal-ready-april

van der Bilt, V. (2019). Assessing emission performance of dredging projects [Tu Delft].

Van Rhee, C. (2002). Modelling the sedimentation process in a trailing suction hopper dredger. *Terra et Aqua*, 18–27.

van Koningsveld, M. (2019). Open source complex logistics simulation. https://openclsim.readthedocs.io/en/latest/

van Koningsveld, M., Verheij, H., Taneja, P., & de Vriend, H. (2021). *Ports and waterways - navigating the changing world*. Delft University of Technology, Hydraulic engineering, Ports; Waterways, Delft,The Netherlands.

van Rhee, C. (2016). *Webinar: Trailing suction hopper dredger - draghead visor control.*

van Rhee, C. (2017). *Lecture notes: Dredging processes 2 (oe4627) - camp based models.*

v. Bergh, P., J.Osnabugge, & d. Keizer, C. (2015). An optimal dredging process by using draghead control concepts [CEDA Dredging days 2015,].

Vlasblom, W. (2003). *University lecture notes: Dredging equipment and technology.* Delft University of Technology.

VOUB. (2010). Pompkarakteristiek van 2 in serie geschakelde pompen [figure], baggerpompen en aandrijvingen.

Weegenaar, R. A., Keetels, G. H., Winkelman, M. O., & van Rhee, C. (2015). Sand erosion with a traversing circular jet. *Proceedings of the Institution of Civil Engineers-Maritime Engineering, 168*(2), 76–83.

Westin, J. (2023). Static vs kinetic. https://jackwestin.com/resources/mcat-content/force/friction-static-and-kinetic

World Economic Forum. (2022). What is the difference between scope 1, 2 and 3 emissions, and what are companies doing to cut all three? https://www.weforum.org/agenda/2022/09/scope-emissions-climate-greenhouse-business/

Acronyms

CTS Constant Tonnage System
CVS Constant Volume System

EHP Effective Horse Power

GHG Greenhouse Gases

HFO Heavy Fuel Oil

IBP Inboard dredge Pump
IWT Inland Water Transport

MGO Marine Gas Oil

TSHD Trailing Suction Hopper Dredger

UWP Underwater dredge Pump

List of Figures

List of Tables

A | Appendix A - Literature

A.1 Cutting force

The cutting forces are determined on the models elaborated in 'The Delft Sand, Clay & Rock Cutting Model' of Sape Miedema. Different models are elaborated in this book for cutting sand, clay and rock. This study makes use of the saturated sand model. A brief explanation of this model is included, for the comprehensive description the book of Miedema can be used as reference S. A. Miedema, 2014.

The rate of the increase of the pore volume in the dilatancy zone, the volume strain rate, is proportional to the cutting velocity. If the volume strain rate is high, there is a chance that the pore pressure reaches the saturated water vapour pressure and cavitation occurs. This also implies that, with a further increasing cutting velocity, the cutting forces cannot increase as a result of the dilatancy properties of the sand. The cutting forces can, however, still increase with an increasing cutting velocity as a result of the inertia forces and the flow resistance." (Miedema, The Delft Sand, Clay and Rock Cutting Model, 2014)

The saturated sand model is related to the pore pressure. The grain particles are dislocated from their structure by the moving cutting teeth. As a result, the sand will increase in volume, also referred to as the dilatancy effect. The created space between the grains will be filled with water, however the grains are still closely packed together. The inflowing water will therefore experience resistance, which cause sub-pressures in the pores. This increase of pore pressure is linked to increase of the cutting velocity.

If this volume strain rate is high (so high cutting velocities) there is a chance that the pore pressure reaches the vapor pressure and cavitation occurs. This cavitation process will then wear the cutting blade, as the little bubbles formed will explode on the blade. This also implies that, with a further increasing cutting velocity, the cutting forces cannot increase due to the properties of the sand. The main parameters which play a role in the cutting of sand are included in figure A.1.
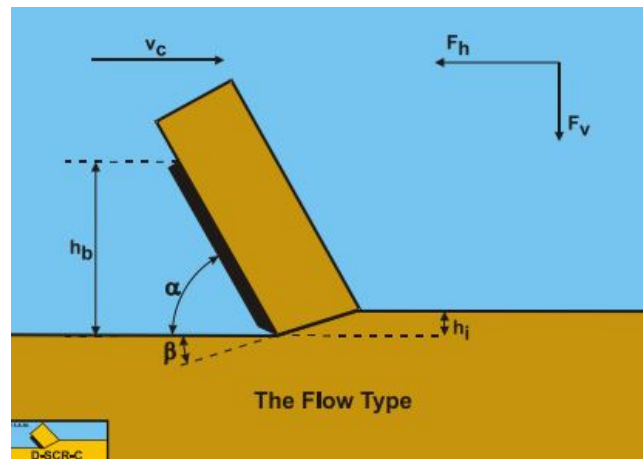

Figure A.1: The cutting of saturated sand, source: S. A. Miedema, 2014

The most important formulas which are used in the determination of the cutting force are described here. The non-cavitating cutting force which is used to calculate the horizontal cutting force until a maximum trailing speeds of 4 knots is expressed with equation A.1.

$$F_{noncav,h} = \frac{c_1 * \rho_w * g * v_t * h_i^2 * \epsilon * w}{k_m} \tag{A.1}$$

Where:

c_1 = Non dimensionless horizontal cutting force coefficient [-]
ρ_w = Water density [kg/m^3]
g = Gravitational acceleration [m/s^2]
v_t = Trailing speed [m/s]
h_i = Cutting layer thickness [m]
ϵ = Dilatancy [-]
w = Total width of draghead teeth [m]
k_m = Effective permeability of soil [m/s]

The non dimensionless cutting coefficient is based on the pore pressure model and blade-, shear- and internal friction angles, described with the following formula:

$$c_1 = \frac{\left(p1m_{\text{dless}} * \frac{\sin(\varphi)}{\sin(\beta)} + p2m_{\text{dless}} * \frac{h_b}{h_i} * \frac{\sin(\alpha+\beta+\varphi)}{\sin(\alpha)}\right) * \sin(\alpha+\delta)}{\sin(\alpha+\beta+\delta+\varphi)} - p2m_{\text{dless}} * \frac{h_b}{h_i} * \frac{\sin(\alpha)}{\sin(\alpha)} \tag{A.2}$$

Where:

φ = Angle of internal friction [rad]
α = Blade angle [rad]
δ = Soil/steel interface friction angle [rad]
h_b = Blade height [m]
h_i = Cutting layer thickness [m]
$p_{1,2mdless}$ = dimensionless pore pressure [-]

The jetting layer thickness $h_{i,jet}$ and the pore pressure Δp_i are in fact also based on different parameters. The input parameters are divided into three different groups: vessel parameters, project parameters and operational parameters.

Vessel parameters	Project parameters	Operational parameters
γ_2 (teeth angle)	ρ_w	v_t
w_{teeth}	g	$Q_{wp,jet}$
n_{teeth}	δ, φ	γ (visor angle)
l_{blade}	n_i, k_i	
	n_{max}, k_{max}	

Table A.1: The cutting parameters sorted into three different groups

A.2   Jetting process

This section will elaborate on the jetting processes, the layer thicknesses which determine the reaction forces on the visor are also elaborated.

Penetration depth

The penetration depth is the length between the jet nozzle and the deepest point in the soil that is reached by the jet flow. The jets, located in the heel of the draghead, will be turned on when the loading process starts. Dependent on the jet pump- and soil characteristics the jets will penetrate the soil with a certain length (penetration depth). The trailing speed plays also an important role in development of the penetration depth, due to the following reason: jetting for a longer period will result in a deeper hole than jetting for a shorter period at one location. So an increase in trailing velocity will result in a decrease of jetting at one location, and therefore a decrease of penetration depth. This processes is shown in figure A.2.
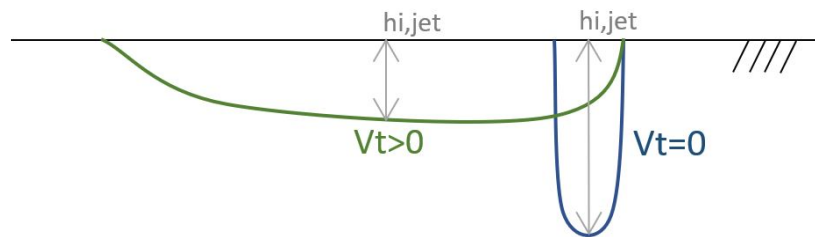
Figure A.2: The layer thickness of the jet based on trailing speed. Trailing with no speed results in a deep hole represented by the blue line, increasing trailing speed will result in a longer thin layer thickness

The visor is dragged along the ground and makes contact with the bed. Due to this contact a layer is created which is affected by the visor. This bed layer can be split up into different layers in which every layer exerts a force on a section of the visor.

The total layer thickness that affects the visor by a reaction force, is referred to as $h_{i,total}$. This layer thickness is based on the geometry and the angle (γ) of the visor and is displayed in figure A.3 and equation A.3. Based on the chosen visor method (explained above) the visor will make contact with the bed layer. The thickness of this bed layer is referred to as $h_{i,total}$ and is dependent on the length and the angle of the visor.

$$h_{i,total} = l_{visor} * sin(\gamma) \tag{A.3}$$

The total layer thickness that affects the visor can be subdivided into three layer thicknesses, the jet, sled and cutting layer. The ratio in which these three layers take place are dependent on two input variables, the visor angle γ and the penetration depth $h_{i,jet}$.
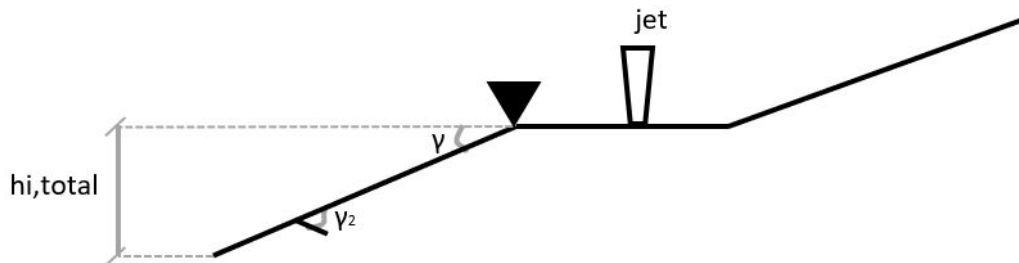

Figure A.3: Total layer thickness that affects the visor, this total layer thickness can be subdivided into three layer thicknesses

Three different situations how the total layer thickness affects the visor will be sketched based on the penetration depth and increasing trail speed. The reaction on the visor will also depend on the visor angle, but for understanding the process, this angle will first be kept constant. The first situation describes the position where the penetration depth is bigger than the total layer thickness that affects the visor ($h_{i,jet} > h_{i,total}$). In this situation a part of the jet water will flow underneath the visor and will therefore be lost. The visor will not be in equilibrium and will sink down until a solid layer has been reached. The jet layer thickness is bigger than the layer thickness which affect the visor. The jetting layer will therefore be aligned with the total layer thickness, since bigger layer thicknesses will not affect the visor ($h_{i,jet} = h_{i,total}$).
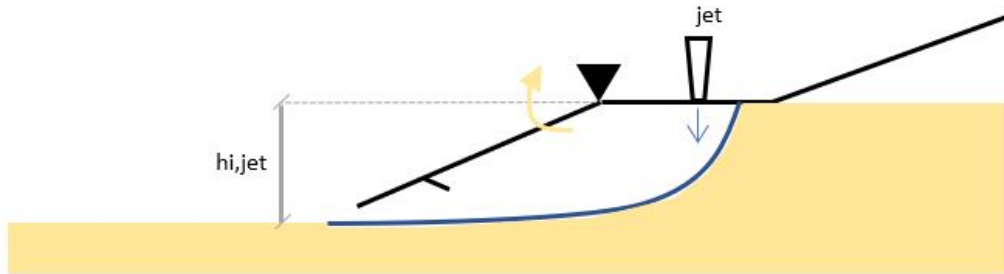
Figure A.4: Layer thickness jet in situation 1: low trailing speed which results in a deep layer. A part of the jet is lost under the visor.

When the trailing speed increases, the penetration depth will decrease and will become less than the layer thickness that affects the visor ($h_{i,jet} < h_{i,total}$). In this situation the visor will make contact with a solid layer and will act as a sled moving along the ground. This sledding movement will result in the second layer thickness, referred to as $h_{i,sled}$. In this case the jet stream will still flow underneath the cutting teeth, as a result the cutting teeth will still not make contact with the soil ($h_{i,jet} > h_{i,total} - h_{i,sled}$). This process is displayed in figure A.5. This sledding layer thickness is dependent on the length of the wearing pieces and can be calculated as equation A.4. The sled layer increases slowly as the trailing speed increases. until the next situation is reached .

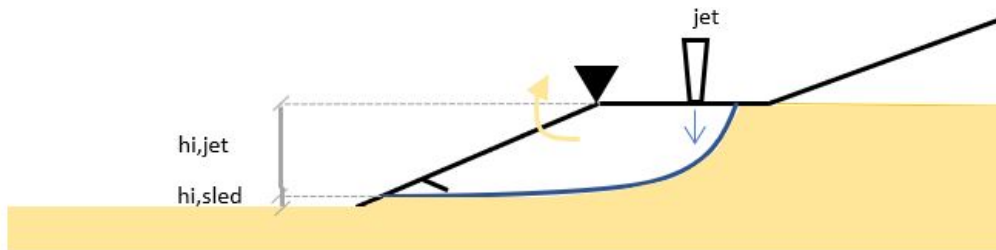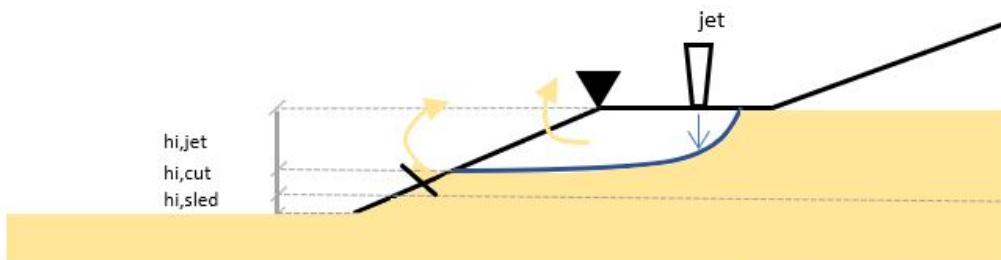$$h_{i,sled} = l_{visor} - l_{cut} * sin(\gamma) \tag{A.4}$$

Figure A.5: Layer thickness jet in situation 2: Increasing trailing speed results in contact with bed layer. An extra layer thickness is created represented by $h_{i,sled}$.

By increasing the trailing speed even more, the decrease in penetration depth will make sure that the cutting teeth make contact with the ground ($h_{i,jet} < h_{i,total} - h_{i,sled}$). This will result in a third layer thickness, namely $h_{i,cut}$. The sledding layer thickness will remain constant since the cutting teeth will take over the increase in layer thickness. The cutting layer is dependent on the ratio of the other layers and can be calculated as follows:

$$h_{i,cut} = h_{i,total} - h_{i,jet} - h_{i,sled} = l_{cut} * sin(\gamma) - h_{i,jet} \tag{A.5}$$


Figure A.6: Layer thickness jet in situation 3: Increasing trailing speed results in contact with bed layer by the teeth. An extra layer thickness is added to the other two layer, namely the cutting layer thickness $h_{i,cut}$.

Sensitivity analysis cutting force

This section analysis shows the sensitivity anlaysis of the cutting force. It can be observed that the soil conditions, especially the porosity, has a great inluence on the output of the cutting force calculation.
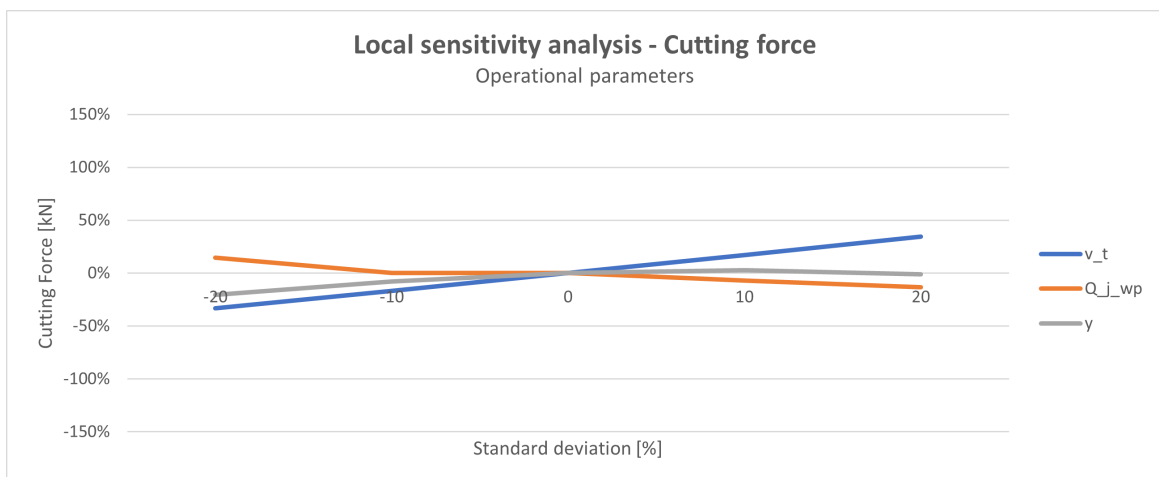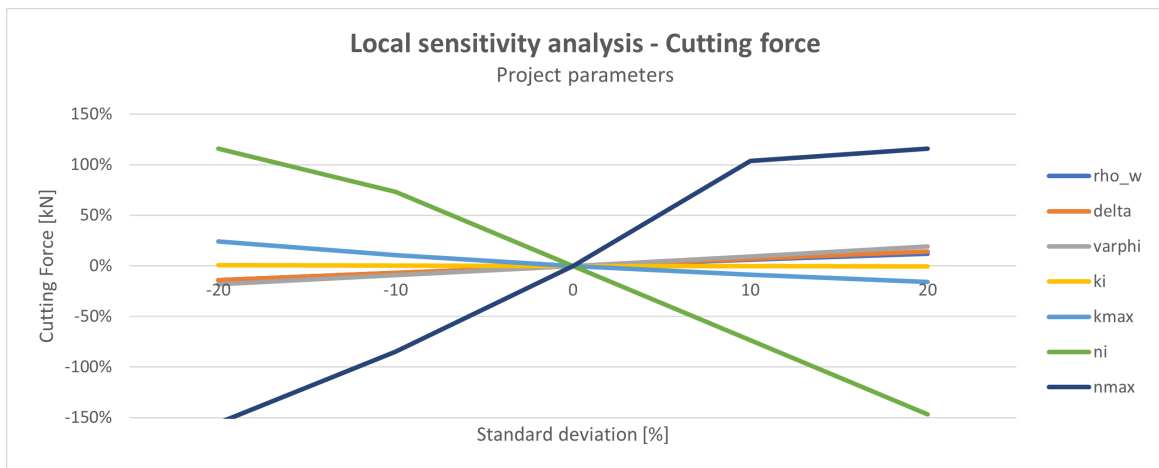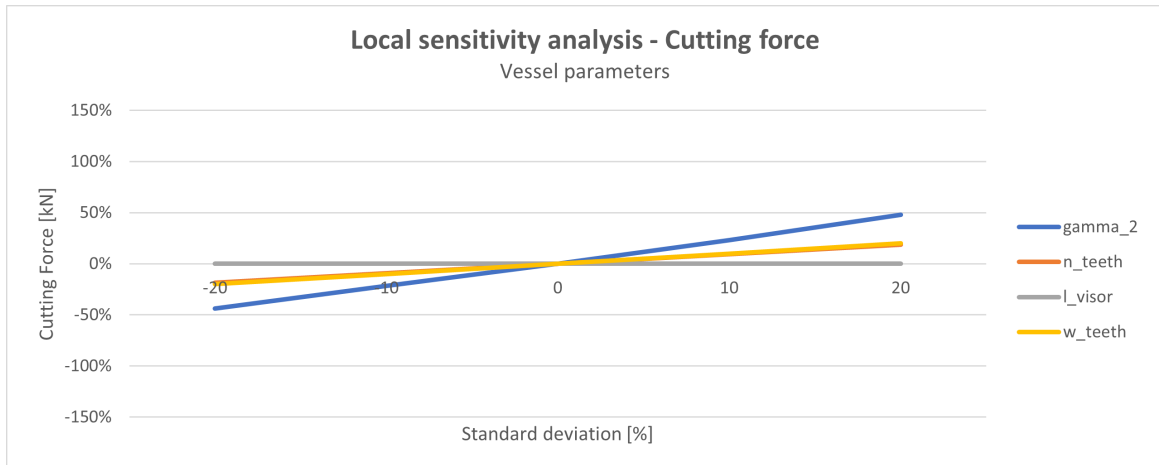
A.3 Visor geometry

To understand the forces working on the visor the free body diagram of the visor and the corresponding geometry of the visor should be well understood. The 3D forces working on the visor will be approximated in a 2D diagram.

The visor angle γ is the angle with respect to the x-axis and the angle of the arm and the cutting teeth are positioned under an angle γ_2.

The location where the forces act on the visor are displayed in figure A.7. The exact location depends on the geometry of the deployed draghead of the TSHD. The cutting force and the gravity force can be found directly of the geometry of the draghead, since the cutting force engages at the teeth and the gravity force at the centre of gravity of the visor. The vacuum force is the resultant force of pushing away the mixture. The point where it engages on the visor is dependent on the opening of the draghead. It is assumed that it engages in the middle of the distance from the cutting teeth until hinge C.

In order to compute the horizontal and vertical forces, it is possible to transfer via geometry and visor angle.

$$l_{vac} = \frac{l_{cut}}{2} \tag{A.6}$$

The sled force is assumed to engage in the middle of the total outer part of the draghead at the wearing pieces:

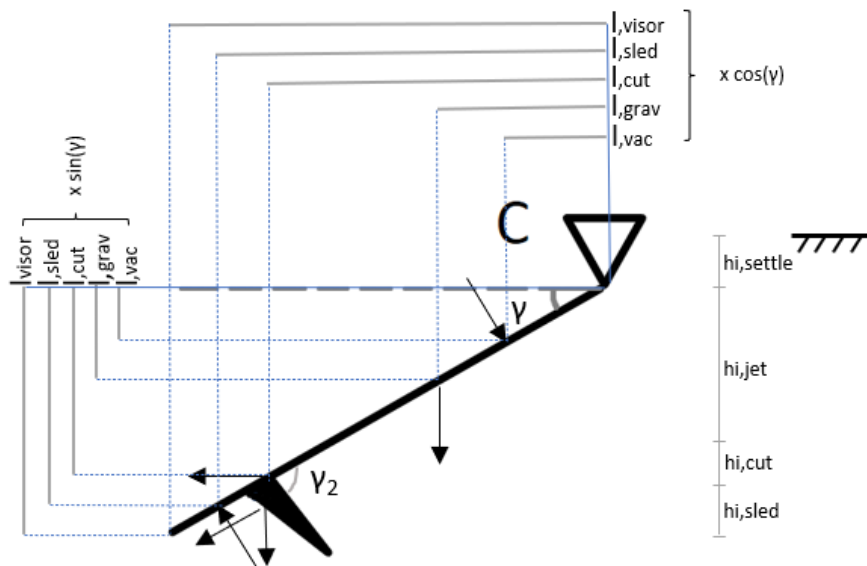$$l_{sled} = \frac{l_{visor} - l_{cut}}{2} + l_{cut} \tag{A.7}$$

Figure A.7: Visor geometry and layer thickness

B | Appendix B - Propeller model

B.1 Estimation model results

This section shows the detailed results of the resistance forces working on visor and draghead. The visor force is the main resistance force (at high trailing speed).
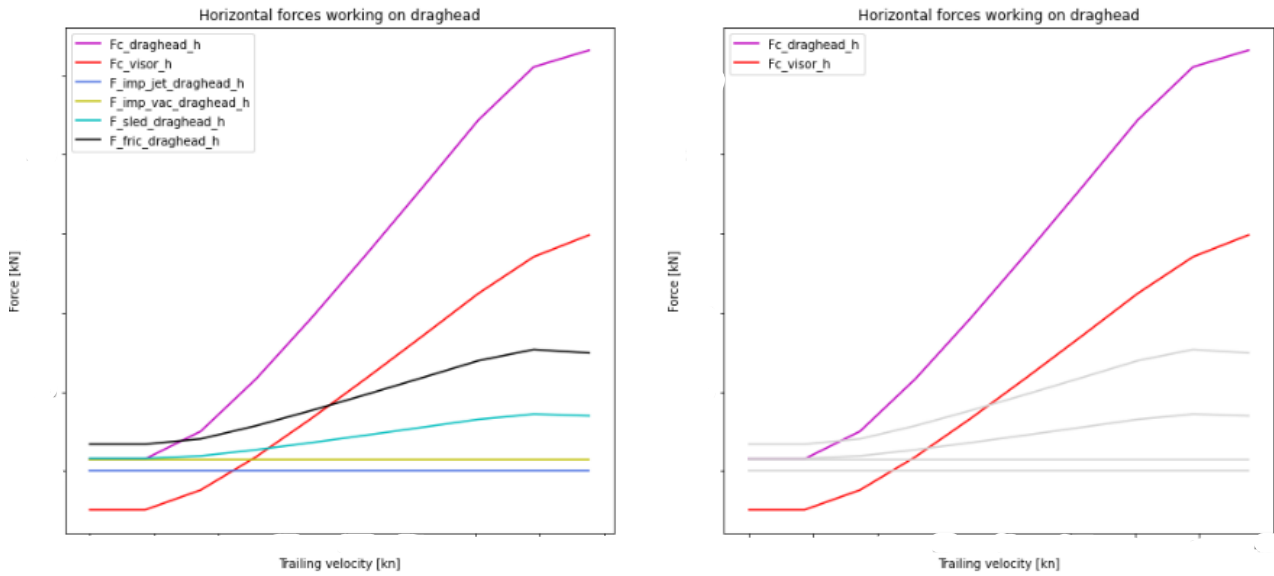

Figure B.1: Left: All resistance terms working on draghead, Right: visor resistance is highlighted since it is the main resistance contributor at higher trailing speeds

The visor analysis shows that the cutting force is the main resistance force at hihger trailing speeds.
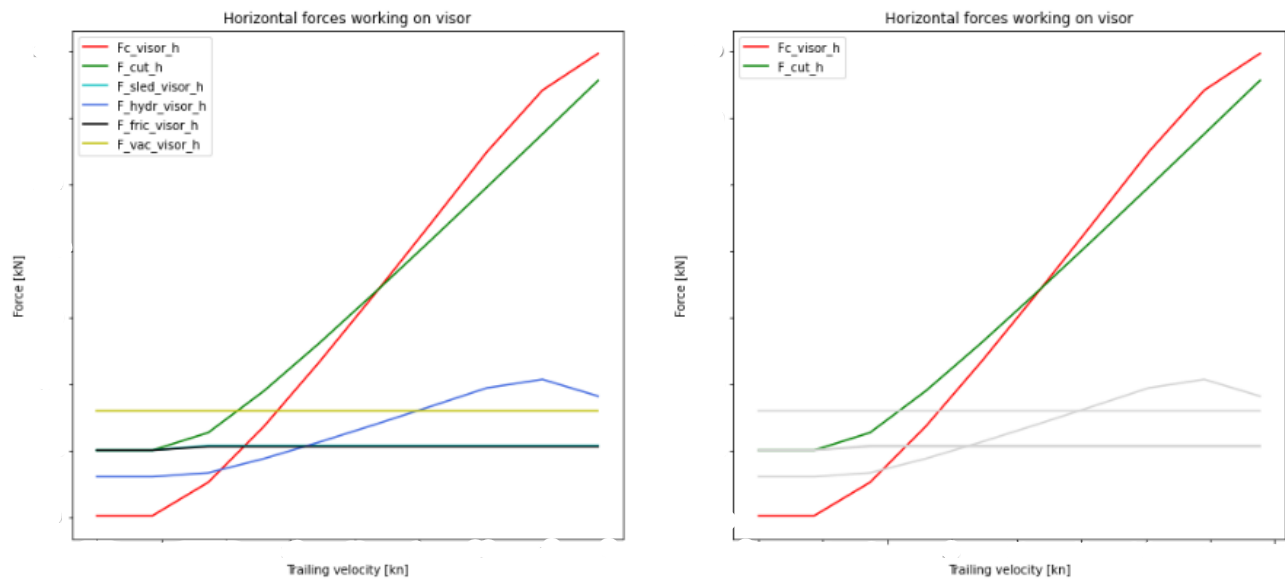

Figure B.2: Left: all resistance terms working on the visor. Right: cutting force is highlighted since it is the main resistance term working on the visor

B.2   ACT - Data analysis

The total results of the correlation and pattern identification research are included in this section. The visor angle has been categorized into distinct angles, and for each angle group, the corresponding power and trailing speed values have been plotted. This research is executed to identify correlations or patterns between the visor angle and the trailing speed.

Three visor angle plots are included in the non stationary analysis, namely $\gamma = -34 : -36$, $\gamma = -32 : -34$ and $\gamma = -30 : -32$. These three angles can be assigned to certain trailing speed limits.
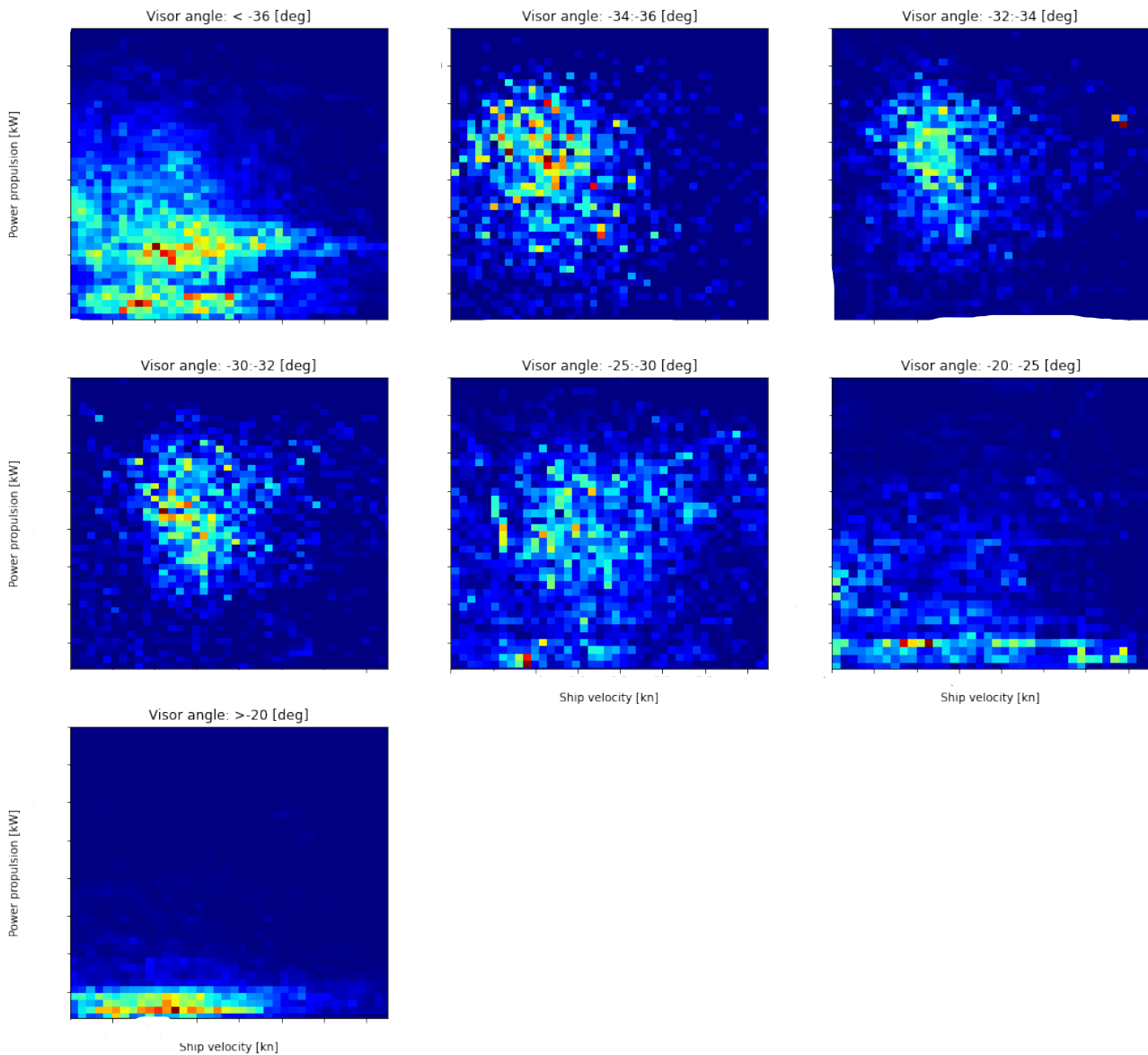

Figure B.3: Correlations between different visor angles and trailing velocities (**Note: axis confidential**).

C | Appendix C - Simulation tool

C.1 OpenCLSim

This section elaborates on the OpenCLSim activities and functions which needs to be used for simulating the total dredging cycle.

Sailing phases

The sailing phases are simulated by the move activity and represents the sailing full and sailing empty sailing phase. The estimation function which calculates the propulsion power during sailing is developed bij Lamers, 2022 and is added to the energy plugin for both phases.

- Move Activity

Loading

The loading cycle OpenCLSim modifications are already elaborated in the recommendation section. The loading area should be divided in smaller boxes based on the center of gravity of the area. The vessel should follow a predefined sailing pattern to be able to better estimate the sailing distance after the loading phase. The activity that should be used to simulate the loading phase are:

- Move Activity
- Shift amount Activity (modified)
- Parallel Activity
- Repeat Activity

Dumping

The dumping phase is simulated by the shift amount activity. For now, only bottom door dumping is included in the dredging cyclus. The dumping area is represented by different point to represent the different dumping locations within the total area. The vessel moves to the point closest to the access channel, when full capacity is reached it should sail to the next point.

- Shift amount Activity
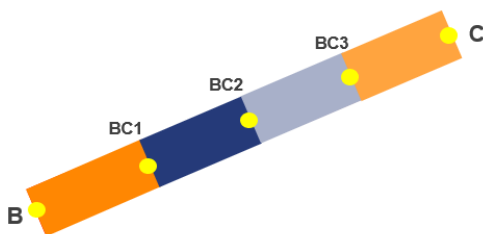
(a) Visualization of the access channel, divided in smaller boxes based on center of gravity
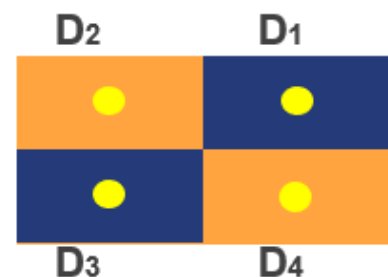
(b) Visualization of the dumping area to be implemented in OpenCLSim

Figure C.1: OpenCLSim visualizations

C.2   Simulation results

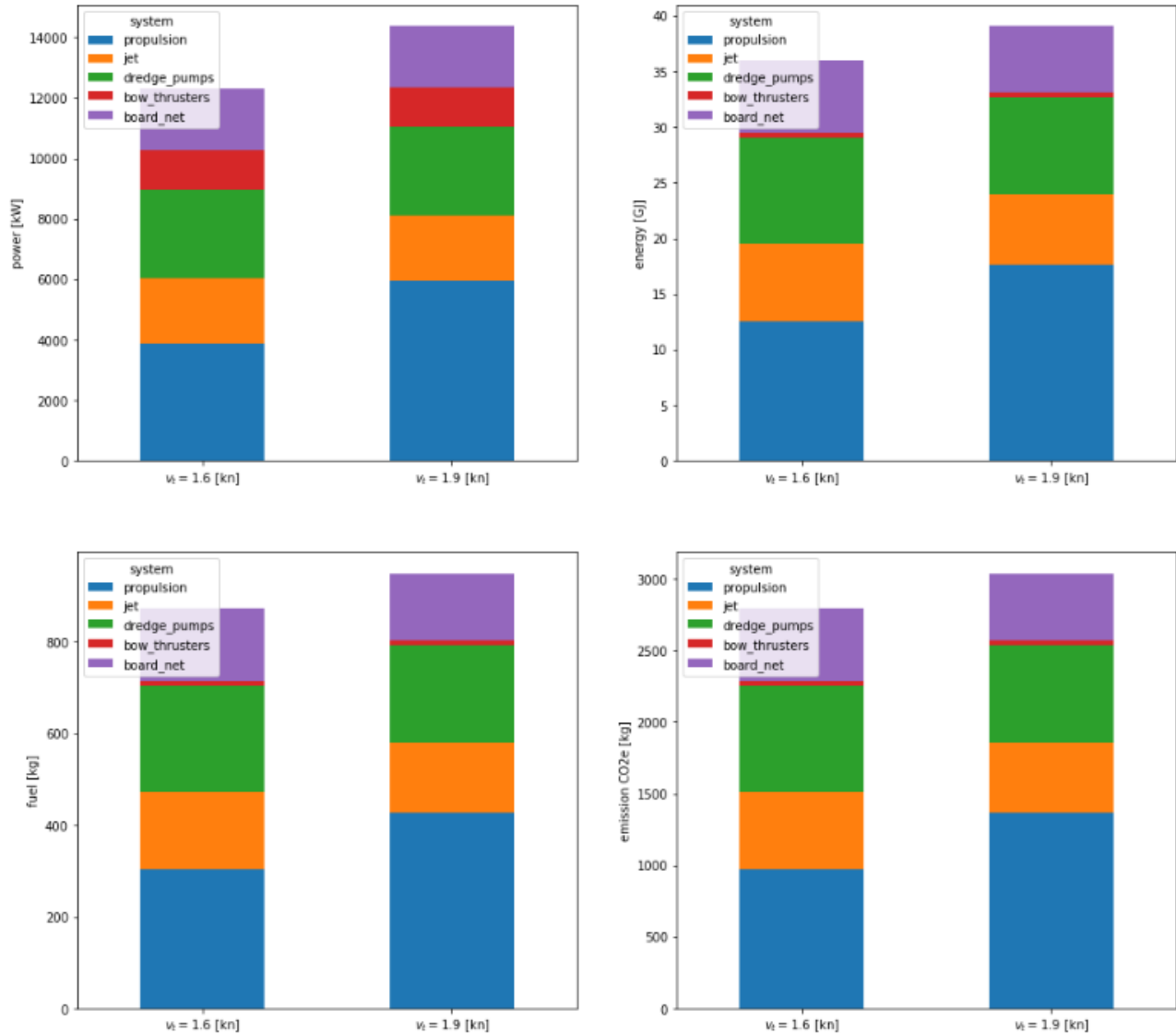This section shows the simulation results of one loading cycle.

Figure C.2: Results of simulation

system	propulsion	jet	dredge_pumps	bow_thrusters	board_net	total
power [kW]	3883.6	2150.1	2948.3	1300.0	2027.0	12309.0
time [hr]	0.9	0.9	0.9	0.1	0.9	0.9
energy [GJ]	12.6	7.0	9.5	0.4	6.6	36.1
fuel [kg]	304.8	168.7	231.4	10.2	159.1	874.2
emission [kg]	975.7	540.2	740.7	32.7	509.2	2798.5

Figure C.3: One loading cycle results with trailing speed $v_t = 1.6[kn]$

system	propulsion	jet	dredge_pumps	bow_thrusters	board_net	total
power [kW]	5946.1	2150.1	2948.3	1300.0	2027.0	14371.5
time [hr]	0.8	0.8	0.8	0.1	0.8	0.8
energy [GJ]	17.6	6.4	8.7	0.4	6.0	39.1
fuel [kg]	427.1	154.4	211.8	9.3	145.6	948.2
emission [kg]	1367.4	494.4	678.0	29.9	466.1	3035.8

Figure C.4: One loading cycle results with trailing speed $v_t = 1.9[kn]$

C.3 Input Data

This section shows the analysis of the bow thrusters power and active time duration. The y-axis represents the power of the bow thrusters, the x-axis the time. A limit is set on 1200 kW. The purple highlighted parts are the data which represent the time the bow thrusters are above 1200 [kW] per loading cycle. It was calculated that the bow thrusters are approximately 5 [min] active per loading cycle. For now it was analysed that the loading cycle takes around 50 [min], this means that the bow thrusters are approximately 10% active during a loading cycle.
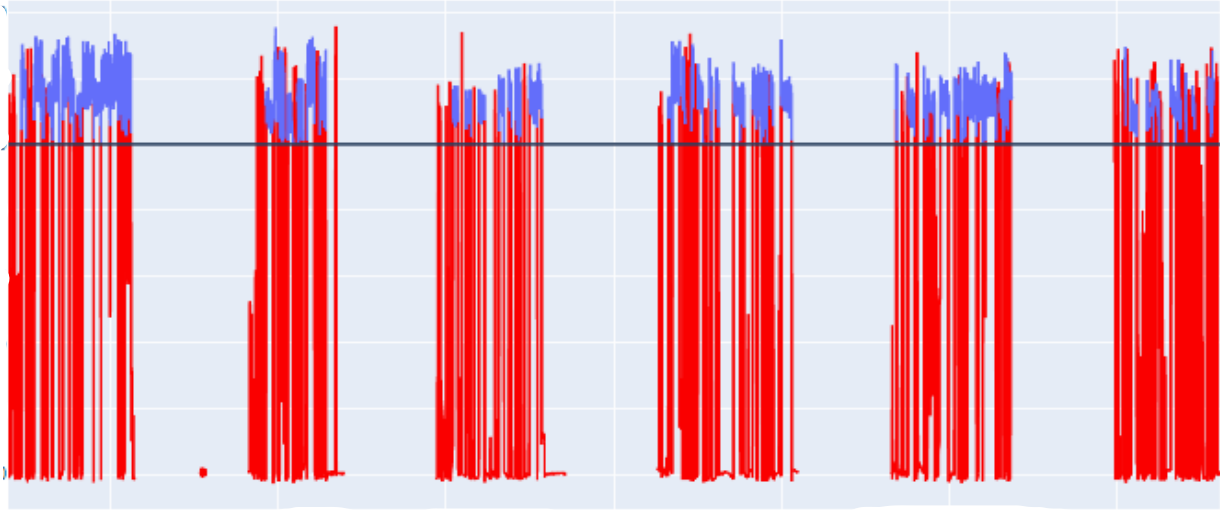

Figure C.5: Result of data analysis bow thrusters. The active time above 1200 [kW] is studied for several loading cycles. The mean of the power and active duration is used as input for the energy plugin (**Note: axis confidential**).